

Determination of distance and stellar parameters by Bayes probabilistic inference

Veselin, Tibor

Master's thesis / Diplomski rad

2024

Degree Grantor / Ustanova koja je dodijelila akademski / stručni stupanj: **University of Rijeka / Sveučilište u Rijeci**

Permanent link / Trajna poveznica: <https://um.nsk.hr/um:nbn:hr:194:355052>

Rights / Prava: [In copyright](#)/[Zaštićeno autorskim pravom.](#)

Download date / Datum preuzimanja: **2025-02-23**



Repository / Repozitorij:

[Repository of the University of Rijeka, Faculty of Physics - PHYRI Repository](#)



UNIVERSITY OF RIJEKA
FACULTY OF PHYSICS

Tibor Veselin

Determination of distance and stellar parameters
by Bayes probabilistic inference

Masters thesis

Rijeka, October 2024

UNIVERSITY OF RIJEKA
FACULTY OF PHYSICS
ASTROPHYSICS AND ELEMENTARY PARTICLE PHYSICS

Master thesis

Determination of distance and stellar
parameters by Bayes probabilistic
inference

Supervisor:

dr. sc. Tomislav Jurkić

Candidate:

Tibor Veselin

Rijeka, October 2024.

Contents

1	Introduction	1
1.1	Other works that used similar approach	4
1.2	Research Objectives	5
2	Stars	6
2.1	History of stellar observations	6
2.1.1	Evolution of stellar observations	6
2.2	What are stars?	8
2.3	The Classification of Stellar Spectra	9
2.4	The Hertzsprung–Russell (H-R) diagram	12
3	Stellar parameters	16
4	Stellar evolution [1]	23
4.1	The Kelvin-Helmholtz timescale	23
4.2	Nuclear timescale	24
4.3	Low-Mass Main-Sequence Evolution	25
4.3.1	The Schönberg–Chandrasekhar Limit	27
4.4	Main-Sequence Evolution of Massive Stars	28
4.5	Late stages of stellar evolution	28
4.6	The Subgiant Branch (SGB)	32
4.7	The Red Giant Branch (RGB)	32
4.8	The Helium Core Flash	33
4.9	The Horizontal Branch (HB)	33
4.10	The Early Asymptotic Giant Branch (AGB)	34
4.11	Death of the star	36
5	Globular Clusters	37
5.1	Spectroscopic Parallax	37
5.2	Messier 92	38
5.3	Messier 13	40
5.4	NGC 6791	42
6	Bayesian Inference	44
6.1	History	44
6.2	Understanding Bayes’ Rule	44
6.2.1	Example: Medical Diagnosis	45
6.3	Bayesian Priors	46
6.3.1	Informative and Uninformative Priors [2]	46
6.3.2	Choosing a Prior [3]	46

6.4	Likelihood Function [3]	47
6.5	Probability density function (PDF) [4]	48
7	Methods: The Bayesian Extinction and Stellar Tool [5]	50
7.1	Stellar Parameter Estimation [6]	50
7.1.1	Age (t)	50
7.1.2	Mass (M)	50
7.1.3	Metallicity (Z)	51
7.1.4	Distance (d)	51
7.2	Fitting Technique [5]	51
7.2.1	Synthetic Photometry [6]	52
7.2.2	Chi-Squared Statistic	52
7.3	Likelihood Function in BEAST	53
7.3.1	Prior Distributions and Posterior Sampling	53
7.4	Dust Extinction Parameter Estimation	54
7.4.1	Visual dust extinction (A_v)	54
7.4.2	Average Grain Size (R_v)	54
7.5	Dust Extinguished Stellar Model [5]	55
7.5.1	Single Star Intrinsic SED	55
7.5.2	Interstellar Dust Extinction	55
7.5.3	Full SED Model	55
7.6	Practical Applications	56
8	Installation and running the BEAST	57
8.1	BEAST filters library files	57
8.2	Step 1: Preparation of Input Catalogs	59
8.3	Step 2: Configuration of the <code>settings.txt</code> File	59
8.4	Step 3: Running the BEAST Models - <code>run_beast.py</code>	59
8.4.1	A) Physics Model Generation (flag command -p)	59
8.4.2	C) Splinter Noise Model	61
8.4.3	E) Trimming for Speed (flag command -t)	61
8.4.4	F) Fitting the Model and Generating Statistics (flag command = -f)	61
8.4.5	G) Plotting Results	62
9	Data and observations	63
9.1	Calculating fluxes	65
9.2	Creating and Viewing FITS file	65

10 Numerical calculations	67
10.1 How BEAST calculates stellar parameters?	67
10.2 Modifying <code>settings.txt</code> file: parameters, models and priors	67
10.3 Modifying <code>run_beast_splinter.py</code> file	69
10.4 The BEAST analysis	70
11 Results and interpretation	72
11.1 Output plots from BEAST analysis	72
11.2 Spatial distribution diagrams	74
11.2.1 M92: Spatial distribution diagrams	74
11.2.2 M13: Spatial distribution diagrams	78
11.2.3 NGC 6791: Spatial distribution diagrams	81
11.3 H-R diagram	84
11.3.1 M92: H-R diagram	84
11.3.2 M13: H-R diagram	89
11.3.3 NGC 6791: H-R diagram	93
11.4 Relationships between stellar parameters	98
11.4.1 M92: Relationships between stellar parameters	98
11.4.2 M13: Relationships between stellar parameters	101
11.4.3 NGC 6791: Relationships between stellar parameters	104
11.5 M92: Comparison between stellar parameters calculated with distance set as constant and distance being variable	107
11.6 M13: Comparison between stellar parameters calculated with distance and age set as constant and distance and age being variable	112
12 Comparison with values from other studies	117
12.1 M92 - Comparison	117
12.2 M13 - Comparison	119
12.3 NGC 6791 - Comparison	121
13 Conclusion	123
14	124
A Python Scripts for Data Handling	130
A.1 Script for Converting Excel to FITS	130
A.2 Script for Exploring HDF5 Files	131
A.3 Script for Converting FITS to Excel	131
A.4 Script for Plotting Spatial distribution diagrams	132
A.5 Script for Flag Assignment Based on Conditions	133
A.6 Script for Generating HR Diagrams with Flagged Data	133

A.7	Script for Plotting HR Diagram with stellar parameters	134
A.8	Script for Multiple Relationship Diagrams	135
A.9	Script for Pairwise Comparison of Fixed and Variable Estimates . .	137
A.10	Tables that show rates (fluxes) for different bands for given stellar positions (R.A. and Decl.)	139
A.11	Tables that show stellar parameters obtained with BEAST	144

Abstract

This thesis is devoted to the study of the stellar parameters and determination of stellar distances. For that purpose, the BEAST (The Bayesian Extinction and Stellar Tool) algorithm was used. BEAST is fitting ultraviolet to near-infrared photometric magnitudes to precomputed model grids. This method precisely evaluates parameters such as age, mass, metallicity, and distance by implementing Bayesian inference combined with prior distributions best-suited to the characteristics of the stellar population under study.

BEAST integrates synthetic photometry and uses chi-squared fitting techniques that handle observational data from large surveys.

This study was focused on globular clusters M92, M13 and NGC 6791 and with the help of BEAST the following parameters were determined: mass, luminosity, surface gravity, radius, temperature, distance, age and metallicity of the stars we studied. We also determined dust parameters: visual extinction and ratio of total to selective extinction.

We later compared values from other science papers and values obtained by the BEAST.

For M92, BEAST determined the mean distance to be 5.46 kpc (accuracy of 66.6%). For age, BEAST determined the value of 7.45 Gyr (accuracy of 67.7%). For visual extinction in magnitude, BEAST got $A_v = 0.12$ (accuracy of 47.3%) and for ratio of total to selective extinction, $R_v = 2.76$ (accuracy of 89%).

For M13, BEAST determined mean distance to be 5.01 kpc (accuracy of 63.67%). For age, it determined 7.67 Gyr (accuracy of 65.84%). For visual extinction in magnitude BEAST got $A_v = 0.16$ (accuracy of 87.5%) and for ratio of total to selective extinction, $R_v = 3.49$ (accuracy of 88.83%).

For NGC 6791, BEAST calculated mean distance to be equal to 4.55 kpc (**accuracy of 92.98%**), which is an excellent result. In that cluster we analysed SGB and RGB stars, while in other clusters we analysed AGB, RGB and HB stars, so it might be the case that BEAST is doing better estimates for stars in earlier stages of their evolution. For age, BEAST estimated the value of 7.77 Gyr (**accuracy of 93.61%**). For visual extinction in magnitude we obtained $A_v = 0.46$ (accuracy of 65.71%) and for ratio of total to selective extinction, $R_v = 3.01$ (accuracy of 97.1%).

We have also shown that fixing stellar age does not influence the determination of other stellar and dust parameters, while fixing distance can greatly influence stellar luminosity and radii.

BEAST is very effective in dealing with the challenges posed by interstellar dust extinction, which can greatly affect the accuracy of photometric data. The results are not perfect, but they show the effectiveness of Bayesian methods in dealing with complex data in astronomy.

Keywords: Stellar parameters, BEAST, Bayes statistics, distance estimation, photometric spectral energy distributions (SED), synthetic photometry, stellar parameters, dust extinction, astronomical surveys, chi-squared fitting.

1 Introduction

The study of stars is a fundamental pursuit in astrophysics, significantly advancing our understanding of the broader universe. Stars are crucial to the dynamics within galaxies. Stars serve as critical catalysts in the synthesis of all elements heavier than hydrogen.

Stellar parameters such as mass, temperature, and luminosity provide insight into nuclear processes and element distribution. That is essential for comprehending the chemical composition of the universe and its potential for life. Additionally, stars are crucial tools in cosmology, enabling astronomers to measure cosmic distances and expand our understanding of the universe's expansion through parameters like the Hubble constant.

For correct determination of stellar parameters, full stellar energy distribution (SED) and fitting to a theoretical models of the stars are being used. The problem with this method is that it is limited to only a small number of stars, and it takes a long time to capture full SED for a star. It is also very expensive.

Today sky surveys are a popular method for doing analysis with stars. The advent of extensive sky surveys like the Sloan Digital Sky Survey (SDSS), Gaia, and future projects like the Vera Rubin observatory and Large Synoptic Survey Telescope (LSST) promises for a vast number of stars spanning from ultraviolet to infrared. They promise to create photometric data for billions of objects. For that, it is necessary to develop a method which will calculate stellar parameters based on wide-band SEDs.

Photometric measurements of these surveys are not full SED for each star. With filters, they capture only integrated flux for specific wavelengths. To obtain precise measurements, we need to use a large number of photometric bands. SDSS uses 5 filters (u, g, r, i and z), from which we used g, r, i and z in this work and we added near-infrared observations from the Two Micron All-Sky Survey (2MASS) in J, K and H filters to get wide-range SED, to avoid the degeneracy that happens because of the big number of parameters that we are determining.

For determining the distance to the star, in most cases we need to know its parallax. In this work, we are testing a way of determining distance to the stars only using photometric measurements.

This thesis aims to leverage these broad datasets to develop robust methods for estimating stellar parameters, distances, and interstellar extinction using Bayesian approaches.

Another reason why it was necessary to use a wide range of bands, from infrared (IR) to ultraviolet (UV) is that up until now photometric measurements and color-magnitude diagrams (CMD) were used to determine stellar parameters, distances and dust extinction. So, some of stellar parameters were assumed and held fixed because of the very large degeneracy of the solutions and the vast parameter space.

And degeneracy is especially large if we use only standard optical measurements in only 3-4 filters.

The determination of stellar parameters such as mass, luminosity, and age only with photometry presents unique challenges, particularly in stars such as red giants (RGB), asymptotic giants (AGB), subgiants (SGB) and horizontal branch stars (HB). They often suffer from parameter degeneration, especially when only limited photometric data are available.

Using the spectroscopic parallax method in giant stars (SGB, RGB, AGB, and HB) to determine stellar parameters and distances is problematic due to degeneration in determining stellar parameters such as mass. The reason for that is that for different extinctions of dust for the same star, we can get two different solutions. They are: main-sequence star with less mass, but greater distance and giant star outside of the main sequence, with greater mass, but closer distance. That can be fixed with adding measurements from bands in the IR spectrum. These are earlier mentioned 2MASS J, H and K filters.

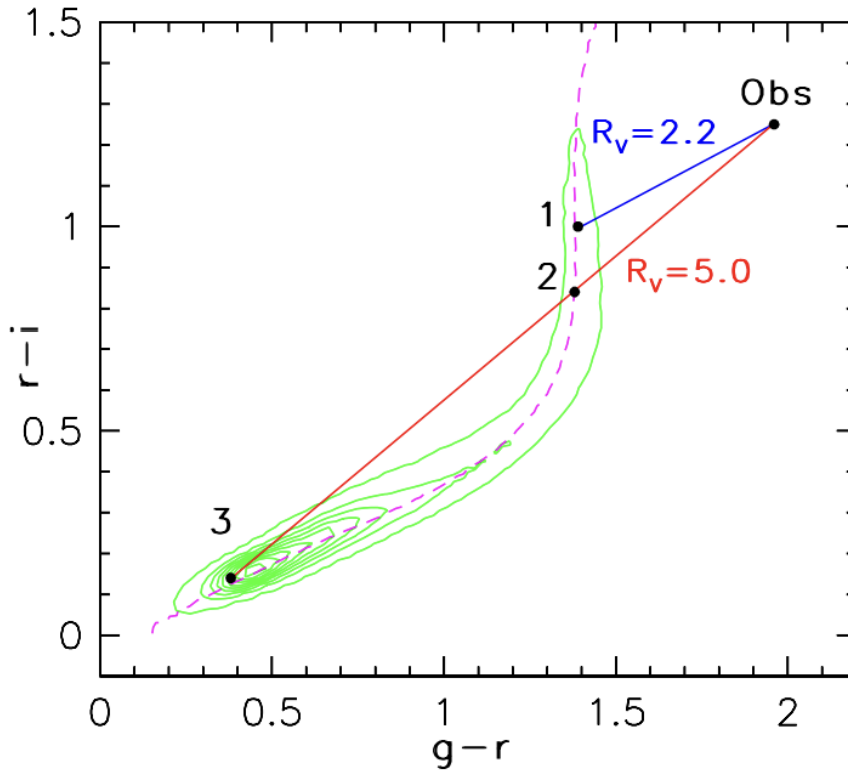


Figure 1: Illustration of the constraints on intrinsic stellar colors, extinction in the r filter band, and the ratio of total to selective extinction. The dashed lines mark the median stellar locus [7].

In figure 1, the dot marked 'Obs' represents a hypothetical observation. Depending on the adopted ratio of total to selective extinction of dust, different combinations of intrinsic stellar colors (i.e., the position along the stellar locus) and extinctions are consistent with the observed $g - r$ color. So, for different selective extinctions we get different solutions. The three solutions are marked 1–3 [7].

So, if we use only 3-4 filters (U, B, V photometry), we have the problem of understanding if particular stars is on the main sequence or is it a red giant. We also can not calculated distance. This is why in this work we used 7 filters, to see if we can get precise results that way.

For our measurements, we used globular clusters. The reason for this is because these stars are all on similar distances from the Earth, with a similar ratio of total to selective extinction and visual extinction of dust. Also, almost all stars within the globular clusters are of similar age. With all of that, it is possible to know how successfully we can determine stellar parameters for giant stars.

1.1 Other works that used similar approach

C. A. L. Baier-Jones et al. [8] used Gaia's publication of 1.47 billion stellar parallaxes to determine their distances. Gaia is precise, but most of the stars are very distant and faint that their fractional parallax uncertainties are large. So, authors decided to use Bayesian inference. Their approach use a prior constructed from a three-dimensional model of our Galaxy. This model includes interstellar extinction and Gaia's variable magnitude limit.

In a similar work, Gregory M. Green et al. [9] created a method to infer reddening and distances to stars based only on their broad-band photometry, and showed how this method can be used to produce a three-dimensional (3D) dust map of the Galaxy. That method samples from the full probability density function of distance, reddening, and stellar type for individual stars, as well as the full uncertainty in reddening as a function of distance in the 3D dust map. They incorporated prior knowledge of the distribution of stars in the Galaxy and the detection limits of the survey.

In another paper, Gregory M. Green et al. [10] created a new three-dimensional map of dust reddening, based on Gaia parallaxes and stellar photometry from Pan-STARRS 1 and 2MASS.

R. Lallement et al. [11] also created 3D maps of the Galactic interstellar matter (ISM) (dust). They did it by inverting individual distance-limited ISM measurements.

Michael Berry et al. [7] used SDSS's photometry of 73 million stars to simultaneously constrain the best-fit main-sequence stellar SED and the amount of dust extinction along the line of sight toward each star. That is the only work that uses linear fitting instead of Bayesian inference.

1.2 Research Objectives

This study aims to:

1. Determine stellar parameters and distances for stars within globular clusters using only photometric data.
2. Determine visual extinction and ratio of total to selective extinction of interstellar dust.
3. Address the degeneracies in parameter estimation for problematic stars like giants by employing a Bayesian methodological framework.
4. Validate the effectiveness of photometric distance and parameter estimations using Bayesian techniques against existing methods.

2 Stars

Stars are these bright objects that we can see on a night sky if we are lucky so that clouds do not cover them. Our experience of looking at stars can greatly differ depending on where we are located. If you are in an urban area with a lot of light pollution and smog, even on a brightest of nights you will not see much. But, if you are lucky and look at the night sky somewhere in African Savanna, or somewhere really high up from the sea level, or maybe close to some of the Earth's poles, you will have the honor of witnessing one of the most beautiful sights that any human can experience. You will see the night sky in all its glory. Countless stars, moon and even our own galaxy, the Milky Way.

2.1 History of stellar observations

That sight captured the imagination of humans for hundreds of thousands of years. Back then, when first humans look at the sky, it did not look the same as today. Stars are not fixed in place; they move through space.

Over thousands of years, these movements can change the constellations we see in the sky. While 100,000 years is a short time in astronomical terms, there can still be noticeable differences in star positions and constellations over such a period. Earth's rotation axis slowly wobbles over a cycle of about 26,000 years. This process, known as precession, means that the stars' apparent positions in the sky change over time. The Milky Way and other galaxies are also moving relative to each other. Although these movements are less noticeable on human time scales over tens of thousands of years, they can slightly alter the appearance of galaxy positions and of the night sky. Stars evolve over time, changing in brightness and even exploding as supernovae. New stars are born, and older stars die out.

All of that contributed in changing the look of the night sky.

2.1.1 Evolution of stellar observations

The evolution of stellar observations has been a cornerstone of scientific progress, advancing from the naked-eye observations of early civilizations to the developments in the sophisticated, technology-driven methods of modern astronomy.

For tens of thousands of years, human beings have been fascinated by the patterns of stars in the sky above Earth. Early on, they noticed that the Moon changed shape from night to night as well as its position among the stars.

Early people noticed constellations of stars in the sky that looked like animals and people, and made up stories about what they thought they saw. In fact, the oldest records we have of astronomical observations are 30,000-year-old paintings found on the walls of caves.

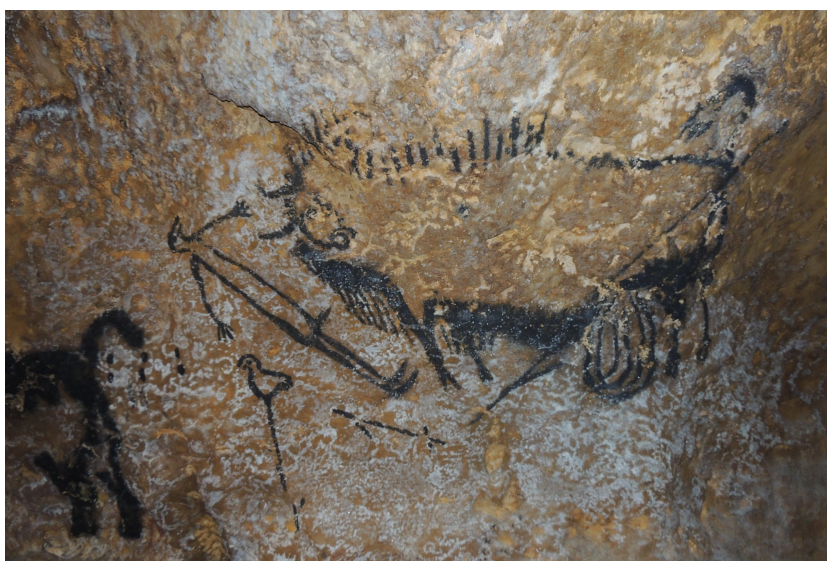


Figure 2: The Shaft Scene in the Lascaux Caves in France. It is featuring a dying man and several animals. Animal symbols represent star constellations in the night sky, and are used to mark dates and events. Artwork might commemorate a comet strike around 15,200 BC, analysis from the University of Edinburgh suggests. [12]

Initially, stars were noted for their brightness and position in the sky. Ancient Greeks and Chinese classified stars into constellations and measured their brightness with a naked eye. These early catalogs were crucial for navigation and calendar systems but offered little insight into the physical nature of stars. Early observers like the Babylonians tracked celestial events such as eclipses and planetary motions.

The invention of the telescope in the early 17th century by Galileo Galilei revolutionized the observation of stars. For the first time, astronomers could resolve individual celestial objects that were not visible to the naked eye. This led to the discovery of moons orbiting Jupiter, the phases of Venus, and detailed observations of sunspots and the rugged lunar surface, revolutionizing our understanding of the universe as a dynamic and varied entity.

The development of spectroscopy in the 19th century allowed astronomers like Joseph von Fraunhofer and later Norman Lockyer to analyze the composition of stellar atmospheres. Spectroscopy enabled astronomers to analyze the light from stars, breaking it into its constituent colors to study the absorption lines in stellar spectra. This technique revealed the presence of various elements in the stars, showing that stars are made of the same elements found on Earth. Spectroscopy became fundamental in classifying stars by their spectral types, which correlate with their temperature.

Advancements in technology and theory in the 20th century, particularly with the creation of the Hertzsprung-Russell diagram by Ejnar Hertzsprung and Henry Norris Russell enabled astronomers to understand the relationship between a star's brightness (luminosity), its surface temperature (color), and its evolutionary stage. The diagram revealed that most stars fall along a main sequence, where stars spend the majority of their lifetimes burning hydrogen into helium. This period also saw the development of the theory of stellar evolution, which describes how stars are born, live out their lives, and die, depending on their initial mass [13].

The late 20th and early 21st centuries have seen big advancements in stellar observations, thanks to the advent of space-based telescopes and modern ground-based facilities. Launching telescopes like the Hubble Space Telescope into space has allowed astronomers to observe the universe without the interference of Earth's atmosphere providing us with unparalleled views across different wavelengths. These observations have been pivotal for studying distant galaxies, star formation, and planetary systems in remarkable detail. On Earth, telescopes have grown in size and sophistication. Facilities such as the Very Large Telescope (VLT) in Chile utilize adaptive optics to correct atmospheric distortion, producing incredibly sharp images.

2.2 What are stars?

Stars are celestial bodies composed of gas and plasma, bound together by gravity. Stars are the most fundamental observable constituents of the universe. They are the engines of energy production in the cosmos.

A typical star, like our Sun, consists primarily of hydrogen and helium with trace amounts of heavier elements. These elements are distributed across various internal layers, each playing a distinct role in the star's lifecycle and characteristics.

A typical structure of solar-like star include[14]:

1. **Core:** The core is the central region where temperatures and pressures are extremely high, which creates nuclear fusion. Nuclear fusion is a process in which lighter atoms fuse to form a larger one, releasing immense amounts of energy, which is the primary source of light and heat of a star.
2. **Radiative Zone:** Surrounding the core, the radiative zone is where energy produced in the core is transported outward by radiation. Photons bounce around in this zone, slowly diffusing outwards. This process can take thousands of years.
3. **Convection Zone:** In many stars, including the Sun, the outer layer of the interior is called the convection zone. Here, energy is transported by convection, a process similar to boiling water. Hot plasma rises from the

lower regions of this zone, cools as it reaches the surface, and sinks back down to be reheated.

4. **Photosphere:** The photosphere is the visible surface of a star and the layer from which light is emitted into space. Here, the star's temperature can be measured by its light.
5. **Atmosphere:** Above the photosphere lies the stellar atmosphere, which includes the chromosphere and the corona. The corona, visible during a solar eclipse, is extremely hot and extends millions of kilometers into space.

Nuclear fusion is very important in understanding stars. The rate of fusion depends on the star's mass. The more massive the star, the greater the gravitational pressure density and temperature in its core, and thus the higher the rate of fusion. This relationship dictates not only the amount of energy a star emits but also significantly influences its lifespan.

Gravity is the governing force in the formation and equilibrium of stars. Also, the nuclear reaction creates an outward pressure gradient and the gravitational force pulls everything to the center. This balance between gravitational forces and the pressure gradient from fusion processes determines a star's stable period, known as hydrostatic equilibrium.

Stars are not just points of light in the night sky. They are complex systems with intricate internal processes. Understanding stars involves exploring their composition, structure, and the nuclear reactions that power them, offering insights into not only their nature but also the broader mechanisms at work in the universe.

2.3 The Classification of Stellar Spectra

When we first started to observe stars with telescopes, we divided them into color classes. White, yellow, red, and deep red. This was later refined, and each color was broken up into letters, A to D for white, E to L for yellow, M and N for red. Later, it was realized that things made more sense if stars were categorized by surface temperature, but this letter system was retained. So, from hottest at around 25,000 K to coolest at around 3,500 K, we now have O, B, A, F, G, K, and M stars, a classification system called the Harvard system. This sequence of letters is rather unintuitive, but to remember the order, we can use the following mnemonic: Oh, be a fine girl, kiss me! [15]

Astrophysics had a major breakthrough with the invention of photometry and spectroscopy. In 1817, Joseph Fraunhofer concluded that not all stars have the same spectra. Harvard professors, Edward C. Pickering and his assistant Williamina P. Fleming in the 1890s labeled spectra of stars with capital letters. They did that based on the strength of hydrogen absorption lines in spectra of

stars. They started with the letter A for the lines that were the broadest. Then, in 1901, Annie Jump Cannon (figure 3) rearranged the sequence of spectra. She placed O and B before A. The way she classified the stars goes: O, B, A, F, G, K and M stars and this is the way that we even today classify the stars. Stars at the start of this sequence are known as early-type stars, while those near the end are called late-type stars. Sun is G-2 type star.



Figure 3: Annie Jump Cannon (1863–1941)[16].

She classified some 200,000 spectra between 1911 and 1914. These results were compiled into the Henry Draper Catalogue, and today, a lot of stars are identified to by their HD numbers. For example, Betelgeuse is HD 39801.

Spectroscopy is the field of study that measures and interprets electromagnetic spectra. The underlying premise of spectroscopy is that light is made of different wavelengths and that each wavelength corresponds to a different frequency. The importance of spectroscopy is centered on the fact that every element in the periodic table has a unique light spectrum described by the frequencies of light it emits and absorbed. That can be explained with the Bohr model and more precisely by quantum physics.

Bohr model was the first successful model of the atom. The atom has an electrons in its orbit. These electrons are at discrete energy levels. That means that the electron in an atom can not be at any radius from its nucleus because that would mean that it can have any energy. Electrons move in fixed circular orbits

around the nucleus without radiating energy, contrary to classical electromagnetic theory which suggests that a charged particle in motion emits radiation. These orbits, or "stationary states," have quantized angular momenta, meaning that the angular momentum of an electron in orbit is an integer multiple of the reduced Planck constant \hbar .

$$L = n\hbar = n\frac{h}{2\pi} \quad (1)$$

where L is the angular momentum, n is the principal quantum number, h is Planck's constant, and \hbar is the reduced Planck constant.

The energy associated with each orbit is also quantized, and electrons can only gain or lose energy by jumping from one allowed orbit to another, emitting or absorbing a photon with energy equal to the difference between these orbits.

$$E_n = -\frac{Z^2 e^4}{8\epsilon_0^2 h^2 n^2} \quad (2)$$

where E_n is the energy of the n -th orbit, Z is the atomic number, e is the electron charge, and ϵ_0 is the permittivity of free space.

When an electron jumps between orbits with different energies, it emits or absorbs a photon with energy equal to the energy difference between these orbits:

$$\Delta E = E_i - E_f = h\nu \quad (3)$$

where E_i and E_f are the initial and final energy states, and ν is the frequency of the photon being emitted or absorbed. This forms the basis for spectroscopy.

Photons created in stars core are exiting star through its photosphere. If the energy of the photon is equal to the energy required for an electron to make an upward transition from a lower to a higher orbital, atom absorbs it. This is how absorption lines are created. For example, the Lyman absorption lines of hydrogen are caused by electrons making upward transitions from the $n = 1$ orbital to higher-energy orbitals.

The hotter the star, the more hydrogen and helium nuclei that have been stripped of their electrons, forming the phase of matter known as plasma. Figure 4 shows that the hottest stars, O stars, show very little hydrogen because most of the hydrogen is without an electron, and thus cannot absorb and emit light. Helium is still able to retain one or both electrons, and thus we do see emission lines correlating with helium. As stars are cooler so hydrogen can hold onto an electron and the spectrum changes. Getting cooler still, some bands show up that correspond with metals, like calcium.

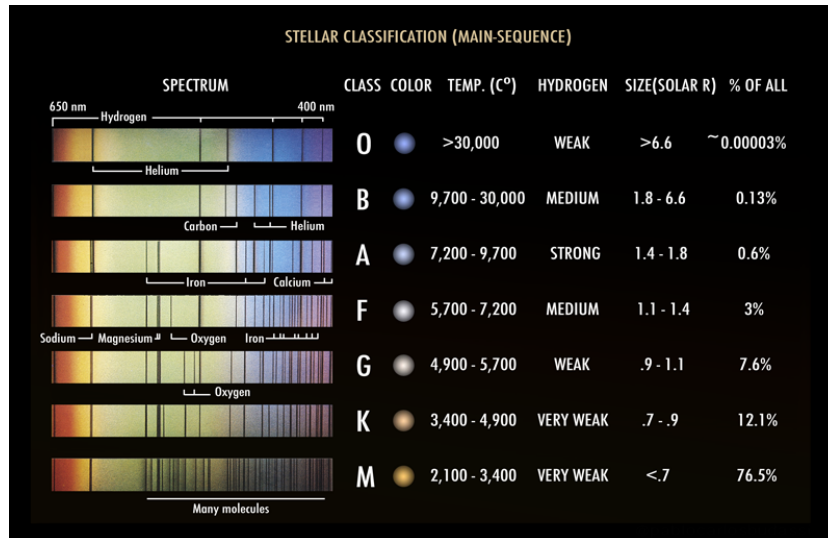


Figure 4: A simple chart for classifying the main star types using Harvard classification[15].

2.4 The Hertzsprung–Russell (H-R) diagram

Astronomers accumulated a lot of data for large samples of stars. They recognized the vast differences in absolute magnitudes and luminosities of stars. M-type stars at the end of the sequence are more dimmer and cooler than O-type stars at the beginning. They deduced that M-type stars are less massive than the O-type stars. That culminated with creation of the theory of stellar evolution that believed that stars started their lives as a O type star (hot bright and blue), and as they age, they use their fuel and became smaller and smaller and cooler over time until they become dim M star.

The theory of stellar evolution requires that the spectral type of the star and its absolute magnitude are in correlation. People did not know that back then. But, Danish amateur astronomer, Ejnar Hertzsprung, in 1905 managed to certify that by analyzing stars with precisely determined absolute magnitudes and spectral types. But, he found it to be strange that G type stars had a range of magnitudes. Hertzsprung called ones with the higher magnitude "giants". That made sense because of Stefan-Boltzmann law:

$$R = \frac{1}{T_e^2} \sqrt{\frac{L}{4\pi\sigma}} \quad (4)$$

Here:

- R : Radius of a star (often in terms of solar radii).

- T_e : Effective temperature of the star (in K).
- L : Luminosity of the star (total energy output per unit time, often in watts).
- σ : The Stefan-Boltzmann constant, which is a physical constant used in blackbody radiation calculations, approximately equal to $5.670 \times 10^{-8} \text{ W} \cdot \text{m}^{-2} \cdot \text{K}^{-4}$.

Having the same spectral type (in that case G type) means that they have the same temperature. From Stefan-Boltzmann law we see that the more luminous star must be larger.

In 1913, Russell published a diagram (Figure ??) illustrating stars' absolute magnitudes on the vertical axis (brightness increasing upward) and spectral types on the horizontal (temperature rising to the left). This early "Russell diagram" laid the groundwork for the modern Hertzsprung–Russell (H–R) diagram. It plotted over 200 stars, with most aligning along the "main sequence" from hot, bright O stars in the upper left to cool, dim M stars in the lower right. Above the main sequence lie giant and supergiant stars, with white dwarfs located below.

At Princeton University, Henry Norris Russell, independently came to the same conclusions as Hertzsprung. In 1913 Russell published the diagram shown in figure 6, illustrating star's spectral type on horizontal axis (temperature decreases to the right) and the absolute magnitude on the vertical axis (brightness decreasing downward). "Russell diagram" laid the groundwork for the modern Hertzsprung–Russell diagram.

The two parallel lines shown in 6 go diagonally from the top left side, where O-type stars (hot and luminous) reside, to the bottom right side of the diagram, where M-type stars (dim and cool) reside. In Russell's diagram shown in figure 6, we can see more than 200 stars within that region of these two parallel lines. This part of the H-R diagram is called main-sequence and stars that reside there are called main-sequence stars. It has 80% - 90% of all stars. There are a lot of different types of stars. Even though around 90% of the stars are on main-sequence, there are a lot of different interesting stars in other regions of H-R diagram. For example, white dwarfs, as their name suggests, are stars with very small radius and hence low luminosity, but they have high luminosities, which puts them below main-sequence in H-R diagram. On the other hand, there are giant stars that have higher luminosities because of their big sizes, which puts them in the region above the lower main sequence on H-R diagram.

There is one similar way to plot H-R diagram. It has temperature instead of spectral type on the x axis and luminosity instead of absolute magnitude on the y axis. It also has dashed lines to indicate lines of constant radius [17]. As it can be seen in figure 5.

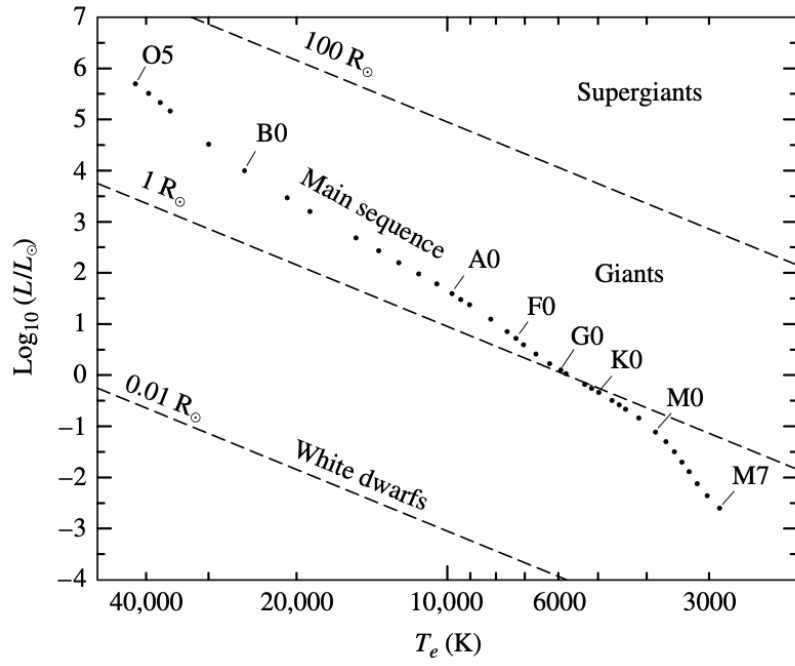


Figure 5: The theorist’s Hertzsprung–Russell diagram. The dashed lines indicate lines of constant radius[17].

The Classification of Stellar Spectra

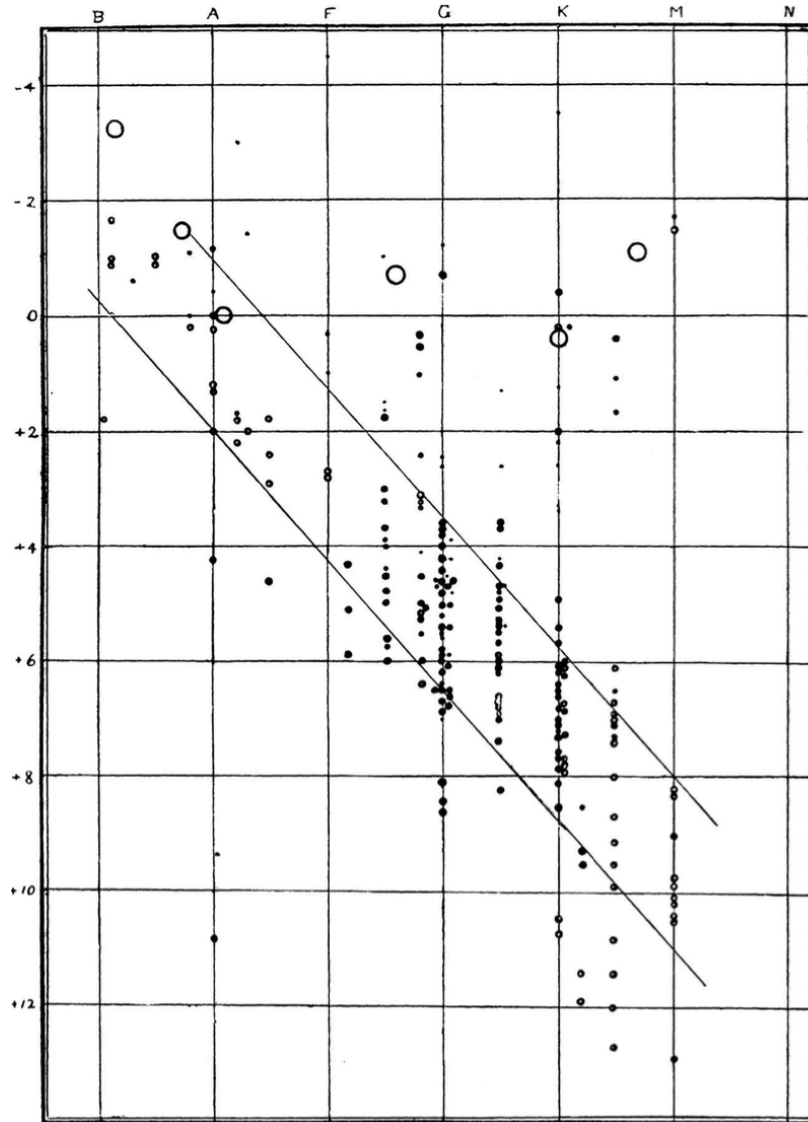


Figure 6: Henry Norris Russell's first diagram, with spectral types listed along the top and absolute magnitudes on the left-hand side. (Figure from Russell, *Nature*, 93, 252, 1914.).

3 Stellar parameters

Stellar parameters such as age, mass, temperature, luminosity, surface gravity, metallicity, and distance are fundamental in understanding the nature and evolution of stars. Each parameter provides insights into different aspects of stellar physics and is determined through a combination of observational techniques and theoretical modeling. In stellar astrophysics, various stellar parameters are interconnected, allowing astrophysicists to infer the properties and evolutionary stages of stars.

Distance

The distance to a star is crucial to derive its intrinsic properties. The history of measuring distances in the cosmos is fascinating. It all started when over 2000 years ago The Greek philosopher Eratosthenes calculated the circumference of the Earth with some simple trigonometry. He observed that at noon at the city of Syene, the Sun shined straight down, and in Alexandria it was not shining straight down, but under an angle. By calculating the angle and distance between these two cities, he calculated the circumference of the Earth. With knowing how big the Earth is we were able to calculate distance to the moon by observing Earth's shadow on it. Great thinkers like Hipparchus and Ptolemy measured distances to the Moon and the Sun with good accuracy over 1000 years before invention of the telescope. With help of Johannes Kepler and Issac Newton mathematics in the 17-th century, we got tools to calculate planetary motions and their distances.

The mapping distances of stars are more complex. For determination of stellar distances, we have 3 main methods:

- *Parallax*: The most direct method of measuring stellar distances is parallax. The parallax is the apparent shift in a star's position on the night sky as a result of Earth's orbit around the Sun [18]. We first measure stars location in the night sky and after half a year we measure it again. We know that the distance from Earth to the Sun is 1 Astronomical unit (AU) or 150 million kilometers, and with measured parallax angle of the star (that angle is shown in figure 7 written as Parallax), we can easily calculate its distance from us. When calculating the distance, the AU is a too small unit because of how large the universe is. So scientists developed a new unit called parsec, to show these large distances. One parsec is the distance we observe for a parallax angle of 1 arc second ($1/3600$ of a degree). That is around 3.26 light years. Closest star to us is at 4.2 ly or 1.3 parsec [19].

The equation to calculate the distance to a star using parallax is given by:

$$d = \frac{1}{p} \quad (5)$$

where:

- d is the distance to the star in parsecs (pc),
- p is the parallax angle in arcseconds.

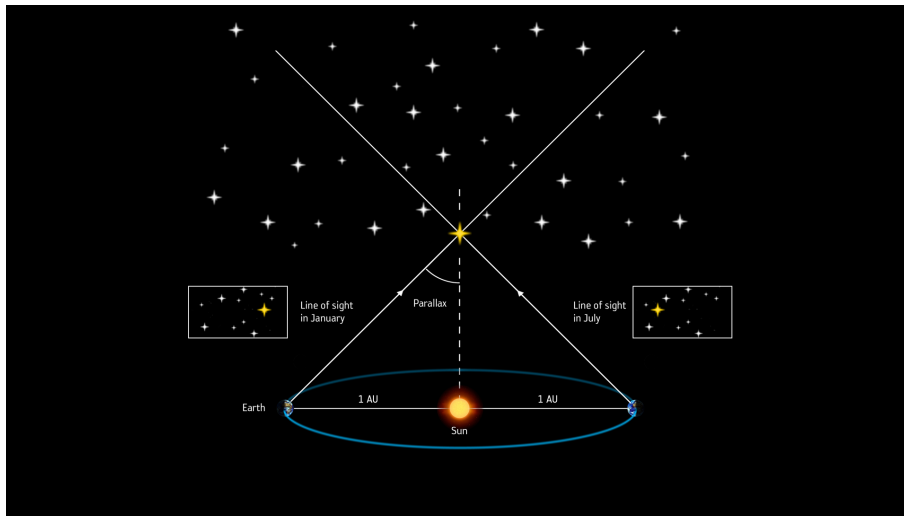


Figure 7: Illustration of measuring stars distance with the parallax (not to scale) (Image credit: ESA).

The problem with measuring parallax is that we need to measure the stars' position on a night sky twice with separation of half an year to measure parallax angle. Also, with that method we can not measure distances to the stars that are further than 1000 light years away because parallax angle becomes too small.

- *Comparison:* If we know distance of closer star and we compare it to the more distant star and determine that they have similar SEDs, then by measuring how much dimmer it is, we can calculate how much more distant it is. Similarly, we can use H-R diagram to obtain luminosity of the star for a given color. By comparing with the apparent magnitude we can determine its distance. This method is called spectroscopic parallax.
- *Standard Candles:* To measure distances far greater than 1000 ly, we need a method of standardized candels.

Harvard computers were a group of women in the early 1900s. They were looking at photos taken by telescopes and naming and classifying stars by their brightness and their type. One of those women, Henrietta Swan Leavitt, was analyzing Magellanic cloud. She deduced that all of the stars in it should be at the similar distance from the Earth. She realized that some of those stars were periodically varying their brightness, getting brighter and dimmer, and again brighter and so on. They were doing it at constant rate [20].

Such objects are stars called Cepheids and RR Lyre. Henrietta Swan Leavitt was looking at the Cepheids. She plotted them putting log of period of pulsation on x axis and magnitude on y axis. By fitting that graph she realised that brighter the star, longer its period will be (figure 8). So if we know the period of the star, we know its luminosity. Cepheids are used to measure the distance of galaxies out to about 30 Mpc. Edwin Hubble used Cepheids to determine the distances of the Andromeda galaxy and derive the Hubble law. Hubble showed that our galaxy is not all there is to a universe and that it is much bigger than the Milky Way, our Galaxy.

Another object with known luminosity is Type 1A supernovae. Supernovae occur when massive star explode at the end of its life. Because the collapse of that particular type of star always happens at the same mass, the luminosity of the explosion is always the same. From this known luminosity we can estimate the distance. Supernovae are very bright – often as bright as all the stars in a whole galaxy put together. Because they are so bright, we can see them at very great distances, up to around 10 Gpc. The disadvantage of supernovae as standard candles is that they don't hang around - you have to spot them when they go off, or shortly afterwards.

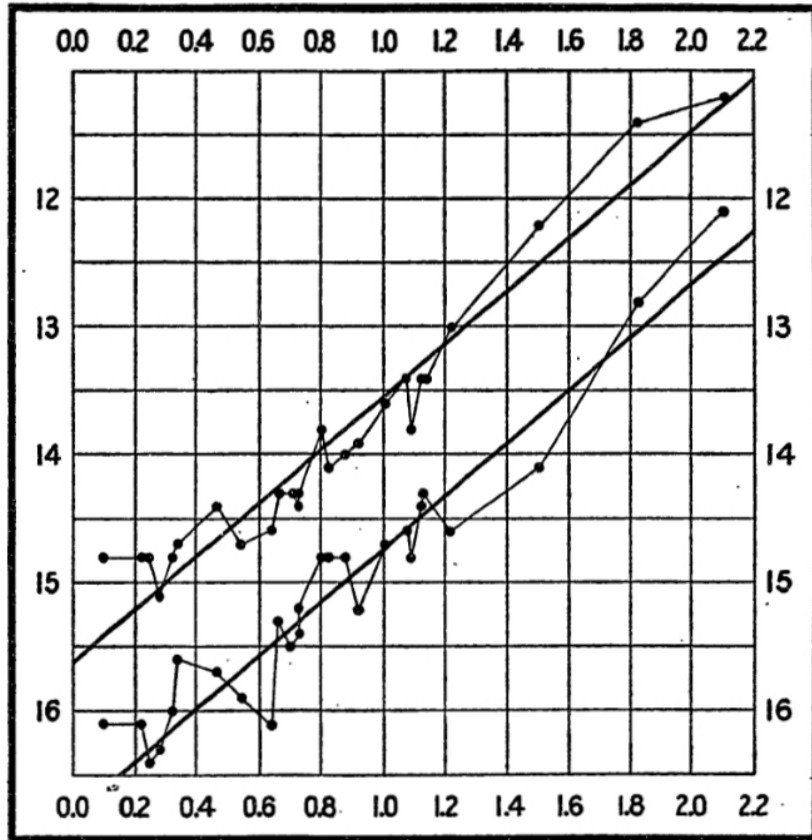


FIG. 2.

Figure 8: Plot from a paper prepared by Leavitt in 1912. The horizontal axis is the logarithm of the period of the brightness variation of the corresponding Cepheid, and the vertical axis is its magnitude. The lines drawn connect points corresponding respectively to the stars' minimum and maximum brightness [21].

Distance modulus is also important because it relates the apparent magnitude m , absolute magnitude M , and the distance d (in parsecs) of an astronomical object.

The distance modulus formula is given by:

$$M = m - 5 \log d + 5 \quad (6)$$

- M is the absolute magnitude, which is the apparent magnitude the object would have if it were 10 parsecs away from the observer.
- m is the apparent magnitude, which is how bright the object appears from Earth.

- d is the distance to the object in parsecs.

The luminosity of a star can be calculated from its absolute magnitude using the following relationship:

$$L = L_0 \times 10^{-0.4 \times (M - M_0)} \quad (7)$$

where:

- L is the luminosity of the star,
- L_0 is the reference luminosity corresponding to the absolute magnitude M_0 (usually the absolute magnitude of the Sun),
- M is the absolute magnitude of the star,
- M_0 is the absolute magnitude of a star with luminosity L_0 (typically $M_0 = 4.83$ for the Sun).

This formula shows how the luminosity of a star increases as its absolute magnitude becomes smaller. It allows astronomers to infer a star's true power output from its observed brightness at a standard distance [22].

Temperature

The surface temperature of a star determines its spectral class. It is important because it determines how the star radiates. When we talk about temperature, almost always we are talking about surface temperature.

Temperature can be determined by:

- *Spectral Fitting*: By fitting observed spectra with theoretical spectra, the effective temperature can be derived from SED.
- *Color Indices*: Temperature can also be estimated from color indices in photometry. That is, by using color-temperature calibration.
- *Spectral classification system*: Spectral classification system categorizes stars based on the absorption lines visible in their spectra. These lines correlate with surface temperature, which dictates the stars color and position in the H-R diagram.

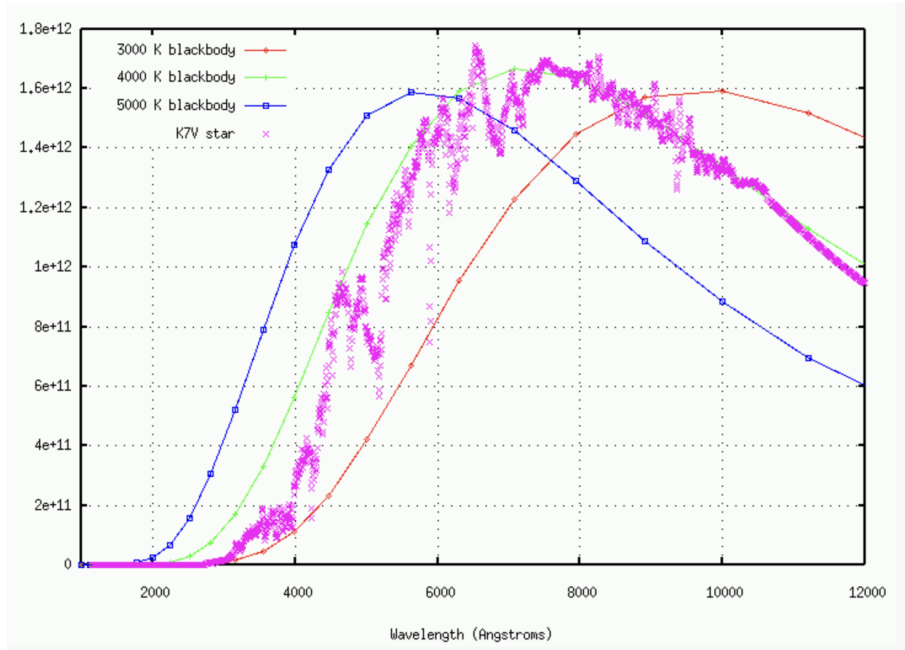


Figure 9: Process of fitting spectrum of a cool star K7V to different blackbody radiations.

Luminosity

Luminosity, denoted as L , is a fundamental characteristic of a star, representing the total amount of energy radiated by the star in all directions per second. Luminosity is expressed in watts (W).

The relationship between luminosity, the radius of the star, and its surface temperature is given by the Stefan-Boltzmann law⁸, if we approximate stellar surface with blackbody, as the stellar atmosphere can be considered to be in local thermodynamic equilibrium.

$$L = 4\pi R^2 \sigma T^4 \quad (8)$$

where:

- σ is the Stefan-Boltzmann constant ($5.67 \times 10^{-8} \text{ W m}^{-2}\text{K}^{-4}$).
- R is the radius of the star.
- T is the temperature of the star, assumed to be a perfect black body.

Determination:

- *Distance and Apparent Brightness:* Knowing the distance to a star and its apparent brightness allows for the determination of its luminosity using the inverse-square law.

- *Bolometric Corrections:* Applying corrections for radiation not observed directly (outside the optical range) to derive the total luminosity from observed magnitudes.

One of the most fundamental relationships in stellar physics is between star's mass and its luminosity. The mass-luminosity relationship is particularly evident in main-sequence stars and can be expressed by the equation:

$$L \propto M^\alpha \tag{9}$$

where α varies typically between 3 and 4 for most main-sequence stars, depending on the mass range considered [23].

Surface Gravity

The surface gravity may be thought of as the acceleration due to gravity experienced by a hypothetical test particle which is very close to the object's surface. Surface gravity affects the pressure broadening of absorption lines in a star's spectrum. Broader lines suggests higher gravity due to greater pressure in the star's atmosphere.

Surface gravity (g) is directly influenced by the mass and radius of the star:

$$g = \frac{GM}{R^2} \tag{10}$$

where G is the gravitational constant. This equation shows that surface gravity is proportional to mass and inversely proportional to the square of the radius [24].

Metallicity

Metallicity measures the abundance of elements heavier than hydrogen and helium in a star. It gives us information about a star's formation and evolutionary history.

The strength of metal absorption lines in a star's spectrum provides a direct measure of its metallicity.

Conclusion: Understanding these stellar parameters allows astronomers to not only classify stars but also to get valuable information on their history and future evolution. The techniques for measuring these parameters are continually refined, providing ever more precise data that goes into models of stellar evolution and galactic dynamics.

4 Stellar evolution [1]

The life cycle of any star, from birth to death, and all the stages in between, will span millions or even billions of years. This is why stars do not seem to change at all, because a human lifetime is too small in comparison.

Space between stars is not empty. It includes interstellar molecular clouds (within interstellar medium or ISM for short). They get large and dense enough to permit the formation of molecules (most commonly molecular hydrogen, H_2), and the formation of H II regions as well as formation of very cold gas and dust. They are very important because stars are being created there. The process starts when some of those clumps reach a critical mass, allowing them to collapse under their own gravity.

The ISM from which the stars are formed is reprocessed in the interiors of stars through nuclear reactions. The ISM is enriched with heavier elements formed in the interiors of stars. The next generation of stars formed from such enriched interstellar material have a higher abundance of heavier elements and higher metallicity, which creates differences in the chemical composition of stars.

The path that will be followed in the evolution of stars depends mainly on its mass, or how much ISM was collected and collapsed to form the star, because that material will serve as the star's fuel. That will define the energy output of the star over time, ultimately determining its final destiny, whether it will become a white dwarf, neutron star or a black hole.

4.1 The Kelvin-Helmholtz timescale

Young stars before the main sequence are mainly influenced by gravitational potential energy. The Kelvin-Helmholtz time scale determines how quickly a pre-main sequence star contracts before nuclear fusion starts. For the Sun it is 3×10^7 years. The Kelvin-Helmholtz time scale also represents the time it would take for a star to radiate away its gravitational energy if its nuclear source were turned off.

Kelvin-Helmholtz timescale:

$$t_{\text{KH}} = \frac{\Delta E_G}{L} = \frac{3}{10} \frac{GM^2}{RL} \quad (11)$$

Where:

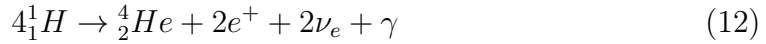
- ΔE_G is the change in gravitational potential energy.
- L is the luminosity of the star, representing the total energy output per unit time.
- G is the gravitational constant ($6.674 \times 10^{-11} \text{ m}^3\text{kg}^{-1}\text{s}^{-2}$).

- M is the mass of the star.
- R is the radius of the star.

4.2 Nuclear timescale

When nuclei of atoms collide with enough energy to overcome the electromagnetic repulsion between them (the Coulomb barrier), a strong nuclear force takes over and the nuclei fuse. That process happens in the stellar core where temperatures and pressures are sufficient. When atomic nuclei fuse, a small fraction of their mass is converted into energy, as dictated by $E = \Delta mc^2$.

A consequence of nuclear reactions in the center of the star:



In equation 12, helium nucleus (4_2He), two positrons ($2e^+$), two electron neutrinos ($2\nu_e$) and a gamma photon (γ) are produced by nuclear fusion from four hydrogen nuclei (1_1H).

Equation 12 represents the proton-proton (pp) chain reaction, which is the primary fusion process in the cores of low-mass stars, such as the Sun. For more massive stars, the CNO cycle is the dominant process. Four hydrogen nuclei do not fuse directly to form helium nuclei, as can be seen in 12. That equation just shows final sum of products at the beginning and at the end of chain of nuclear reactions leading to this.

Stellar evolution is a consequence of changes in chemical composition due to nuclear reactions and the influence of gravitational force.

$$L = \text{const.} \Rightarrow \text{constant source of energy:}$$

Time it takes for star to burn up its nuclear energy:

$$t_{\text{nuc}} = \frac{E_{\text{nuc}}}{L} \approx \frac{p \cdot 0.007 \cdot Mc^2}{L} \quad (13)$$

For the Sun:

- Kelvin-Helmholtz timescale: $t_{\text{KH}} \approx 10^7$ years
- Nuclear timescale: $t_{\text{nuc}} \approx 10^{10}$ years

We can see that t_{nuc} is much longer (around 1000 times) than t_{KH} .

Almost all stars spend most of their time on the main sequence. Approximately 80% to 90% of the stars in the vicinity of the Sun are main-sequence stars.

Later evolutionary stages occur much more rapidly.

4.3 Low-Mass Main-Sequence Evolution

The Zero Age Main Sequence (ZAMS) is the phase where stars begin their evolution with hydrogen fusion as the primary energy source.

While all main sequence stars convert hydrogen into helium and exhibit similar evolutionary patterns, they do have notable differences.

- For stars with $M > 1.2M_{\odot}$: The core is convective due to the temperature-sensitive CNO cycle.
- For stars with $0.3M_{\odot} < M < 1.2M_{\odot}$: The core is radiative, and energy is generated mainly through the proton-proton (pp) chain, which is less sensitive to temperature compared to the CNO cycle.
- For stars with $M < 0.3M_{\odot}$: The core is convective due to the high surface opacity.

M_{\odot} symbol represents the mass of the Sun.

Sun will be on the ZAMS approximately 4.57 billion years.

The luminosity, radius, and temperature of a low mass star such as Sun increase over time due to the rise in the mean molecular weight μ in the core as hydrogen is converted to helium.

$$\frac{1}{\mu_i} \approx 2X + \frac{3}{4}Y + \left\langle \frac{1+z}{A} \right\rangle_i Z \quad (14)$$

where:

- X is the mass fraction of hydrogen,
- Y is the mass fraction of helium,
- Z is the mass fraction of heavier elements (metals),
- A is the atomic mass number of an element, and
- z is the charge of the nucleus.

Because the mean molecular weight is increasing, according to the ideal gas law, the temperature and density must also increase.

That results in a core compression and therefore, the core density increases. That leads to releasing of the gravitational potential energy. That is consequence of virial theorem. Half of the energy is emitted as radiation, while the other half increases the gas's thermal energy, raising its temperature. That leads to increase in luminosity and radius of star.

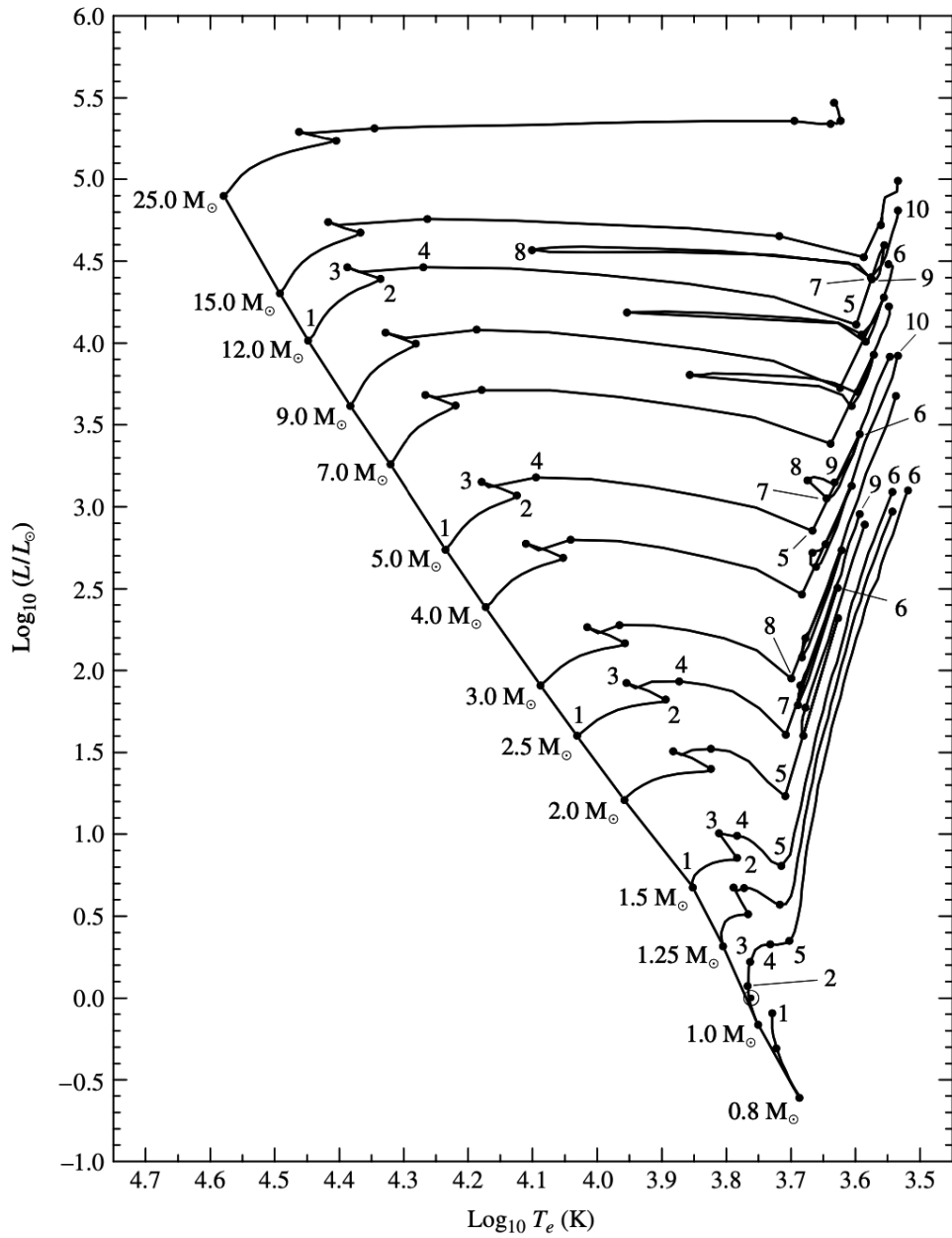


Figure 10: Main-sequence and post-main-sequence evolutionary tracks of stars with an initial composition of $X = 0.68$, $Y = 0.30$, and $Z = 0.02$ [25].

Figure 10 represents the evolutionary path for stars from $0.8M_{\odot}$ to $25M_{\odot}$. We can see changes in luminosity (y-axis) and temperature (x-axis) through their lives. The Sun as it is today is located between the points 1 and 2 on the $1M_{\odot}$ track.

As a star evolves, its hydrogen in core is being depleted until it runs out. That happens around 9.8 Gyr after star with $1M_{\odot}$ arrives at ZAMS (point 3).

The depletion of hydrogen in the core leads to the end of nuclear reactions. The temperature in the core is sufficiently high to initiate nuclear reactions in a thick shell surrounding a small helium core. The luminosity is almost zero in the center of the star (3% of the mass), where an inert isothermal helium core is located.

For an isothermal core to maintain hydrostatic equilibrium and support the material above it, its density must increase. The luminosity in the thick shell is higher than during the hydrogen burning phase in the core, leading to an increase in luminosity, point 3 in figure 10. Part of the energy is used for the slow expansion of the envelope, causing the effective temperature to drop, and the track shifts to the right.

4.3.1 The Schönberg–Chandrasekhar Limit

This evolutionary phase concludes when the mass of the isothermal core becomes too large, and the core can no longer support the material above it. The maximum fraction of a star’s mass that can reside in an isothermal core while still supporting the overlying layers is:

$$\left(\frac{M_{\text{ic}}}{M}\right)_{\text{SC}} \approx 0.37 \left(\frac{\mu_{\text{env}}}{\mu_{\text{ic}}}\right)^2 \quad (15)$$

Where:

- M_{ic} is the mass of the isothermal core.
- M is the total mass of the star.
- μ_{ic} is the mean molecular weight of the isothermal helium core.
- μ_{env} is the mean molecular weight of the envelope surrounding the helium core.

That equation was created by Schönberg and Chandrasekhar in 1942. The Schönberg–Chandrasekhar limit is another direct consequence of the virial theorem.

The largest portion of the star’s mass that can be contained within the isothermal helium core depends only on the mean molecular weight of the isothermal core and the surrounding envelope.

$$\left(\frac{M_{\text{ic}}}{M}\right) > \left(\frac{M_{\text{ic}}}{M}\right)_{\text{SC}} \Rightarrow \text{CORE COLLAPSE} \quad (16)$$

Once the mass of the isothermal helium core exceeds this threshold, the core undergoes collapse on a Kelvin–Helmholtz timescale (point 4). After that, the star no longer remains on the main sequence, which indicates the end of main-sequence evolution for low-mass stars.

The star can postpone the Schönberg–Chandrasekhar limit if it creates an additional pressure source in its core. This happens when the electrons in the gas begin to exhibit degeneracy. When density becomes extreme, electrons come to the lowest possible energy states. Electrons are fermions and obey the Pauli exclusion principle. As a result, electrons begin to occupy higher energy states in succession, starting with the ground state. When complete degeneracy is reached, the pressure exerted by the gas arises entirely from the nonthermal motion of the electrons, making it independent of the gas temperature.

4.4 Main-Sequence Evolution of Massive Stars

Evolution of massive stars on the main-sequence is very similar to low-mass stars. The only important difference is that massive stars in that stage have a convective core. Their cores mix material making the core composition homogeneous. Convective zone is shrinking while the star is on main-sequence. When the mass fraction of hydrogen reaches about $X = 0.05$ in the core of a $5M_{\odot}$ star, the entire star begins to contract (point 2 in figure 10). The gravitational potential energy is released and the luminosity increases. As the radius decreases, the effective temperature must increase accordingly. This is end of main-sequence stage of life for stars with mass greater than a $1.2M_{\odot}$. For massive stars, Schönberg–Chandrasekhar limit is:

$$\left(\frac{M_{\text{ic}}}{M}\right)_{\text{SC}} \approx 0.54 \left(\frac{\mu_{\text{env}}}{\mu_{\text{ic}}}\right)^2 \quad (17)$$

4.5 Late stages of stellar evolution

This section is very important as we are studying stars in the late stages of evolution.

The star ends its journey on a main-sequence after series of complex evolutionary phases. Nuclear burning is turning on and off in the core and shell around it. The star’s structure changes by contracting and expanding the core and shell. Significant loss of the mass takes place at the end of the main-sequence.

In the stars with small masses at around $1M_{\odot}$, the core contracts, which leads to an increase in temperature, and therefore in luminosity. The envelope expands slightly, and the effective temperature decreases.

In the massive stars with masses around $5M_{\odot}$, the entire star rapidly contracts, releasing gravitational energy. Its luminosity increases, radius decreases, and effective temperature increases. After that, the temperature in the shell becomes sufficient for fusion (point 3 in figure 10). Burning of the hydrogen shell leads to expansion of the envelope. Part of that energy is being absorbed, so luminosity decreases and the effective temperature drops. After the whole core becomes helium, the temperature outside the helium core rises enough to trigger the combustion of a thick hydrogen shell.

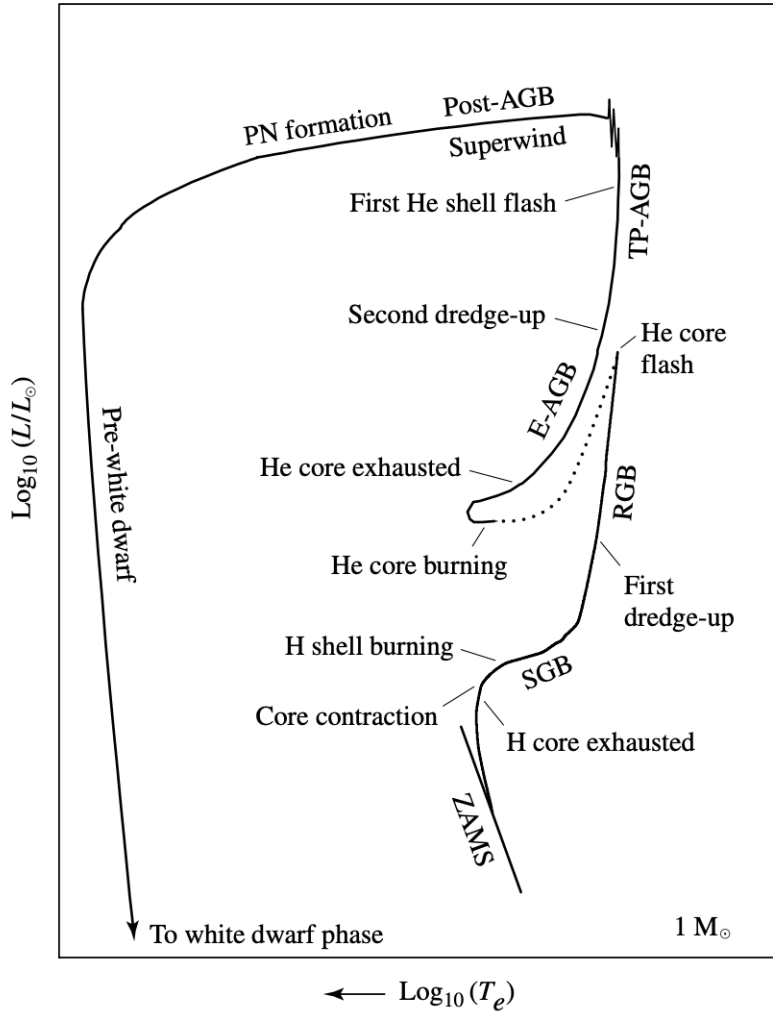


Figure 11: A schematic diagram of the evolution of a low-mass star of $1M_{\odot}$ from the zero-age main sequence to the formation of a white dwarf star. The dotted phase of evolution represents rapid evolution following the helium core flash. The diagram is labeled according to figure 10. Figure was taken from [1].

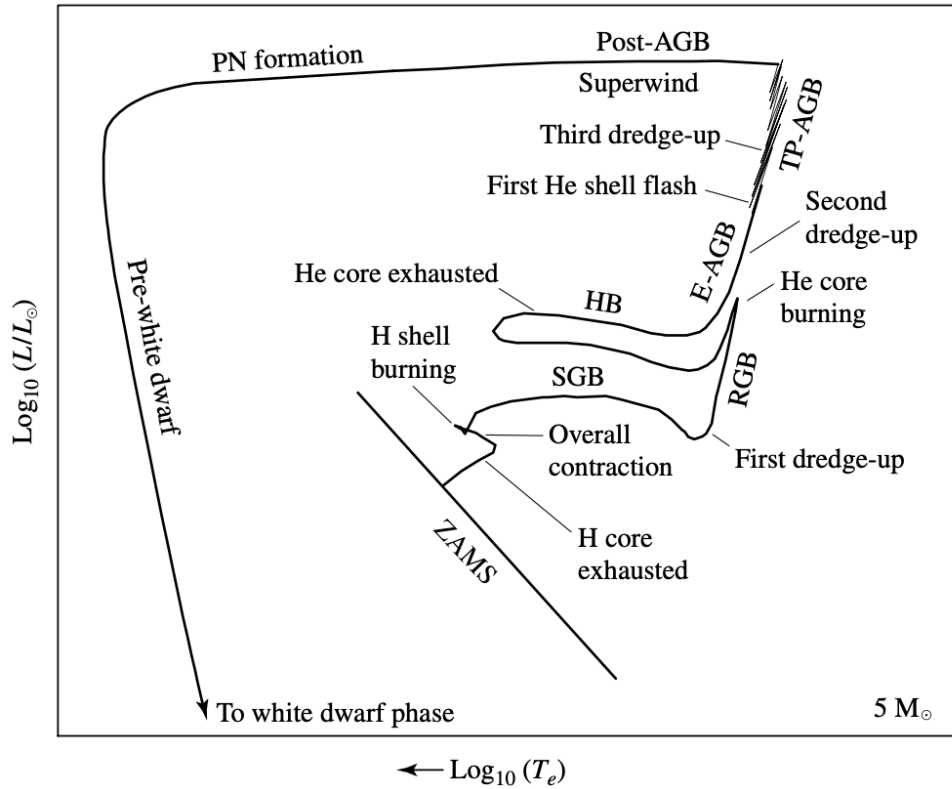


Figure 12: A schematic diagram of the evolution of an intermediate-mass star of $5M_{\odot}$ from the zero-age main sequence to the formation of a white dwarf star. The diagram is labeled according to figure 10 with the addition of the Horizontal Branch (HB). Figure was taken from [1].

4.6 The Subgiant Branch (SGB)

In stars with low and intermediate masses, as the hydrogen shell at the base of the star's envelope continues to burn, the mass of the helium core increases in a steady rate, until it becomes nearly isothermal. At that point, the Schönberg–Chandrasekhar limit is reached, which makes core to become unstable and it begins rapidly contract. In figure 10 we see that in point 4. The gravitational energy that was released by the rapidly contracting core causes the star's envelope to expand, resulting in a decrease in the effective temperature. Contraction of the core, which is no longer isothermal, leads to an increase in the temperature and density of the shell, which in turn increases the energy production rate in the shell, causing the envelope to expand and cool, which absorbs part of the released energy. Expanding envelope absorbs enough energy released in the shell to reduce luminosity and increase effective temperature for stars with mass of $5M_{\odot}$. In figure 10 we see that in point 5.

4.7 The Red Giant Branch (RGB)

The expansion of the envelope and the decrease in effective temperature is why we call stars in that part of their evolution red giants. Because of the lower temperature they are red. Their size is increased dramatically, which explains "giants" in their name. They are also much brighter (higher luminosity). Decrease of the effective temperature leads to an increase in photospheric opacity due to formation of H^{-} ions, resulting in the formation of a convective zone near the surface. The convective zone becomes deep, with high efficiency in energy transfer, which causes such high luminosity. The convective zone is so deep that it extends to the nuclear burning zone. Transport of material from the interior to the surface starts to happen, so called first dredge-up. At the RGB tip, temperature and density have become high enough to allow triple alpha process to start:



New source of energy (burning of helium) is very sensitive to temperature. The hydrogen shell is pushed toward the surface. Hydrogen burning is the dominant energy source. The shell cools and energy production decreases, resulting in a rapid drop in luminosity. The envelope contracts, and the effective temperature rises.

4.8 The Helium Core Flash

Stars with masses smaller than $1.8 M_{\odot}$ behave differently from more massive stars. They go through something called helium core flash. The helium core collapses on the tip of the red giant branch, leading to strong degeneracy. Neutrinos carry away energy, causing the core to cool. The core becomes cooler than its surroundings.

Helium ignites in the shell around the core, but the entire core quickly becomes involved with a triple-alpha process. That leads to the helium core flash. The ignition is sudden and explosive. The released energy is of the same order as the energy of an entire galaxy:

$$L \sim 10^{11} L_{\text{Sun}}$$

The energy released is absorbed in the outer layers. Initially, it is used to eliminate electron degeneracy in the core, and then it contributes to the kinetic energy and expansion of the core, leading to a decrease in the temperature and density of the core and slowing down nuclear reactions. The evolution of low-mass stars "jumps" until the stable helium core burning and hydrogen shell burning begin because we can not calculate what happens in between due to extremely rapid changes in the interior of the star.

4.9 The Horizontal Branch (HB)

After the tip of the red giant branch, the contraction of the envelope and compression of the hydrogen shell lead to an increase in temperature and the rate of energy release in the hydrogen shell. This results in an increase in the released energy and an increase in the effective temperature, causing the formation of a deep convective zone in the envelope and the convective core.

Helium burning is analogous to hydrogen burning on the main-sequence but has a much shorter duration, resulting in the horizontal evolution, towards blue color on H-R diagram.

For star with $5 M_{\odot}$, an increase in the mean molecular weight of the core leads to core contraction, followed by expansion and cooling of the envelope. In figure 10 we see that in point 8. Helium exhaustion in the core causes the carbon-oxygen core to contract, and the star moves horizontally to the red on the HR diagram, analogous to the SGB phase. The duration of the HB phase is short. Contraction of the core and an increase in temperature lead to the formation of a thick layer around the inert CO core where helium burns. The layer thins and compresses, increasing energy production. The upper layers expand and cool, temporarily shutting down the hydrogen shell. Neutrinos cool the core, causing

strong degeneracy in the CO core due to the increase in density and the decrease in temperature of the core.

4.10 The Early Asymptotic Giant Branch (AGB)

It is similar to the hydrogen exhaustion phase. The AGB phase and helium shell burning are analogous to the RGB phase and hydrogen shell burning. A rapid increase in luminosity leads to the star's ascent along the Asymptotic Giant Branch. The dominant burning occurs in the helium shell. The envelope that is expanding, absorbs most of the released energy, causing the radius to increase and the effective temperature to decrease, leading to the development of a deep convective envelope. Convection reaches the zone between the outer hydrogen layers and the helium region above the helium shell, resulting in the second dredge-up. That leads to an increase in the helium and nitrogen content in the envelope.

The inactive hydrogen shell ignites and dominates. The helium shell is very thin, it ignites and extinguishes periodically which leads to periodic helium flashes. This occurs because the hydrogen-burning shell is dumping helium ash onto the helium layer below.

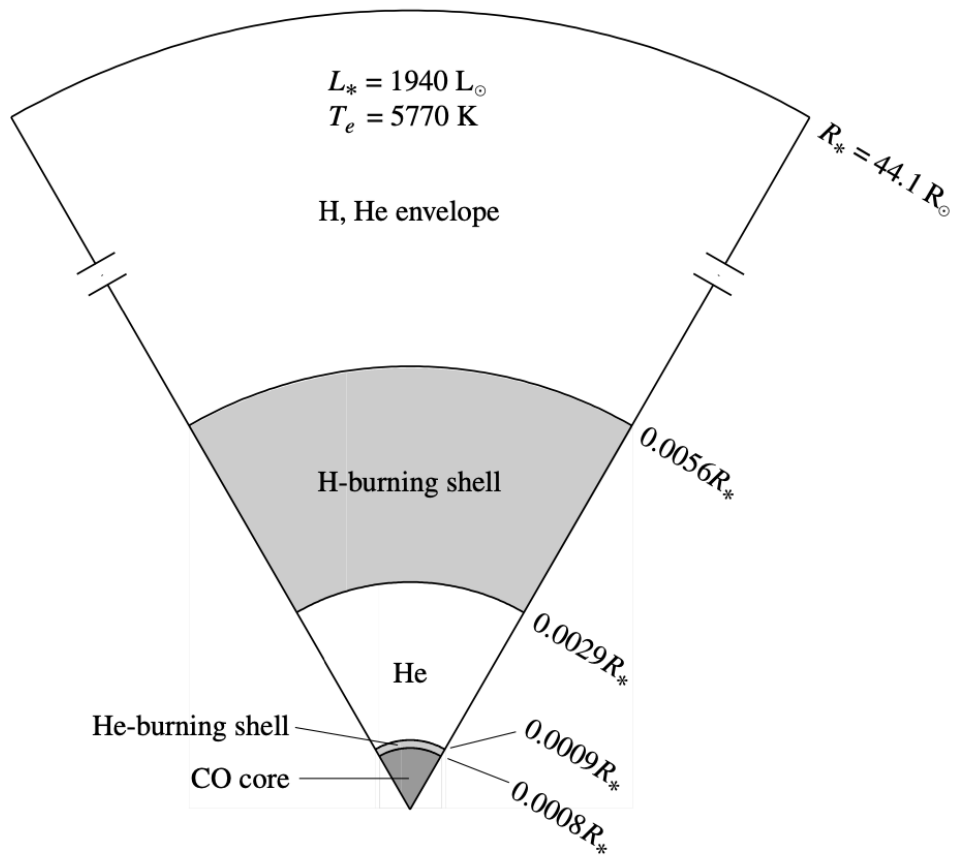


Figure 13: A $5 M_{\odot}$ star on the early asymptotic giant branch with a carbon–oxygen core and hydrogen- and helium-burning shells. Figure was taken from [26].

4.11 Death of the star

AGB stars lose mass very rapidly. The further evolution of AGB stars depends exclusively on initial mass and mass loss.

At the end of the life, massive stars, $M > 8M_{\odot}$, have their cores collapsed under the force of gravity, resulting in a supernova explosion.

At the end of their life, low-mass star, $M < 8M_{\odot}$, shed their outer layers, forming a planetary nebula while leaving behind a dense remnant called a white dwarf. These white dwarfs cool and fade over billions of years. That happens because, the helium shell produces more carbon and oxygen, increasing the mass of the CO core in AGB star. The central density becomes high enough for the formation of electron degeneracy. These stars do not have enough mass to beat electron degeneracy.

Mass loss plays a significant role in preventing core collapse. If mass loss is significant enough, additional burning and nucleosynthesis can take place in the core before its collapse, resulting in the formation of an ONeMg (Oxygen-Neon-Magnesium) core.

The maximum possible mass for a completely degenerate core is $1.4M_{\odot}$, known as the Chandrasekhar limit. That is also the maximum mass of the white dwarf.

If the core is between $1.4M_{\odot}$ and $3M_{\odot}$, gravity will be too strong and the core will collapse creating a supernova, that finally creates the neutron star.

If the mass of the core is greater than $3M_{\odot}$, gravity will be so strong that it will surpass even neutron degeneration and the core will collapse in a black hole.

5 Globular Clusters

A globular cluster is a spheroidal conglomeration of stars that is bound together by gravity, with a higher concentration of stars towards its center. They are associated with all types of galaxies. Traditionally, it was thought that globular clusters were formed by the collapse of the giant molecular clouds. More recent studies show that their formation is complex and differs significantly between very old and young globular clusters. Old globular clusters are formed at the same time as the galaxy, which is considered "in situ" formation assisted by the dark matter halo formation, followed by the mass growth. A large fraction of globular clusters are formed "ex situ", which is outside of the galaxy and accreted. Many globular clusters are accreted remnants of the dwarf galaxies. Globular clusters are very interesting to study because every member of a given cluster formed from the same region, with essentially identical compositions, and within a relatively short period of time, which is ideal for studying star formation and evolution. They are very densely packed, so it is very challenging to observe individual stars and obtain their photometry, within globular clusters. A special technique was developed to measure photometry called crowded field photometry. The Vogt-Russell theorem indicates that the differences in evolutionary states among the stars in a cluster are attributed entirely to their initial masses [27].

Globular clusters are stable because of their strong gravitational attraction, which allows them to live very long, even billions of years. They have tens of thousands to millions of stars. In the Milky Way, they are found in the halo and the bulge. Globular clusters are similar in form to dwarf spheroidal galaxies, and the distinction between the two is not always clear.

Before the invention of the telescope, people thought that clusters were stars. With the invention of the telescope in the 17th century, globular clusters appeared as fuzzy blobs. French astronomer Charles Messier included many of them in his catalog of astronomical objects, so today many clusters are named after him. In the 18th century, astronomers recognized that globular clusters are groups of many individual stars. One of the first evidence that the Sun is far from the center of the Milky Way was provided at the beginning of the 20th century by studying the distribution of globular clusters in the sky [1].

5.1 Spectroscopic Parallax

Without knowing the exact distances to the globular clusters and the absolute magnitude of each star, we can still create H-R diagrams. Although clusters are huge, they are small in comparison with their distance from Earth. For that reason, we can assume that all star members of the cluster are at the same distance from Earth. So, we can use the apparent magnitude instead of the absolute magnitude in

H-R diagram. This essentially involves shifting the position of each star vertically by the same amount on the diagram. By aligning the observed main sequence of the cluster with a main sequence calibrated in absolute magnitude, the distance of the cluster can be determined, which in turn reveals the distance of the cluster from the observer. This method of measuring the distance to the globular clusters is called spectroscopic parallax, or main-sequence fitting. That reminds me of my favourite movie, *Interstellar*.

5.2 Messier 92

Messier 92 (also known as M92, or NGC 6341) is a globular cluster of stars in the northern constellation of Hercules.

It was discovered by Johann Elert Bode on December 27, 1777. It was rediscovered by Charles Messier on March 18, 1781, and added as the 92nd entry in his catalog. William Herschel first resolved individual stars in 1783.

It is located on the northern hemisphere, where it is one of the brighter of its sort with apparent magnitude 6.3[28]. When the viewing conditions are good, it can be seen with the naked eye.

It is also one of the oldest clusters in the Milky Way galaxy. It is located 10 kpc from the galactic center and 8.2 kpc away from the Earth [29]. Its metallicity is $[\text{Fe}/\text{H}] = 0.0051$ [30]. Its age is estimated to be between 11 and 13 Gyr old [31].



Figure 14: NASA/ESA Hubble Space Telescope image of the M92.

This Hubble image of Messier 92 core is a composite made using observations at visible and infrared wavelengths. M92 contains roughly 330,000 stars in total, it is very tightly packed with stars. The predominant elements within M92 are hydrogen and helium, with only traces of others, so it belongs to a group of metal-poor clusters, in accordance with its old age.

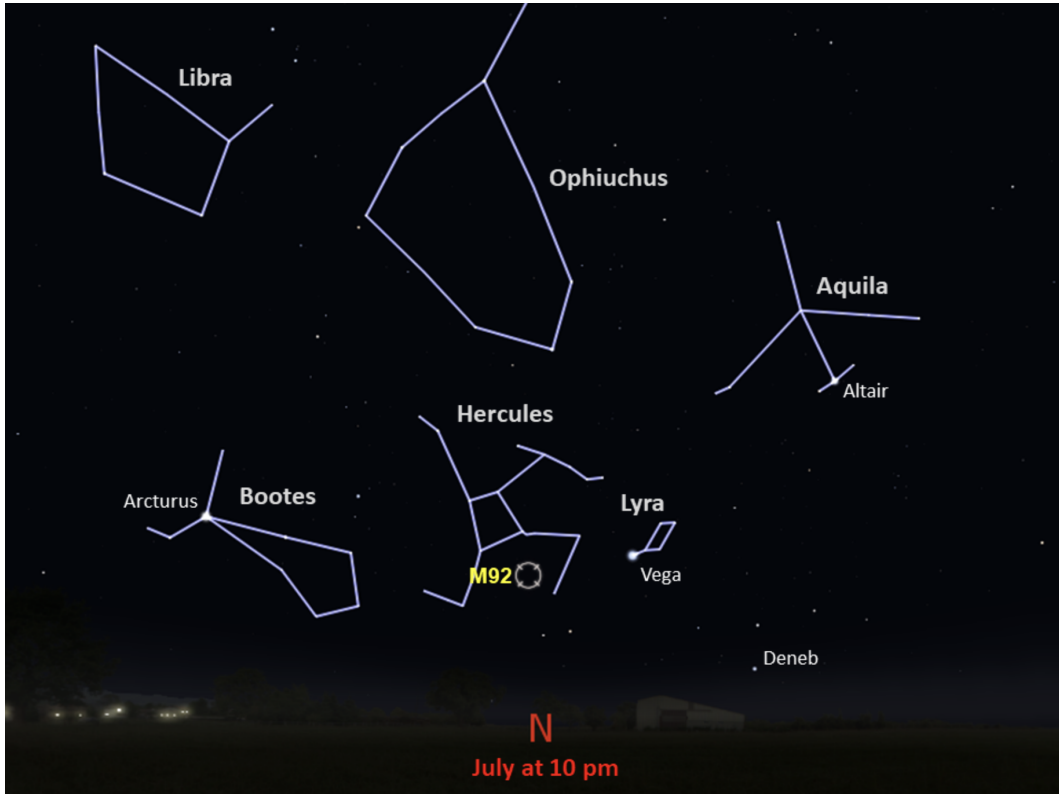


Figure 15: This star chart for M92 represents the view from mid-southern latitudes for the given month and time. Source: NASA

5.3 Messier 13

Messier 13 or M13 (also known as NGC 6205), is a globular cluster in the constellation of Hercules.

Messier 13 was discovered by Edmond Halley in 1714 [32], and cataloged by Charles Messier on June 1, 1764. It is located in the northern hemisphere at right ascension 16h 41m 41.6s, and declination $+36^{\circ}27.7'$ [33]. Its apparent magnitude is 5.8 [33]. Messier 13 is often described by astronomers as one of the most magnificent globular clusters.

M13 is about 145 light-years in diameter. It consists of several hundred thousand stars, with estimates varying from around 300,000 to over half a million. M13 has parallax 0.127 mas which is equal to a distance of 7.87 kpc away from Earth [34]. Its radial velocity is -244.4 km/s [35]. M13 metallicity is 0.033 [36]. Its estimated age is 11.65 Gyr [37]. Also, M13 visual extinction is $A_v = 0.012$ and ratio of total to selective extinction $R_v = 3.1$ [38].

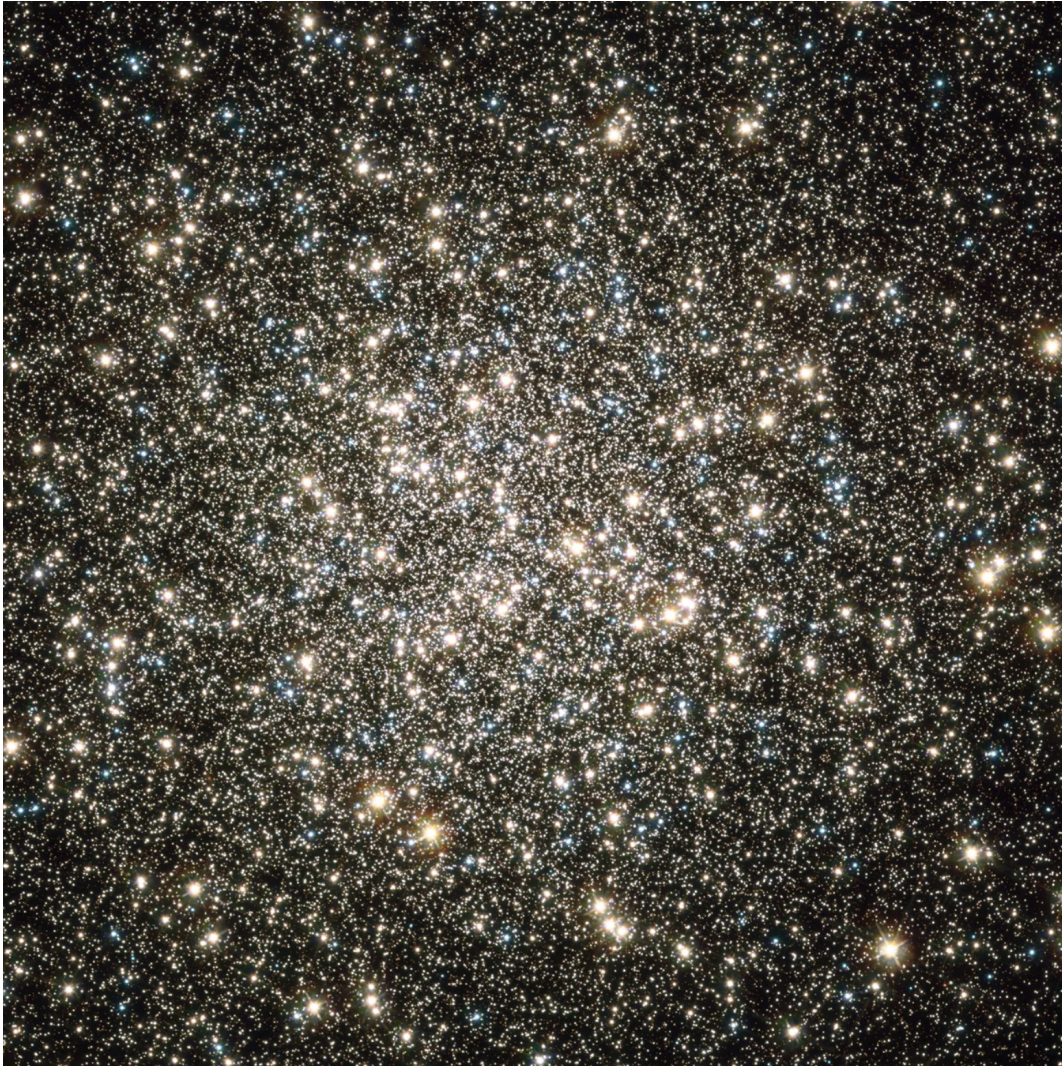


Figure 16: NASA/ESA Hubble Space Telescope image of the M13.



Figure 17: This star chart for M13 represents the view from mid-northern latitudes for the given month and time. Source:NASA.

5.4 NGC 6791

NGC 6791 is an open star cluster in the Lyra constellation.

It was discovered by Friedrich August Theodor Winnecke in 1853. It is one of the oldest and most metal-rich clusters in the Milky Way. It is located in the northern hemisphere at right ascension 19h 20m 53s, and declination $+37^{\circ}46.3'$ [39]. Its apparent magnitude is 9.5 [39]. Its distance is 4.23 kpc away from Earth [40]. NGC 6791 radial velocity is -47.75 kpc [39]. It is 8.3 Gyr old [41] and has metallicity of 0.0258 [42].

Also, NGC 6791 has visual extinction of $A_v = 0.7$ and its ratio of total to selective extinction $R_v = 3.1$ [41].

In March 2009 NASA launched the Kepler Mission spacecraft. In April 2009 the project released the first light images from the spacecraft and NGC 6791 was one of two objects highlighted on figure 18.

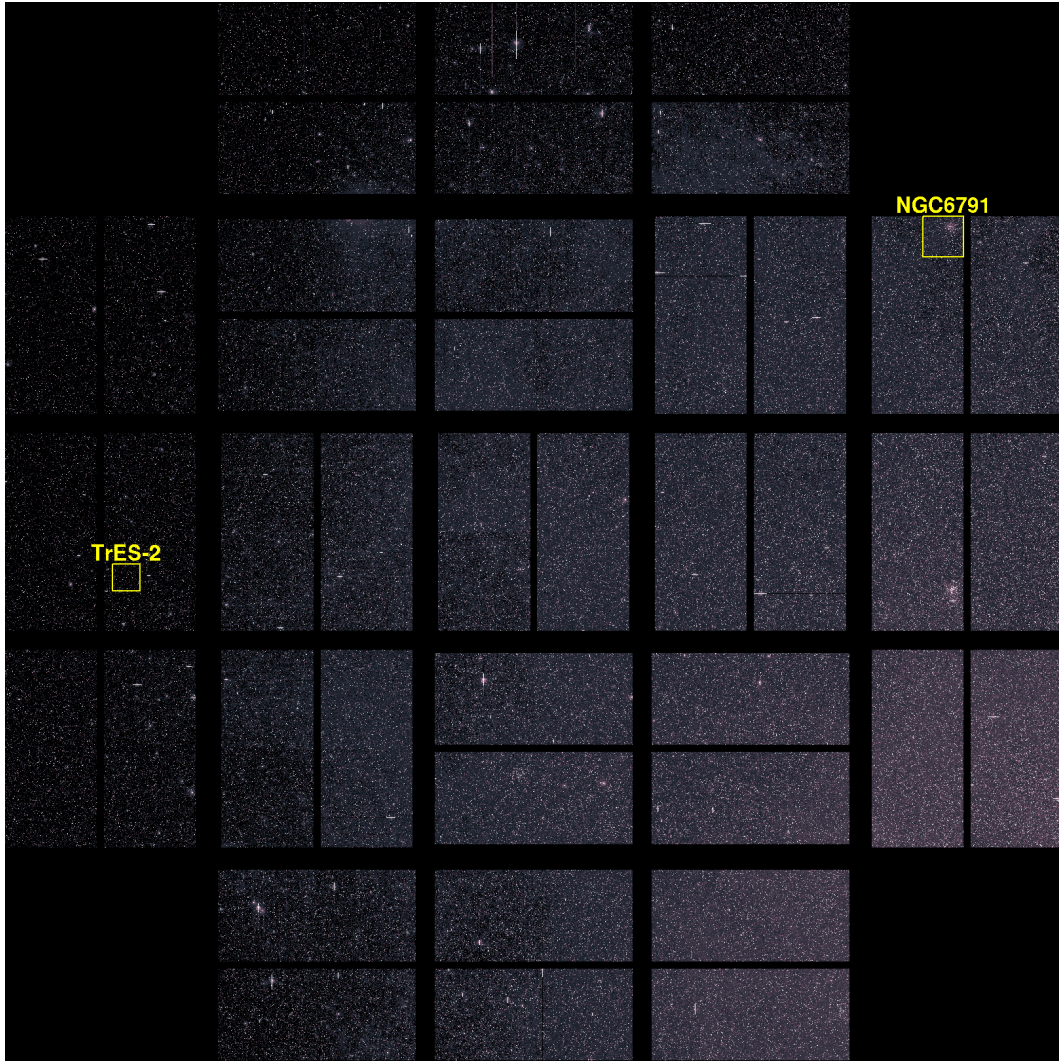


Figure 18: An image from Kepler with NGC 6791 and another point of interest outlined. Celestial north is to the left. Source: NASA.

6 Bayesian Inference

6.1 History

Throughout history, there have been many ways to deal with probabilities. Historically, the most important one is the frequentist approach. In the 18th century, the British mathematician Reverend Thomas Bayes (1702–1761) wrote a manuscript on how to combine an initial belief with new data to arrive at an improved belief, which was later called Bayesian statistics. The mathematician who popularized Bayesian methodology was Pierre-Simon Laplace. He rediscovered and greatly clarified Bayes' principle back in 1774. He applied the principle to a variety of contemporary problems in astronomy, physics, population statistics, and even jurisprudence. One of the most famous results is his estimate of the mass of Saturn and its uncertainty, which remain consistent with the best measurements of today.

Despite that, Bayes' statistic did not stick around, but frequentist did. The reason is probably because computations in Bayes' statistics require a lot of computing of complex math problems, so today with development of computer, Bayes' statistics made comeback.

The core of methodology we used in this work is Bayesian statistics, a statistical technique that updates the probability estimate for a hypothesis as more evidence or information becomes available. The Bayesian method extends the concept of the data likelihood function by adding prior information to the analysis and assigning probability density functions (PDFs) to all model parameters and models themselves [3].

6.2 Understanding Bayes' Rule

Bayes theorem gives a mathematical rule for inverting conditional probabilities, allowing us to find the probability of a cause given its effect. It updates prior belief with new information, making us more informed, giving us posterior probability. Mathematically, the Bayes theorem is written as [43]:

$$P(\theta | D) = \frac{P(D | \theta) \cdot P(\theta)}{P(D)} \quad (19)$$

where:

- $P(\theta | D)$ is the probability of the hypothesis θ given the data D (posterior probability).
- $P(D | \theta)$ is the probability of observing the data D given that the hypothesis θ is true (likelihood).

- $P(\theta)$ is the initial probability of the hypothesis before seeing the data (prior probability).
- $P(D)$ is the probability of the data under all possible hypotheses (evidence).

The formulation of the data likelihood is very important. If we do not make good likelihood function that describes the process, then the resulting posterior PDF will be inaccurate, too.

The posterior PDF is determined using the Bayes theorem. In practice, this step can be computationally intensive for complex multidimensional problems.

In search of the parameter θ , we need to find θ that maximizes the likelihood function. That will give us best (maximum) posterior.

6.2.1 Example: Medical Diagnosis

Consider a scenario where a doctor is determining the likelihood of a patient having a disease based on a diagnostic test. Suppose:

- The disease affects 1% of the population, so $P(\text{Disease}) = 0.01$ (prior probability).
- The test is 99% accurate, which means:
 - $P(\text{Positive} \mid \text{Disease}) = 0.99$ (likelihood of a positive test if the patient has the disease).
 - $P(\text{Positive} \mid \text{No Disease}) = 0.01$ (likelihood of a positive test if the patient does not have the disease).

To find $P(\text{Disease} \mid \text{Positive})$, the probability that the patient has the disease given a positive test result, we first need to calculate $P(\text{Positive})$:

$$\begin{aligned}
 P(\text{Positive}) &= P(\text{Positive} \mid \text{Disease}) \cdot P(\text{Disease}) + P(\text{Positive} \mid \text{No Disease}) \cdot P(\text{No Disease}) \\
 &= 0.99 \cdot 0.01 + 0.01 \cdot 0.99 \\
 &= 0.0099 + 0.0099 \\
 &= 0.0198
 \end{aligned}$$

Now, applying Bayes' Rule:

$$P(\text{Disease} \mid \text{Positive}) = \frac{P(\text{Positive} \mid \text{Disease}) \cdot P(\text{Disease})}{P(\text{Positive})} = \frac{0.99 \cdot 0.01}{0.0198} = 0.5 \tag{20}$$

This result means that even if the test is positive, there is only a 50% chance that the patient actually has the disease, because of the low number of disease incidence in the general population.

6.3 Bayesian Priors

The prior incorporates all other knowledge or assumptions that might exist about the values of parameters before data is observed, but is not used when computing the likelihood. Prior is its assumed probability distribution before some evidence is taken into account. The prior you choose can greatly influence the outcome of a Bayesian analysis, especially when there is not much data [3].

6.3.1 Informative and Uninformative Priors [2]

Informative priors are used when it is essential to include significant information in the prior: to incorporate previously collected data, or the results of a former analysis, to include data from another source or to account for theoretical considerations. An example might be a prior distribution centered around a value given by other studies or historical data. For example, if previous measurements suggest a parameter's value with some uncertainty, we can use a Gaussian distribution as an informative prior with the mean set to the previously estimated value and the standard deviation reflecting the uncertainty.

Uninformative priors are used when not much prior information is available and when there is a premium placed on the objectivity of analysis. They have minimal influence on the posterior distribution. Examples include the uniform prior, which assigns equal probability to all possible values of a parameter within a given range, and Jeffreys' prior.

In a scenario where 1 in 10000 people die on the way to work every year, an informative prior might be a binomial distribution reflecting this incidence rate, whereas an uninformative prior might assume any incidence rate from 0 to 1 is equally likely.

6.3.2 Choosing a Prior [3]

The selection of a prior is crucial and can be based on various methodologies:

- **Empirical Priors:** Empirical Priors are derived from earlier data measurements or studies that are relevant to the current analysis. Rather than integrate out priors as in the standard approach, they are set to their most likely values. Empirical Bayes is also sometimes known as the maximum marginal likelihood. This approach is particularly useful in fields where a lot of data from studies before are available.
- **Conjugate Priors:** They are used in special combinations of priors and likelihood functions when the posterior probability has the same functional form as the prior probability. This property simplifies the calculation of the

posterior a lot, making it much easier to perform Bayesian updates as new data becomes available.

- **Objective Priors:** Objective priors represent a state of minimal information. These priors are being used when we want to maintain objectivity. Example is the Jeffreys' prior.

Understanding these different types of priors and their appropriate applications is crucial in performing proper Bayesian statistical analysis. Each prior type offers distinct advantages and is suited to different analytical situations.

6.4 Likelihood Function [3]

In Bayesian inference, the likelihood function measures how well a statistical model explains observed data by calculating the probability of seeing that data under different parameter values of the model. This function is for updating the beliefs about model parameters based on the observed data.

The likelihood function, which can be written as $P(D | \theta)$, represents the probability of the data D given the model parameters θ .

If we know the distribution from which our sample was drawn, we can compute the probability, or likelihood, of observing any given value.

For a set of independent and identically distributed observations, the likelihood function of the entire data set, is then the product of likelihoods for each particular value. We can write that as:

$$P(D | \theta) = \prod_{i=1}^n f(x_i | \theta),$$

where $f(x_i | \theta)$ is likelihood of the i -th observation x_i and θ is model parameter.

The example of computing likelihood would be the case where we are computing the heights of individuals with a normal distribution, with unknown mean μ and known variance σ^2 . Here, the likelihood of observing the data given the mean μ is:

$$P(D | \mu) = \prod_{i=1}^n \frac{1}{\sqrt{2\pi\sigma^2}} \exp\left(-\frac{(x_i - \mu)^2}{2\sigma^2}\right).$$

The likelihood can be considered both as a function of the data and as a function of the model. In practice, computing the likelihood can be computationally very hard and may require numerical methods such as Markov Chain Monte Carlo (MCMC) for integration over multiple parameters.

6.5 Probability density function (PDF) [4]

There are two main types of random variables: discrete and continuous. Discrete random variables have countable outcomes, while continuous random variables take on values across a continuum. The concept of a Probability Density Function (PDF) is used in describing the behavior of continuous random variables.

If we have histogram that is smooth curve, that is PDF. Its height at a point is not the probability of that point. Probability is equal to zero at every point. Instead, the height of the curve measures how dense is the probability at that point. So instead of looking at the individual values and their probabilities, as we do with discrete values, we need to look interval between two values.

For a continuous random variable X , the PDF $f(x)$ is a function that describes the relative likelihood for this random variable to take on a given value. The key properties of a PDF are:

- $f(x) \geq 0$ for all x (non-negativity).
- The integral of $f(x)$ over the entire space is 1. The total probability is normalized:

$$\int_{-\infty}^{\infty} f(x) dx = 1.$$

- For any two numbers a and b where $a \leq b$, the probability that X lies between a and b is given by the integral of $f(x)$ from a to b :

$$P(a \leq X \leq b) = \int_a^b f(x) dx.$$

The Bayesian method extends the concept of the data likelihood function by adding prior information to the analysis and assigning PDFs to all model parameters and models themselves.

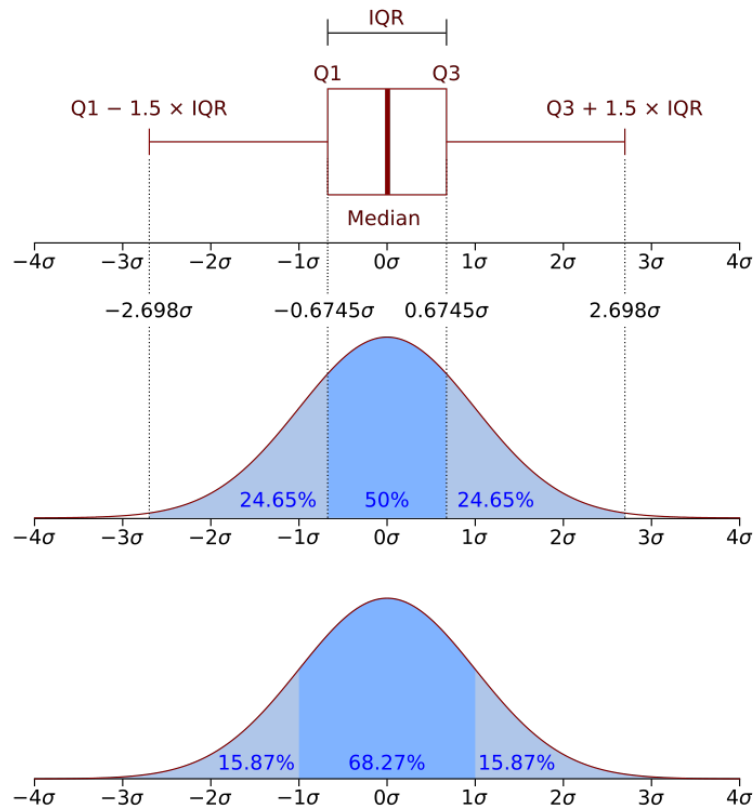


Figure 19: Box plot and probability density function of the normal distribution $N(0, \sigma^2)$. The box plot provides a summary of the distribution's quartiles and outliers, while the PDF shows the distribution's overall shape and spread (Q_1 , Q_2 and Q_3 and quantiles) [44].

7 Methods: The Bayesian Extinction and Stellar Tool [5]

The Bayesian Extinction and Stellar Tool (BEAST) is a Python package that fits the ultraviolet to near-infrared photometric SEDs of stars to extract stellar and dust extinction parameters.

It uses Bayes statistics. It models dust extinguished SED for each individual star while taking into consideration observational uncertainties common to large resolved star surveys. BEAST estimates stellar parameters using stellar evolution and atmospheric models. It also constrains the line of sight extinction with a set of photometric measurements and an observational uncertainty model. For that, it uses a newly developed mixture model that encompasses the full range of dust extinction curves seen in the Local Group. The BEAST is specifically created for use with large multi-band surveys of resolved stellar populations.

Using Bayesian statistics, BEAST gives stellar parameters for each individual star. With Bayesian statistics, BEAST uses prior knowledge for calculations which helps to handle the uncertainties associated with photometric measurements. With prior data, BEAST calculates the posterior distribution for stellar parameters taking into account uncertainties and correlations between different parameters. That approach is statistically more advanced, which helps with more complex datasets and gives better results.

7.1 Stellar Parameter Estimation [6]

BEAST calculates the probability density function for stellar parameters. They are age, mass, metallicity, distance, luminosity, surface gravity, radius and temperature. Each parameter affects the photometric SED in specific ways. Stellar evolution models provide the BEAST model grid with stellar parameters (luminosity, temperature...) as a function of age, metallicity, and stellar mass.

7.1.1 Age (t)

The age of a star affects its luminosity and spectral characteristics. BEAST uses stellar evolution models to predict the SED for different stars, for which by fitting can predict the most precise age.

7.1.2 Mass (M)

Stellar mass influences the star's evolution and luminosity. BEAST fits the observed SEDs using models that relate mass to stellar properties. Mass is derived parameter, determined from the stellar age.

7.1.3 Metallicity (Z)

Metallicity affects the color and intensity of the SED. BEAST estimates metallicity by comparing the observed SEDs with models that include different metallicity values.

7.1.4 Distance (d)

Distance affects the apparent brightness of the star. BEAST estimates the distance by fitting the observed SED and correcting for luminosity. The distance is calculated with equation:

$$m - M = 5 \log d - 5 + A_v \quad (21)$$

where m is the apparent magnitude, M is the absolute magnitude, d is the distance and A_v is visual extinction.

7.2 Fitting Technique [5]

We undertake a probabilistic approach to modeling the SED of a single star. Our data consists of N photometric measurements of a single source. Given flux measurements F_D of a star, the likelihood of observing these measurements, given our model parameters θ , is given as a multivariate Gaussian distribution:

$$P(F_D|\theta) = \frac{1}{Q(\theta)} \exp\left(-\frac{1}{2}\chi^2(\theta)\right), \quad (22)$$

where

$$Q^2(\theta) = (2\pi)^{N_{\text{det}}} |\mathbf{C}(\theta)|, \quad (23)$$

$$\chi^2(\theta) = \Delta^\top \mathbf{C}(\theta)^{-1} \Delta, \quad (24)$$

$$\Delta = F_D - F_M(\theta) + \mu(\theta). \quad (25)$$

Here, $\mathbf{C}(\theta)$ is the covariance matrix for the N photometric bands, $F_M(\theta)$ represents the predicted flux, and $\mu(\theta)$ is the crowding bias in each band. The covariance matrix $\mathbf{C}(\theta)$ is composed of three terms:

$$\mathbf{C}(\theta) = \mathbf{C}_P(\theta) + \mathbf{C}_\mu(\theta) + \mathbf{C}_C(\theta), \quad (26)$$

where $\mathbf{C}_P(\theta)$ is the diagonal covariance matrix of the photon counting uncertainties, $\mathbf{C}_\mu(\theta)$ is the covariance matrix due to crowding uncertainties, and $\mathbf{C}_C(\theta)$ is the covariance matrix giving absolute flux calibration uncertainties.

The model grid in BEAST is constructed by varying stellar parameters such as age, mass, metallicity, and extinction, which are then used to generate synthetic photometry.

7.2.1 Synthetic Photometry [6]

Synthetic photometry is a technique for comparing theoretical models with observed photometric data. The principle is to calculate the expected magnitude of an astronomical object as observed through a specific filter. This is done by integrating its SED over the filter's transmission function. We used it to calculate the magnitude from the theoretical SED and compare it with the observed magnitude.

The total flux $F_{\text{filter}}(\theta)$ observed through a filter is obtained by integrating the SED over the filter's transmission function:

$$F_{\text{filter}}(\theta) = \int_0^{\infty} F_{\lambda}(\theta)T(\lambda)\lambda d\lambda \quad (27)$$

SED of a star, denoted by $F_{\lambda}(\theta)$, represents the flux as a function of wavelength λ for a given set of parameters θ . Each photometric filter has an associated transmission function $T(\lambda)$, which describes the fraction of incident light that passes through the filter at each wavelength.

The synthetic magnitude m_{syn} is calculated by comparing the integrated flux $F_{\text{filter}}(\theta)$ to a reference flux $F_{\text{filter},0}$ through the same filter [45]:

$$m_{\text{syn}} = -2.5 \log \left(\frac{\int_0^{\infty} F_{\lambda}(\theta)T(\lambda)\lambda d\lambda}{\int_0^{\infty} F_{0,\lambda}T(\lambda)\lambda d\lambda} \right) \quad (28)$$

Here, $F_{0,\lambda}$ is the reference SED typically corresponding to a standard star such as Vega, and the denominator normalizes the observed flux.

7.2.2 Chi-Squared Statistic

The chi-squared statistic is crucial in fitting models to observational data, especially in astrophysics when dealing with photometric measurements.

In the least-squares method, we are minimizing the sum of squared differences (residuals) between the observed data points $\{x_i, y_i\}$ and the predicted values by our model (or theoretical values) $f(x_i; \theta)$, where θ represents the model parameters [46]:

$$S(\theta) = \sum_{i=1}^N (y_i - f(x_i; \theta))^2 \quad (29)$$

When observational uncertainties σ_i are present, the residuals are weighted by the inverse of the variance. We get weighted least-squares approach:

$$\chi^2(\theta) = \sum_{i=1}^N \left(\frac{y_i - f(x_i; \theta)}{\sigma_i} \right)^2 \quad (30)$$

In the context of photometric data, where we compare observed magnitudes $m_{\text{obs},i}$ with synthetic magnitudes $m_{\text{syn},i}(\theta)$ predicted by the model, the chi-squared statistic is given by:

$$\chi^2 = \sum_{i=1}^{N_{\text{filters}}} \left(\frac{m_{\text{obs},i} - m_{\text{syn},i}(\theta)}{\sigma_{m,i}} \right)^2, \quad (31)$$

with $m_{\text{obs},i}$ being the observed magnitude in the i -th filter, $m_{\text{syn},i}(\theta)$ the synthetic magnitude, and $\sigma_{m,i}$ the observational uncertainty.

This formula is used to assess how good is the fit between the observed photometric data and the model, taking into account the measurement uncertainties.

The likelihood $P((F_D)|\theta)$ is computed based on the chi-squared statistic.

7.3 Likelihood Function in BEAST

The likelihood function $P(D | \theta)$ represents the probability of observing photometric data given a model star with parameters θ .

The parameter θ includes both stellar and dust parameters, and D represents the observed photometric data.

For photometric SEDs, the likelihood function is:

$$P(D | \theta) = \prod_{i=1}^N P(D_i | \theta) = \prod_{i=1}^N \frac{1}{\sqrt{2\pi\sigma_i^2}} \exp\left(-\frac{(D_i - M_i(\theta))^2}{2\sigma_i^2}\right) \quad (32)$$

where:

- D_i represents the observed flux in the i -th photometric band,
- σ_i is the measurement uncertainty in the i -th band, and
- $M_i(\theta)$ is the model flux predicted with the stellar and dust parameters θ ,
- N is the number of photometric bands.

The same is true for photometric magnitudes, so 32 becomes 22 with corresponding chi-square statistic given in 31.

7.3.1 Prior Distributions and Posterior Sampling

Prior distributions $P(\theta)$ take into account our initial beliefs about the parameters. The choice of priors $P(\theta)$ is crucial in Bayesian analysis. In BEAST, priors are chosen based on existing knowledge of stellar populations. Common priors used in BEAST include:

- Age Prior:

The age of stars is assumed to follow a distribution based on theoretical stellar evolution models. That is uniform or logarithm if uniform distribution within a certain range.

- Metallicity Prior:

Metallicity priors are Gaussian distributions centered around typical values for the stellar population.

- Mass Prior:

Stellar masses follow an initial mass function (IMF). An example might be the Salpeter IMF, or Kroupa IMF.

- Dust Parameters Prior:

For dust parameters, priors are chosen based on typical observational constraints or theoretical models of dust grain properties.

To sample from the posterior distribution, BEAST employs Markov Chain Monte Carlo (MCMC) methods.

7.4 Dust Extinction Parameter Estimation

Not only does BEAST compute stellar parameters, it also models dust extinction. Dust extinction impacts how starlight is absorbed and scattered by interstellar dust.

7.4.1 Visual dust extinction (A_v)

Visual dust extinction A_v represents the total extinction due to interstellar dust along the line of sight. It is estimated by comparing observed and model SEDs with varying extinction values. The extinction A_v is related to the observed flux F_{obs} and the intrinsic flux F_{int} :

$$F_{\text{obs}} = F_{\text{int}} \cdot 10^{-0.4A_v} \quad (33)$$

7.4.2 Average Grain Size (R_v)

The average grain size R_v affects how dust scatters and absorbs light. It is ratio of total to selective extinction. BEAST estimates R_v by fitting extinction curves to the observed data.

7.5 Dust Extinguished Stellar Model [5]

7.5.1 Single Star Intrinsic SED

The star's intrinsic SED can be described by a combination of stellar atmosphere and stellar evolutionary models. The intrinsic SED, of a single star is described by its mass M , age t , and metallicity Z :

$$L_\lambda(M, t, Z) = 4\pi R(M, t, Z)^2 S_\lambda(T_{\text{eff}}, \log(g), Z), \quad (34)$$

where $R(M, t, Z)$ is the stellar radius, given by stellar evolution models, and $S_\lambda(T_{\text{eff}}, \log(g), Z)$ represents star's surface flux.

7.5.2 Interstellar Dust Extinction

Interstellar dust extinguishes stellar light as it travels from the star's surface to the observer. Dust extinction is modeled by a mixture of two components, A and B , describing the full range of observed extinction curves:

$$k_\lambda(R(V), f_A) = f_A \left[\frac{A(\lambda)}{A(V)} \right]_A + (1 - f_A) \left[\frac{A(\lambda)}{A(V)} \right]_B, \quad (35)$$

where f_A is the fraction of the A -type extinction and $(1 - f_A)$ is the fraction of the B -type extinction. The extinction in the V-band, $A(V)$, and the parameters $R(V)$ and f_A characterize the dust's effect on the observed SED.

7.5.3 Full SED Model

Combining intrinsic stellar SED with dust extinction, at a distance d the observed monochromatic flux $F_{\text{Mod},\lambda}$ for a star is:

$$F_{\text{Mod},\lambda}(\theta) = \frac{L_\lambda(\theta_{\text{star}}) D_\lambda(\theta_{\text{dust}})}{4\pi d^2}, \quad (36)$$

To compare with photometric observations, we need to compute model fluxes in the same bands as the observations. We calculate the model band flux in bandpass i using:

$$F_{\text{Mod},i} = \frac{\int \lambda B_i(\lambda) F_{\text{Mod},\lambda}(\theta) d\lambda}{\int \lambda B_i(\lambda) d\lambda}. \quad (37)$$

where, $B_i(\lambda)$ is the bandpass response function for i -th band in fractional photon units.

To calculate SED, the stellar evolution code Padova was used, which calculates stellar structure. That model does not calculate only SEDs, but it also calculates

isochrones. For each star, it calculates how the star ages and how its spectrum changes, from which we can determine stellar age.

7.6 Practical Applications

The BEAST has a lot of practical applications in astrophysics. It gives valuable information on stellar populations. When studying globular clusters, BEAST analyzes the SED for each star of cluster members to calculate stellar parameters for each star. This analysis helps to determine the history of cluster formation and stellar evolution.

In studying galactic surveys, BEAST is mapping the distribution of stellar populations and interstellar dust. With this information, we get better understanding of galactic structure, dust distribution and star formation.

8 Installation and running the BEAST

Installation of the BEAST

Minimum system requirements for running the BEAST are:

- **Python Version:** Python 3.8 or higher, with Python 3.11 recommended. Recommended using Anaconda Python.
- **Astropy Version:** Astropy 1.3 or higher.
- **Numpy**
- **hd5** item **PyTables**

We have installed all the required software and we run calculations on MacBook Air with M1 processor chip.

BEAST was installed using the appropriate Conda environment. For more information on installing BEAST, consult manual and instructions at BEAST Installation instructions.

For BEAST to function properly, specific library files related to filters, stellar atmospheres, and stellar evolution models must be installed.

BEAST library files, as well as instructions on how to use them, can be found in BEAST Installation instructions.

8.1 BEAST filters library files

BEAST supports filters for different instruments and surveys including: GALEX, SPITZER, WISE, 2MASS, SDSS, HST, AKARI, JOHNSON. Filters catalogue files download location (`~/beast`):

- **filters.hd5**
- **vega.hd5**

```
list(hd_file[list(hd_file.keys())[0]])
(b'GALEX_FUV', b'GALEX', b'GALEX', b'FUV', 92.87649047, 1539.78123994, 1536.33336172, b''),
(b'GALEX_NUV', b'GALEX', b'GALEX', b'NUV', 449.81448569, 2313.89225863, 2299.24499411, b''),
(b'GROUND_2MASS_J', b'GROUND', b'2MASS', b'J', 1626.37650654, 12407.21682434, 12389.68375913, b''),
(b'GROUND_2MASS_H', b'GROUND', b'2MASS', b'H', 2509.40449271, 16513.66459849, 16494.94709132, b''),
(b'GROUND_2MASS_Ks', b'GROUND', b'2MASS', b'Ks', 2620.70199282, 21655.83871164, 21638.14405982, b''),
(b'SPITZER_IRAC_36', b'SPITZER', b'IRAC', b'36', 3181.966405, 35634.29391089, 35569.27067798, b''),
(b'SPITZER_IRAC_45', b'SPITZER', b'IRAC', b'45', 4664.68082, 45110.14161368, 45020.21995468, b''),
(b'SPITZER_IRAC_58', b'SPITZER', b'IRAC', b'58', 2116.064825, 57593.36760732, 57450.41367546, b''),
(b'SPITZER_IRAC_80', b'SPITZER', b'IRAC', b'80', 8138.00526, 79594.93105685, 79157.67051198, b''),
(b'WISE_RSR_W1', b'WISE', b'RSR', b'W1', 0.60038843, 3.37919174, 3.36822494, b''),
(b'WISE_RSR_W2', b'WISE', b'RSR', b'W2', 0.78808484, 4.62929655, 4.61791056, b''),
(b'WISE_RSR_W3', b'WISE', b'RSR', b'W3', 2.7116615, 12.3337576, 12.07302227, b''),
(b'WISE_RSR_W4', b'WISE', b'RSR', b'W4', 1.18356282, 22.25323592, 22.19429619, b''),
(b'GROUND_SDSS_U', b'GROUND', b'SDSS', b'U', 60.58749975, 3561.78873416, 3556.52396878, b''),
(b'GROUND_SDSS_G', b'GROUND', b'SDSS', b'G', 418.52000097, 4718.87224629, 4702.49527931, b''),
(b'GROUND_SDSS_R', b'GROUND', b'SDSS', b'R', 546.14500065, 6185.19447695, 6175.57888104, b''),
(b'GROUND_SDSS_I', b'GROUND', b'SDSS', b'I', 442.15249882, 7499.70417496, 7489.97684637, b''),
(b'GROUND_SDSS_Z', b'GROUND', b'SDSS', b'Z', 88.50499982, 8961.48833673, 8946.70956512, b''),
```

Figure 20: filters.hd5 file „content” table

```
list(hd_file[list(hd_file.keys())[0]])
(b'HST_NIC3_F222M', 22164.09884343, 3.88222891e-11, 26.02729715),
(b'HST_NIC3_F240M', 23976.70722308, 2.91955146e-11, 26.33670966),
(b'CFHT_MEGAPRIME_CFH9702', 7552.45543911, 1.372377e-09, 22.15631642),
(b'J', 12407.21682434, 3.11337676e-10, 23.7669208),
(b'H', 16513.66459849, 1.13533175e-10, 24.86219304),
(b'Ks', 21655.83871164, 4.27901763e-11, 25.92163981),
(b'36', 35634.29391089, 6.6166846e-12, 27.94839892),
(b'45', 45110.14161368, 2.67156925e-12, 28.93308391),
(b'58', 57593.36760732, 1.04224721e-12, 29.95507315),
(b'80', 79594.93105685, 3.04242189e-13, 31.29195141),
(b'W1', 3.37919174, 0., inf),
(b'W2', 4.62929655, 0., inf),
(b'W3', 12.3337576, 0., inf),
(b'W4', 22.25323592, 0., inf),
(b'U', 3561.78873416, 3.67247815e-09, 21.08760195),
(b'G', 4718.87224629, 5.42964565e-09, 20.66307128),
(b'R', 6185.19447695, 2.50324369e-09, 21.50374217),
(b'I', 7499.70417496, 1.39811991e-09, 22.13613895),
(b'Z', 8961.48833673, 8.4400587e-10, 22.68413633)]
```

Figure 21: vega.hd5 file „sed” table

Running BEAST

8.2 Step 1: Preparation of Input Catalogs

The first step in running BEAST is the preparation of the necessary input catalogs:

- **Observed Photometric Catalog:** This file contains the observed photometric data in different filters for the stars under study. It includes columns such as normalized fluxes (e.g., `FILTERNAME_RATE`), magnitudes in the system you study, and optional RA and DEC coordinates. Its should be in FITS format.

8.3 Step 2: Configuration of the `settings.txt` File

The `settings.txt` file is crucial for configuring BEAST runs. It contains information about project details, stellar and dust parameters and grid definitions.

Key Sections of `settings.txt`:

- **Project Details:** Includes project name, filters, base filters, and observation file details.
- **Grid Definition Parameters:** Sets parameters for velocity, distance, stellar parameters (e.g., `logt`, `Z`), and dust parameters (e.g., `Avs`, `Rvs`).
- **Model Priors:** Links to prior models can be found at BEAST Priors Documentation.

Important Note: Any change in parameters within the `settings.txt` file requires renaming the output directory to avoid overwriting previous results.

8.4 Step 3: Running the BEAST Models - `run_beast.py`

8.4.1 A) Physics Model Generation (flag command `-p`)

This command generates physics model grid based on the grid parameters in `settings.txt` file. Procedure runtime for our model was from 30 seconds up to 30 minutes.

Outputs:

- `seds.grid.hd5`: The main grid file containing the physics model.
- `spec_grid.hd5` and `spec_w_priors.grid.hd5`: Additional files generated during the process.

```

#####
# Distances, Velocity
#####

# velocity of galaxy
velocity = -244.4 * units.km / units.s

# Distances: distance to the galaxy [min, max, step] or [fixed number]
#distances = [2.0,10.0,1]
distances = [7.87]
distance_unit = units.kpc
distance_prior_model = {'name': 'flat'}

#####
# Stellar Parameters
#####

# Age (logt) -- [min,max,step] to generate the isochrones in years
# example [6.0, 10.13, 1.0]
#logt = [9.6, 10.13, 0.1]
logt = [10.0, 10.1, 0.05]
#age_prior_model = {'name': 'flat', "sfr": 1e-5}
age_prior_model = {'name': 'flat'}
#age_prior_model = {'name': 'exponential', "tau": 0.1}

# note: Mass is not sampled, instead the isochrone supplied
# mass spacing is used instead
#mass_prior_model = {"name": "kroupa"}
mass_prior_model = {"name": "salpeter", "slope": 0.3}
#mass_prior_model = {"name": "flat"}

# Metallicity : list of floats
# Given as relative to solar which has 0.0152 (Z_solar)
# Here: Z == Z_initial, NOT Z(t) surface abundance
# PARSECv1.2S accepts values 1.e-4 < Z < 0.06
# example z = [0.03, 0.019, 0.008, 0.004]
#z = np.array([0.0001,0.0005,0.001,0.005,0.01,0.015,0.02]).tolist()
#z = (10 ** np.array([-2.1, -1.5, -0.9, -0.3]) * 0.0152).tolist()
z = [0.0001, 0.0005, 0.0008, 0.002, 0.005]
met_prior_model = {"name": "flat"}

# Isochrones: current choices are: Padova or MIST
# PadovaWeb() -- `modeltype` param for iso sets from ezipadova
# (choices: parsec12s_r14, parsec12s, 2010, 2008, 2002)
# MISTWeb() -- `rotation` param (choices: vvcrit0.0=default, vvcrit0.4)
#
# Default: PARSEC+COLIBRI
iso = isochrone.PadovaWeb()

# Stellar Atmospheres library definition
psl = stellib.Tlusty() + stellib.Kurucz()

#####
# Dust Parameters
#####

# Dust extinction grid definition
# recommended extinction mixture model
extLaw = extinction.Generalized_RvFLaw(ALaw=extinction.Generalized_DustExt(curve='F19'),

```

Figure 22: part of the settings.txt file.

8.4.2 C) Splinter Noise Model

This is a simple model that assumes the noise is a fraction of the model SED flux and there is no bias. Using the photometric uncertainties for each observation and each band, we have estimated that the flux uncertainty is no more than 4% of the flux value. Therefore, we have used Splinter noise model with generous flux uncertainty of 10%. Splinter Noise Model produces noise model grid (noisemodel.grid.hd5).

8.4.3 E) Trimming for Speed (flag command -t)

The physics model can be trimmed of sources that are so bright or so faint that they will by definition produce effectively zero likelihood fits. Such trimming will speed up the fitting.

Outputs:

- `seds_trim.grid.hd5`
- `noisemodel_trim.grid.hd5`

8.4.4 F) Fitting the Model and Generating Statistics (flag command = -f)

The core step of BEAST involves fitting the model to the observed data.

Outputs:

- `*_stats.fits`: Statistics for each of the fitted and derived parameters, including the 16th 50th 84th percentiles, mean, and expectation value.
- `*_pdf1d.fits`: Marginalized 1D PDFs for each of the fitted and derived parameters.
- `*_pdf2d.fits`: Marginalized 2D PDFs for pairs of parameters.
- `*_lnp.hd5`: Sparsely sampled log likelihoods.

Our calculation runtime was few minutes.

8.4.5 G) Plotting Results

Plotting the resultant SEDs can be done with the command::

```
$ beast plot_indiv_fit project/project --starnum=starnumber
```

This generates plots for the SEDs of individual stars, allowing detailed analysis of the fitting results.

9 Data and observations

As input, BEAST needs the Flexible Image Transport System (FITS) file format. The easiest way is to first create an .xlsx file or .txt file and then convert it to .fits file.

Optical photometry data for this theses are from article:"GLOBULAR AND OPEN CLUSTERS OBSERVED BY SDSS/SEGUE: THE GIANT STARS" [47], from which data for globular cluster M92 and M13, as well as for open cluster NGC 6791 were taken. SDSS can not observe photometry for a lot of stars in globular clusters. Reason for that is, when there is a lot of stars in one place, telescopes can not distinguish one star from another (crowded field) because they are too bright and too close to each other. So, authors of this article had to develop a new special techniques to do it. The article provided data for the magnitude in the g, r, i and z bands, with error for the r band, for given R.A. and Decl. for each star. It also provided a velocity for each star in km/s. This paper focuses in particular on the red giant branch stars in the clusters. By studying velocities of the stars, authors determined if the particular star was in fact from the same cluster. They all had similar angular velocities and kinematics.

The Sloan Digital Sky Survey or SDSS is a major multi-spectral imaging and spectroscopic redshift survey using a dedicated 2.5-m wide-angle optical telescope at Apache Point Observatory in New Mexico, United States. Its main goal is to map the distribution of galaxies, stars, and quasars to understand the structure of the universe, the nature of galaxies, and the scale of cosmic time. Over its various phases, SDSS has expanded its scope to include studies on dark energy, the Milky Way, and extra-solar planets, significantly enriching our understanding of the cosmos through massive data releases accessible to astronomers worldwide [48].

The Sloan Extension for Galactic Understanding and Exploration (SEGUE) is a survey designed to map the structure and stellar content of the Milky Way. This part of the SDSS is devoted to understanding what components make up our galaxy, such as the thick disk, the halo, and the thin disk. SEGUE observed the spectra of about 240,000 stars that can be used by astronomers to determine the chemical compositions, distances, and velocities of individual stars. This is especially valuable when it comes to understanding the birth and growth of our own galaxy, telling us more about its make-up in terms of structure and star types [49].

After converting the data from the article to the.xlsx file, the next step was to add magnitude for the J, H and K bands. After adding J, H and K magnitudes, these magnitudes finally needed to be converted to fluxes.

Magnitudes for the J, H, and K bands were found in IRSA/IPAC catalog23. For each star, R.A. and Decl. were needed to be inputted to get J, H and K magnitudes. The near-infrared J, H and K magnitudes were obtained from 2MASS survey using

IRSA/IPAC catalog. Infrared Science Archive (IRSA) chartered to serve calibrated science products from NASA's infrared and submillimeter missions, including the 2MASS, IRAS and MSX surveys. After collecting all of the stars J, H and K magnitudes, the next step was to convert all of the magnitudes to fluxes.

The Two Micron All-Sky Survey (2MASS), was an astronomical survey of the whole sky in infrared light. It took place between 1997 and 2001. 2MASS produced an astronomical catalog with over 300 million observed objects, including minor planets of the Solar System, brown dwarfs, low-mass stars, nebulae, star clusters and galaxies [50].

Table 1: SDSS (g,r,i,z) and 2MASS (J,H,K) Photometric Bands and Their Characteristics [51]

Band	Effective Wavelength Midpoint	Type of Light
g	464 nm	Visible (Green)
r	658 nm	Visible (Red)
i	806 nm	Near-Infrared
z	900 nm	Near-Infrared
J	1220 nm	Near-Infrared
H	1630 nm	Near-Infrared
K	2190 nm	Near-Infrared

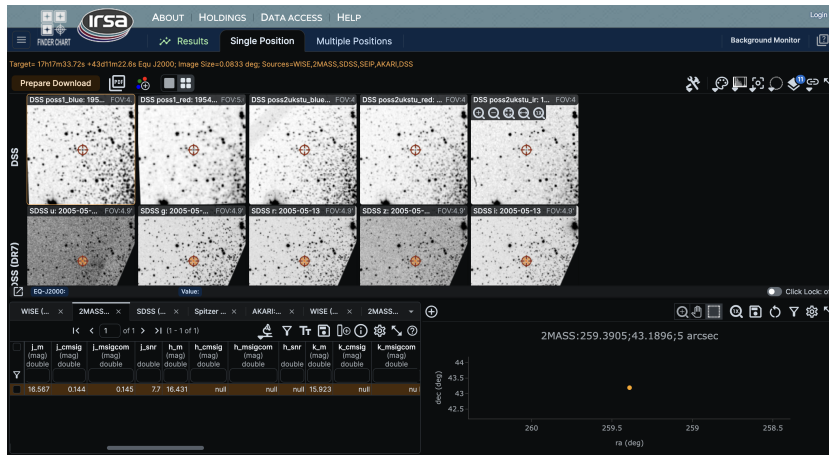


Figure 23: Example for random star in IRSA webpage.

9.1 Calculating fluxes

The SDSS photometric system uses a flux-based magnitude conversion that involves a specific function for each band. The flux f is related to the observed flux parameter b , a reference flux f_0 and the observed magnitude m through the following relation [52]:

$$f = 2bf_0 \sinh \left(\frac{m}{\frac{-2.5}{\ln(10)}} - \ln(b) \right) \quad (38)$$

Table 2 lists the values of b and f_0 for each SDSS band used in this work

Table 2: SDSS Photometric Conversion Parameters

Band	b	f_0 (Jy)
g	0.9	3631
r	1.2	3631
i	1.8	3631
z	7.4	3631

Using equation 38, for each magnitude in the g, r, i, and z filters, flux was calculated.

To calculate fluxes in J, H and K bands, the formula used was:

$$f = 10^{-0.4m} f_0 \quad (39)$$

With all fluxes calculated for all bands, we got the final table ready for BEAST analysis. We can see how these finished tables look like for all of our studied clusters in A.10.

9.2 Creating and Viewing FITS file

For BEAST to perform its analysis, we need to convert our .xlsx file to .fits file.

The FITS file format is a common way to store and share data in astronomy, especially for images and tables. It is flexible enough to handle a wide range of data types, like multi-dimensional arrays (such as images) and binary tables, which makes it great for storing complex datasets. A key feature is that it includes metadata, details about how the data were collected, such as instrument settings and observation specifics, right in the file header. It is popular in the astronomy world because it makes data easy to share and work with across various systems and software [53].

The way that our XLSX file was converted into FITS format is by Python code presented in Appendix A.1.

To view the FITS file, NASA has developed the software called fv FITS viewer, which can be easily downloaded on any OS from NASA's website. The installation is very straightforward and so is the use of it. The opened FITS file looks like this:

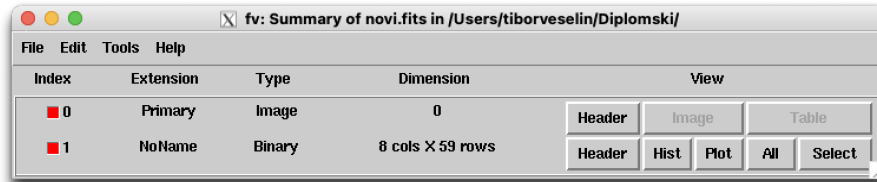


Figure 24: FITS file opened with fv viewer.

10 Numerical calculations

10.1 How BEAST calculates stellar parameters?

Stellar parameters, distances and dust extinction are calculated with BEAST by first setting the grid of theoretical stellar models and evolutionary tracks. From them BEAST constructs SEDs, calculates photometric magnitudes in given bands and fits them with theoretical photometric magnitudes using Bayes Inference.

Theoretical models and stellar evolution models we used are: Padova model, Colibri evolution model and Trusty.

10.2 Modifying `settings.txt` file: parameters, models and priors

In this section, the parameters we used are for M92, but to perform BEAST analysis for other clusters, parameters were changed accordingly. Firstly, in `settings.txt` file we need to set survey name. In my case it is SEGUE survey, so in file I put:

```
surveyname = "SEGUE"
```

The BEAST creates hidden folder `.beast`. The `.beast` folder is automatically created by BEAST in your home directory and contains essential library files needed to run BEAST models. These include files that store information about the filters and stellar models used in the analysis.

Two important files within this directory are:

- **filters.hd5**: This file contains data on various astronomical filters, including their wavelength and throughput information. It is used to define how light from stars is measured through different instruments. It must also include g, r, i, z SDSS and J, H and K 2MASS filters, needed for this theses.
- **vega.hd5**: This file contains reference data for the star Vega, a standard calibration star in astronomy. BEAST uses this file to adjust the magnitudes and fluxes of stars in the dataset to be consistent with Vega's properties.

These files are crucial for ensuring accurate stellar modeling by applying proper calibrations and filtering during the analysis.

We needed to see the content of the `filters.hd5` file, so we can see how each filter is called, so we can put that information in the `settings.txt` file. The code used to look at the content of the `filters.hd5` file is shown in Appendix A.2.

Example of a few rows that this code outputs:

```

filters/GROUND_SDSS_R: <class 'h5py._hl.dataset.Dataset'>
filters/GROUND_SDSS_U: <class 'h5py._hl.dataset.Dataset'>
filters/GROUND_SDSS_Z: <class 'h5py._hl.dataset.Dataset'>
filters/HST_ACS_WFC_F435W: <class 'h5py._hl.dataset.Dataset'>
filters/HST_ACS_WFC_F475W: <class 'h5py._hl.dataset.Dataset'>
filters/HST_ACS_WFC_F550M: <class 'h5py._hl.dataset.Dataset'>

```

Filters I used (line in `settings.txt` file):

```

filters = ["GROUND_SDSS_G", "GROUND_SDSS_R", "GROUND_SDSS_I",
↪ "GROUND_SDSS_Z", "GROUND_2MASS_J", "GROUND_2MASS_H",
↪ "GROUND_2MASS_KS"]

```

As we can see from 12, the names of columns with fluxes in each band are `G_RATE`, `R_RATE`, `I_RATE`, `Z_RATE`, `J_RATE`, `H_RATE` and `K_RATE`. That looks in `settings.txt` file like this:

```
basefilters = ["G", "R", "I", "Z", "J", "H", "K"]
```

Next in `settings.txt` file we have:

```
obs_colnames = [f.upper() + "_RATE" for f in basefilters]
```

- `basefilters`: This is a list containing the names of filters.
- `f.upper()`: This method converts each filter name in `basefilters` to uppercase. If the filter names were in lowercase or mixed case, this ensures consistency by converting them to uppercase.
- `"_RATE"`: This string is appended to each uppercase filter name. It signifies that the observational data being referenced is the flux rate

In `settings.txt` file we also have put velocity of cluster, which is in our case -121.2 km/s for M92 [54].

We know that the distance to M92 is 8.2 kpc [29], but we put distance as an unknown, so that we can check how BEAST estimates distances. We put that distance between 2 and 10 kpc, and gave BEAST 0.2 kpc step to analyze. We also used flat prior. We also did analysis with fixed distance to get more precise values of other parameters.

For age, we did a similar thing. We put the logarithm of the age between 9.5 and 10.13 with step of 0.1. That is defined with the grid of evolutionary models (Padova models). In clusters like these, there is no creation of new stars. From age, mass, radius, and log g is being calculated. We put exponential age prior at

first, but that prior yielded very bad results, so we changed it to flat prior, which gave much better results.

For mass we used Salpeter prior [55].

Since this is a very old globular cluster, with almost no gas or dust and no formation of new stars, the metallicity must be quite low. The fitting has been adjusted to very low metallicities, ranging from 0.0001 to 0.005. Prior was out to flat.

For the Stellar Atmospheres standard prior models were used: Tlusty and Kurucz.

Also, important are the dust parameters.

For the dust extinction, we used general model.

The dust column density (A_v) is very small according to previous studies, so the fit is set between 0 and 0.6 with the step of 0.1. Prior is flat.

Average grain size (R_v) is determining the size of the grain and it is expected to be around 2.5 in the direction of this open cluster. For that reason, fit is between 2.35 and 3.1 with the step of 0.25. Prior is logarithmic.

Mixing fraction (f_A) determines the mix between the extinction curves for the Milky Way disk and the center of the Small Magellanic Cloud (SMC). The fit is set between 0 and 1 with step of 0.25. Prior is logarithmic.

Other parameters in `settings.txt` file, can be left as they are. Finally, we can put our noise model at the end, and with that, our `settings.txt` file is complete and our data is ready for the analysis. The next step is to do the BEAST analysis with our data.

10.3 Modifying `run_beast_splinter.py` file

This file is a Python script configured to run the BEAST analysis. BEAST is fitting the spectral energy distributions (SEDs) of stars to determine stellar and dust extinction parameters, and this script configures and automates that process. It is preparing the necessary environment and processing steps required for the BEAST's complex computational processes.

We had to modify this file to create a noise model for the flux of our stars. We calculated that the average magnitude error for all the filters is 2.13%. We did that by calculating upper and lower boundaries for magnitude values by adding and subtracting error for magnitudes and then dividing it with actual values. We did that for all filters and calculated average of errors of 2.13%. Splinter noise model assumes that every photometric band is independent from the others and has a fractional flux uncertainty and no bias. This model has standard fractional flux uncertainty of 10%. We used the same value which gives us more than 4 sigma certainty. The way that we implemented `splinter_noise_model` is by adding following code in our `run_beast_splinter.py`:

```

if args.splinter:

    print("Generating splinter noise model.")
    import beast.observationmodel.noisemodel.splinter as noisemodel1
    modelsgedgridfile = settings.project + '/' + settings.project +
    ↪ '_seds.grid.hd5'
    modelsgedgrid = SEDGrid(modelsgedgridfile)

```

10.4 The BEAST analysis

Firsts, we need to open terminal and get to the folder with our files. In that folder we need to have `settings.txt` file, `run_beast_splinter.py` file and "Data" folder with our FITS file of observed fluxes.

BEAST code is run by:

```
$ ./run_beast_splinter.py -pstf
```

Now the BEAST does its analysis which looks like this:

```

~/Diplomski/Beast_splinter --zsh
(base) tiborveselin@fibors-Air Beast_splinter % ./run_beast_splinter.py -pstf
Padova CMD Isochrones
Working on the PARSEC isochrone
Interrogating http://stev.oapd.inaf.it...
Downloading data...http://stev.oapd.inaf.it/tmp/output636379121824.dat
Interrogating http://stev.oapd.inaf.it...
Downloading data...http://stev.oapd.inaf.it/tmp/output848968511468.dat
Interrogating http://stev.oapd.inaf.it...
Downloading data...http://stev.oapd.inaf.it/tmp/output502534989247.dat
Interrogating http://stev.oapd.inaf.it...
Downloading data...http://stev.oapd.inaf.it/tmp/output554088289857.dat
Interrogating http://stev.oapd.inaf.it...
Downloading data...http://stev.oapd.inaf.it/tmp/output222413855672.dat
Padova/Proba Isochrones
Make spectra
applying 1 distances
Adding spectral properties: True
Spectral grid: 180% | 1488/1488 [00:00:00:00, 5264.861t/s]
Spectral grid: 100% | 4859/4859 [00:01:00:00, 4894.211t/s]
Distance grid: 100% | 1/1 [00:00:00:00, 38.221t/s]
Make prior weights
computing the distance plus weights for dist = 8200.0
computing the age-mass-metallicity grid weight for Z = 0.0001
computing the age-mass-metallicity grid weight for Z = 0.0004
computing the age-mass-metallicity grid weight for Z = 0.0008
computing the age-mass-metallicity grid weight for Z = 0.002
computing the age-mass-metallicity grid weight for Z = 0.005
Make SEDS
number of initially requested points = 98
number of valid points = 36 (based on restrictions in R(V)
versus T-A plane)
Generating a final grid of 228204 points | 36/36 [00:02:00:00, 15.781t/s]
SED grid: 100%
Generating splinter noise model.
Writing to disk into Proba/Proba_noisemodel.grid.hd5
Trimming the model and noise grids
number of original models = 228204
number of ast trimmed models = 228204
working on filter # = 0
working on filter # = 1
working on filter # = 2
working on filter # = 3
working on filter # = 4
working on filter # = 5
working on filter # = 6
number of original models = 228204
number of ast trimmed models = 228204
number of trimmed models = 91897
Writing trimmed sedgrid to disk into Proba/Proba_seds_trim.grid.hd5
Writing trimmed noisemodel to disk into Proba/Proba_noisemodel_trim.grid.hd5
not using full covariance matrix
Calculating lnp(Aster): 100% | 59/59 [00:01:00:00, 35.331t/s]
Done fitting on grid Proba/Proba_seds_trim.grid.hd5
None
time to fit: 0.06093395823228638 min
(base) tiborveselin@fibors-Air Beast_splinter % beast plot_indiv_fit Beast_splinter/Beast_splinter --sternum1
Traceback (most recent call last):
  File "/opt/miniconda3/bin/beast", line 8, in <module>
    sys.exit(main())

```

Figure 25: BEAST analysis in terminal.

When the BEAST is done with analysis, the new folder with output analysis is created:

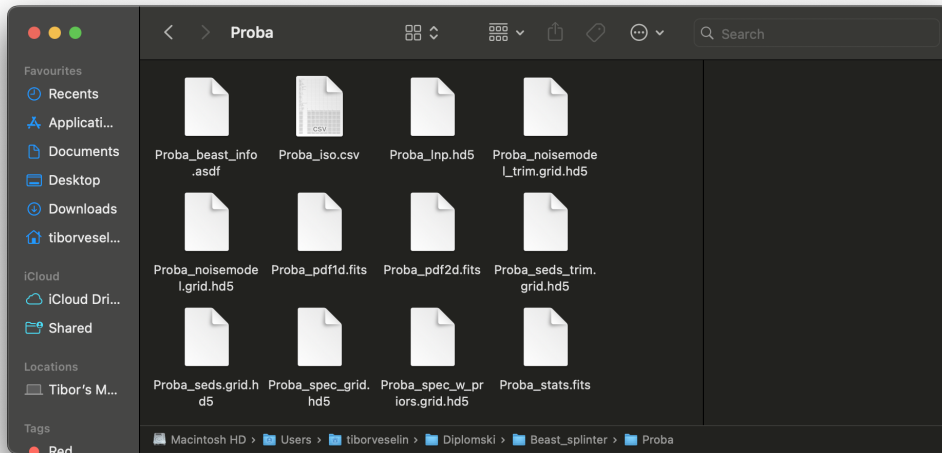


Figure 26: Output data from the BEAST analysis.

Here, the most important file is `Proba_stats.fits`. In this file we have all of the data that was calculated with the BEAST analysis, such as age, mass, temperature etc for each star. So, the next step is to convert FITS file to XLSX. The conversion of FITS data to Excel format is detailed in Appendix A.3.

Finally, we got `zavrсна.xlsx` file that has all stellar parameters. Now, the next step is to analyze that data.

You can see the stellar parameters obtained with BEAST for each of the stars in 3 clusters in Appendix A.11.

11 Results and interpretation

For M92, we performed the analysis with the distance being variable and the distance constant. When we put the distance as constant, we get more precise parameters values. For that reason, we used an analysis in which the distance is constant for all parameter values except with age (figures are 28 and ??). For age we used analysis where we set distance to be variable, so that we can see how BEAST calculates distance and age.

For M13, we performed the analysis with the distance being variable and the distance constant. We also put the age of the cluster as a large fitting interval and as a narrow fitting interval (between 10 and 13 Gyr). When we put the distance as constant and age in narrow fitting interval, we get more precise parameters values. For that reason, we used an analysis in which the distance is constant and the age is in a narrow fitting interval, for all parameter values except of age (figures are 34 ??). For age we used analysis where we set distance to be variable and age a wider fitting interval (3 to 13 Gyr), so that we can see how BEAST calculates age.

BEAST did a very good job in its analysis of NGC 6791. We also performed analysis with distance being constant and being variable and age being in a very narrow and in a wider fitting interval. It calculated the parameters for NGC 6791 very well with very small deviations in all of these cases. For that reason, we presented the values of parameters that were calculated in analysis with the distance as variable and the age in a wide fitting interval.

11.1 Output plots from BEAST analysis

After running Beast analysis and after we get output files, we can plot them in Beast, running command in terminal:

```
beast plot_indiv_fit distance_constant2/distance_constant2 --starnum=50
```

In "starnum=x", x represents the sequence number of the star we want to plot. The plot for the sample star is shown in figure 27.

In figure 27 we see SED of the star on the top. On x axis wavelength λ is shown in μm and on y axis stellar flux is shown. Besides that, we also get PDF for stellar parameters and their uncertainties. On diagrams of PDF for each derived star and dust parameter, best fitted model value is shown in cyan, while 16%, 50% and 84% percentiles are shown in violet. 16% and 84% percentiles correspond to $\pm\sigma$ (one standard deviation). In that particular case, effective temperature, log gravity and luminosity are well constrained. SED with observed fluxes and best fitted theoretical model is also shown.

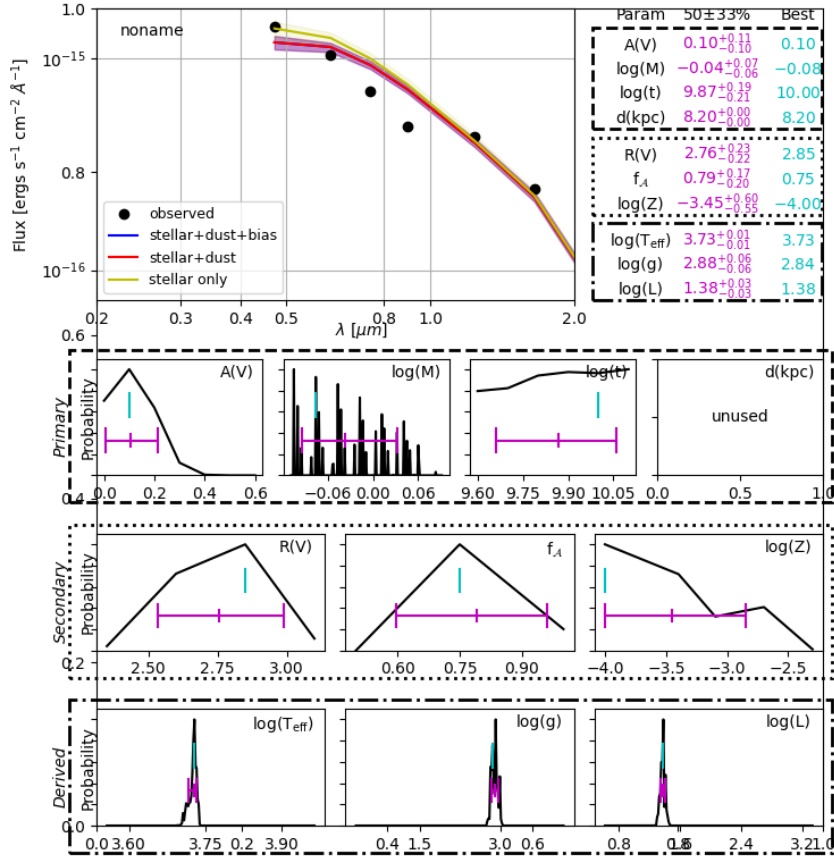


Figure 27: Plot of SED with observed fluxes and best fitted models, as well as PDF for fitted stellar parameters for 50th sequence number of star in M92 cluster.

11.2 Spatial distribution diagrams

Great way to visualise our data in physical scale is by making spatial distribution diagrams. On 2D plain we put right ascension (RA) and declination (Decl).

Decl is the celestial sphere's equivalent of latitude and it is expressed in degrees, as is latitude. For DEC, + and - refer to north and south, respectively. The celestial equator is 0° DEC, and the poles are $+90^\circ$ and -90° .

RA is the celestial equivalent of longitude. RA can be expressed in degrees, but it is more common to specify it in hours, minutes, and seconds of time: the sky appears to turn 360° in 24 hours, or 15° in one hour. So an hour of RA equals 15° of sky rotation.

We put stars coordinates (RA and Decl) on x and y axis and on the z axis we put stellar parameter such as luminosity. Stars with higher luminosities, are shown in brighter and warmer colors such as yellow, and less luminous stars have darker and colder colors such as blue and purple. The spatial distribution diagrams for all six stellar parameters are shown below:

11.2.1 M92: Spatial distribution diagrams

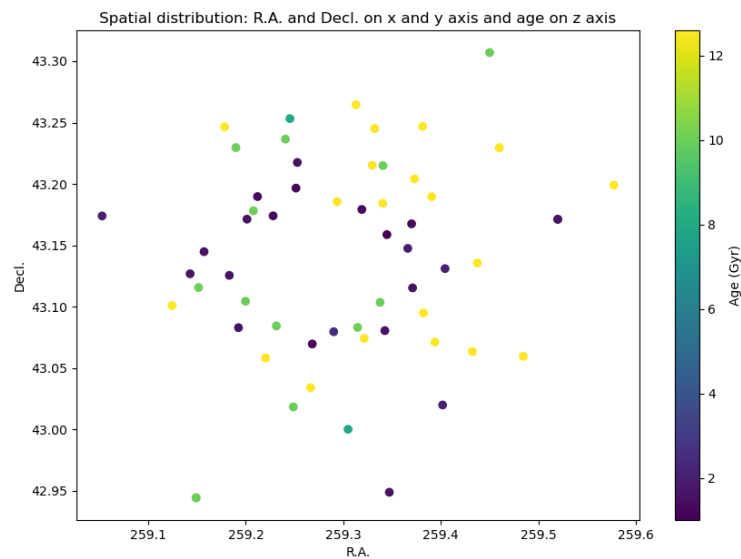


Figure 28: Spatial distribution diagram of age.

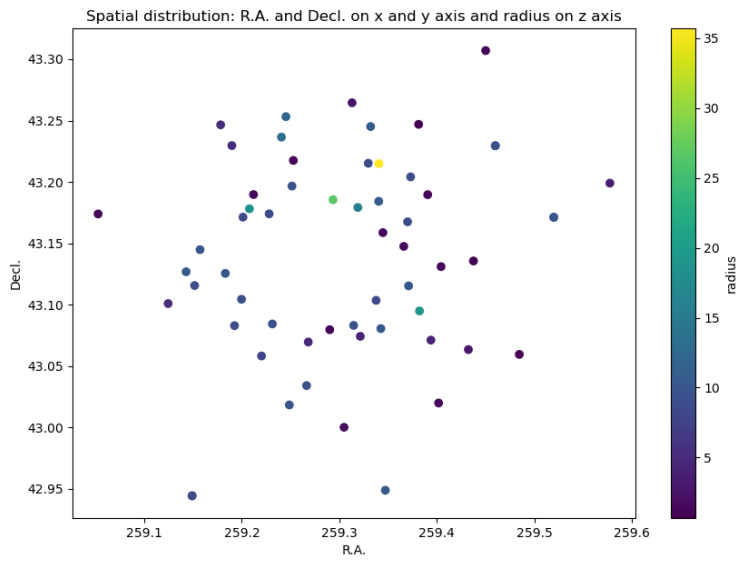


Figure 29: Spatial distribution diagram of radius.

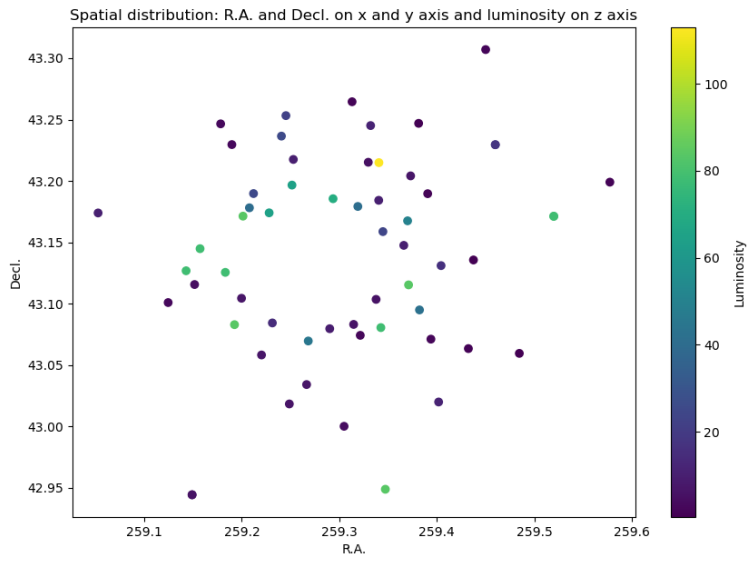


Figure 30: Spatial distribution diagram of luminosity.

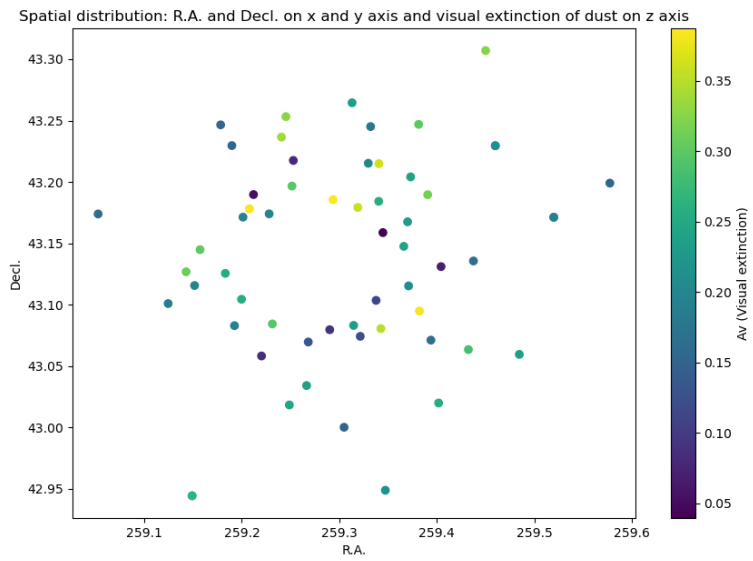


Figure 31: Spatial distribution diagram of visual extinction.

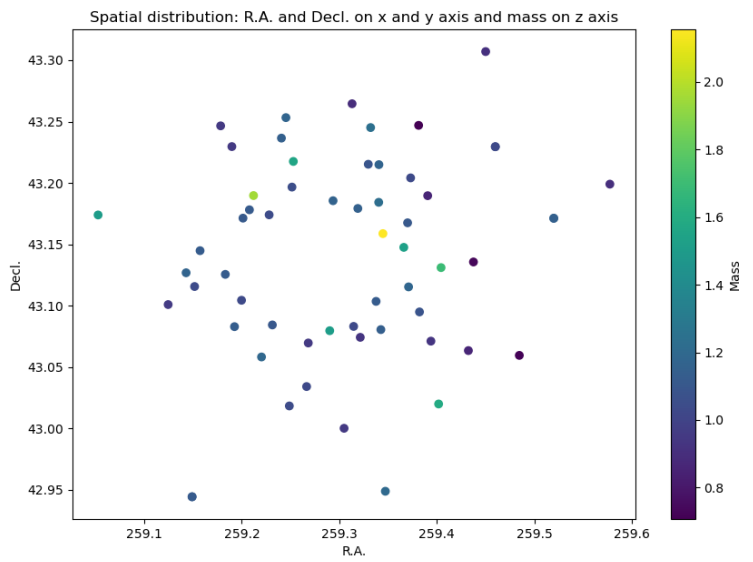


Figure 32: Spatial distribution diagram of mass.

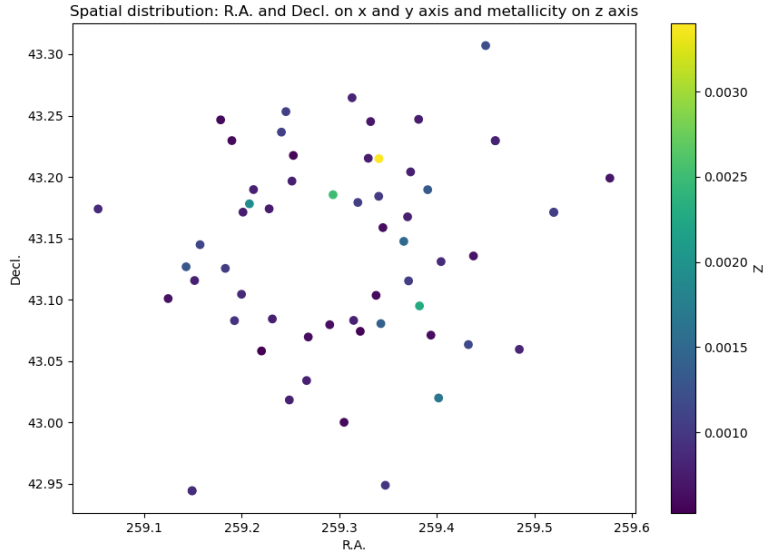


Figure 33: Spatial distribution diagram of metallicity.

In the spatial distribution diagrams we can see an empty space in the middle. The reason for that is because in the center of the M92 cluster, the density of the stars is so high that we cannot distinguish one star for itself.

The method for plotting the spatial distribution diagram is explained in Appendix A.4.

We can also see in Appendix A.11 values of all calculated parameters for each star with given R.A. and Decl. for every cluster that we studied.

It seems that younger and more luminous giant are found nearer to the center of the cluster. All other parameters seems to be randomly distributed in space.

11.2.2 M13: Spatial distribution diagrams

We can make spatial distribution diagrams for M13 the same way we did for M92:

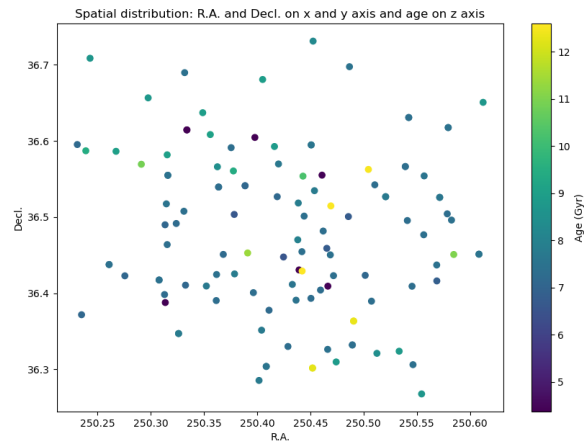


Figure 34: Spatial distribution diagram of age.

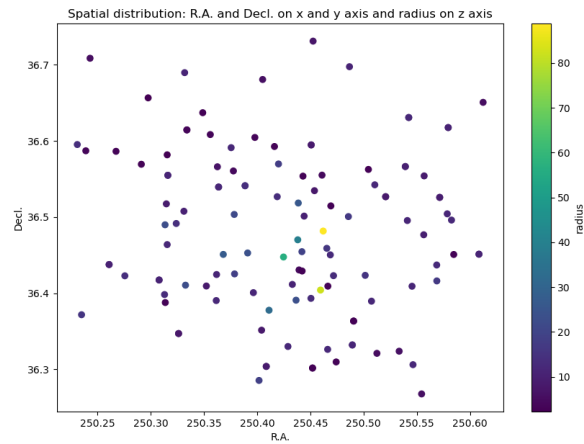


Figure 35: Spatial distribution diagram of radius.

Analysed giants seems to have similar stellar parameters that are randomly distributed in the cluster.

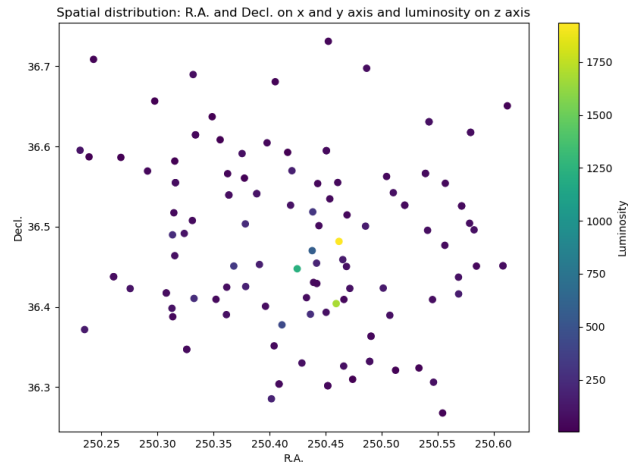


Figure 36: Spatial distribution diagram of luminosity.

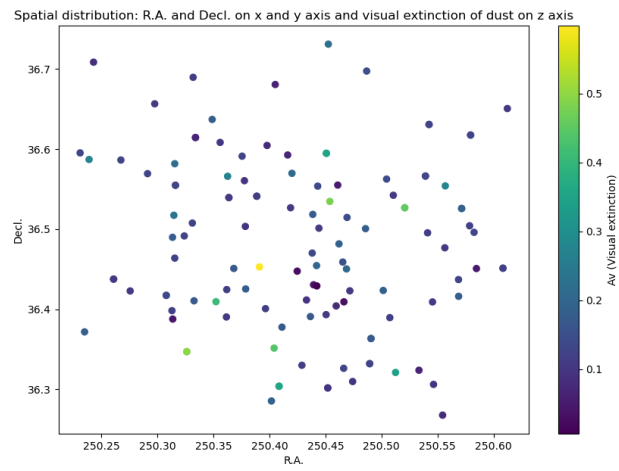


Figure 37: Spatial distribution diagram of visual extinction.

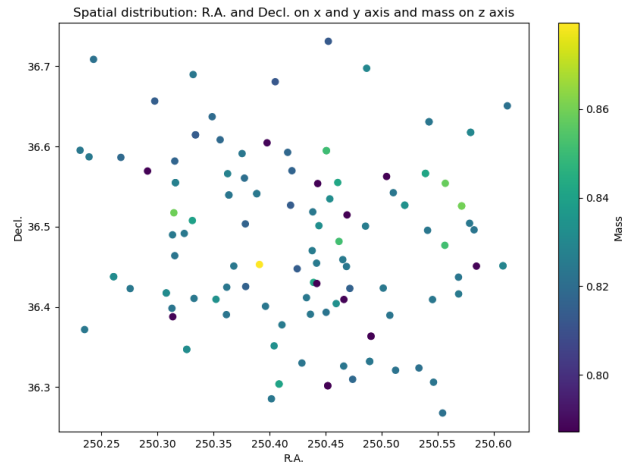


Figure 38: Spatial distribution diagram of mass.

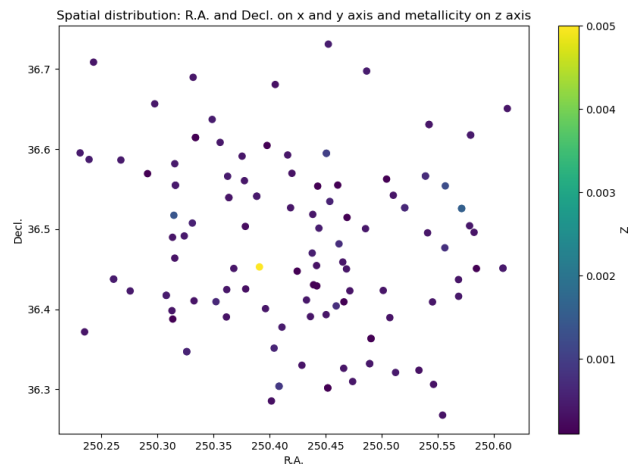


Figure 39: Spatial distribution diagram of metallicity.

11.2.3 NGC 6791: Spatial distribution diagrams

We can make spatial distribution diagrams for NGC 6791 in the same way as we did for clusters before:

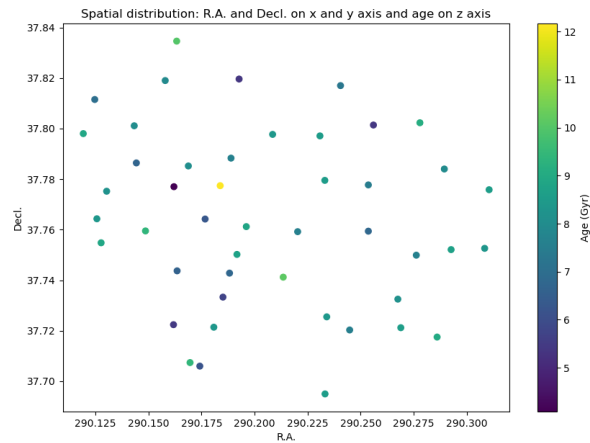


Figure 40: Spatial distribution diagram of age.

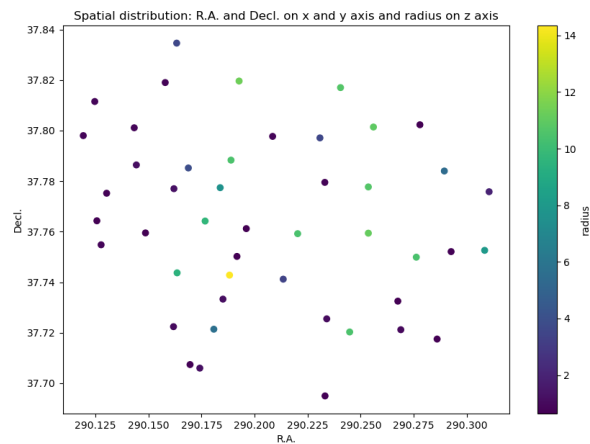


Figure 41: Spatial distribution diagram of radius.

Again it seems that all stellar parameters are randomly distributed in the cluster, with the possible exception of luminosity and radius, as it seems there are more larger and luminous giants towards center of cluster.

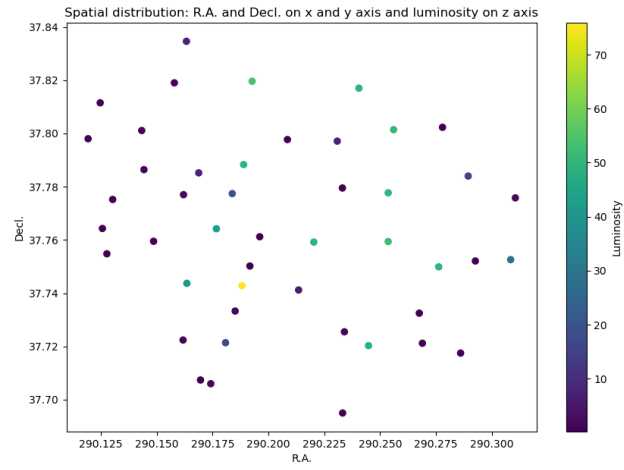


Figure 42: Spatial distribution diagram of luminosity.

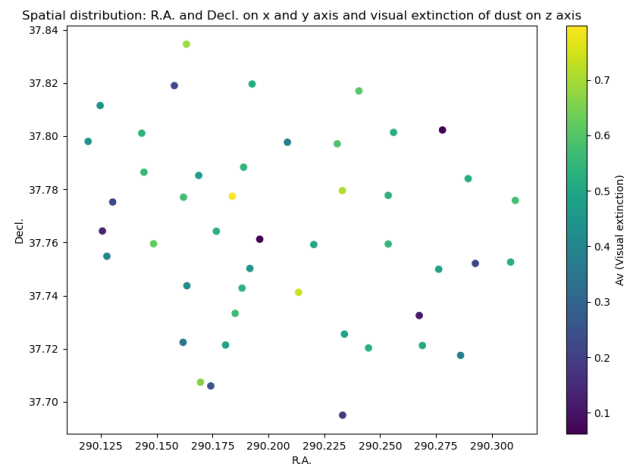


Figure 43: Spatial distribution diagram of visual extinction.

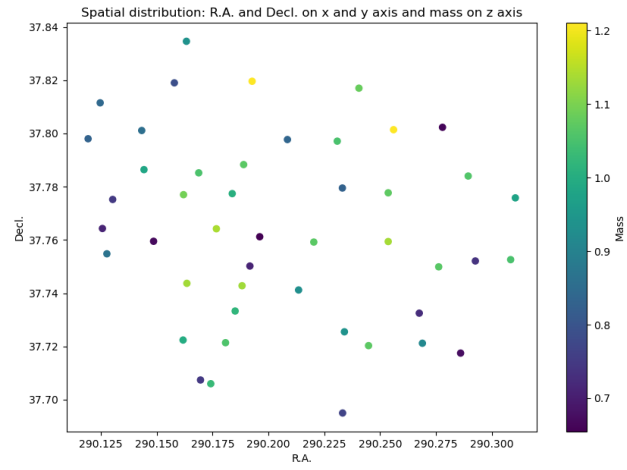


Figure 44: Spatial distribution diagram of mass.

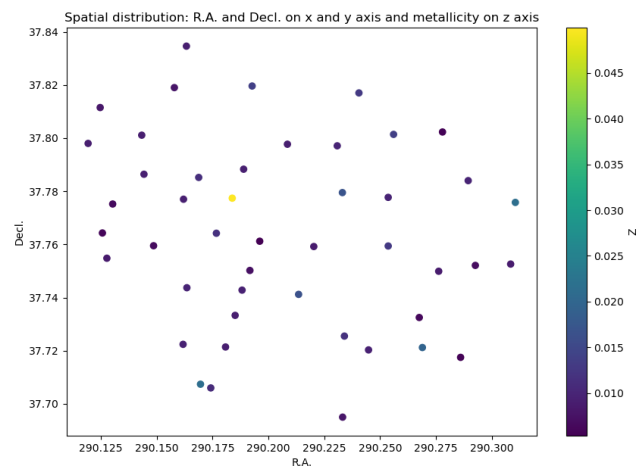


Figure 45: Spatial distribution diagram of metallicity.

11.3 H-R diagram

To make a H-R diagram, we need to measure two quantities: luminosity and temperature. In astronomy, a star's color is defined as the difference between its magnitudes as seen through two different filters. B-V color in Johnson photometric system, often used to represent effective temperature in H-R diagram, corresponds to g-r in SDSS photometric system. Stellar luminosity can be represented by g or r SDSS magnitude. Therefore, corresponding H-R diagram can be represented as g or r magnitude versus g-r color. Traditionally, astronomers have taken images through blue, yellow, and red filters denoted by the letters B, V, and R. If we subtract a star's V magnitude from its B magnitude, we get a color called B-V. Stars with lower B-V colors have higher temperatures, so we can use B-V color to make a H-R diagram. Since SDSS uses u, g, r, i and z filters, to make your H-R diagram, we can use the green and red filters, which both fall in the visible part of the spectrum. From the magnitudes of stars in these filters, we can calculate the color g-r.

11.3.1 M92: H-R diagram

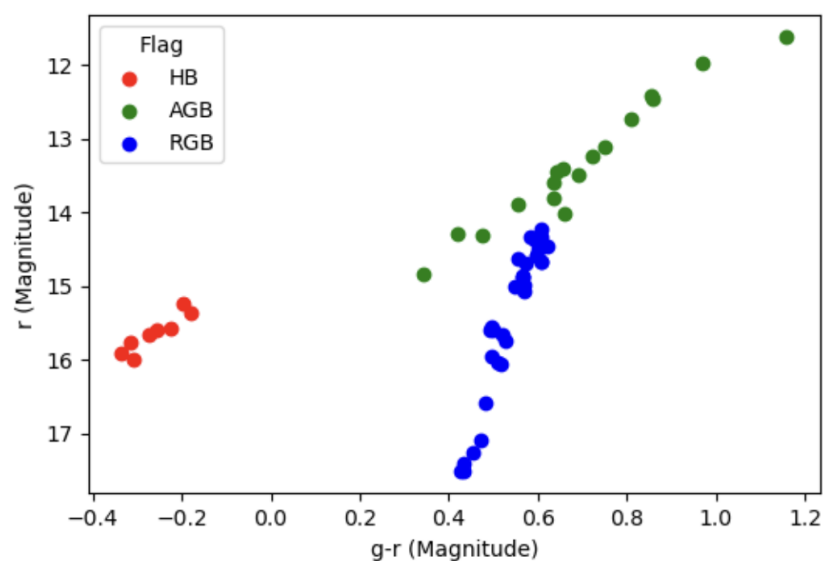


Figure 46: H-R diagram for M92 giants.

H-R DIAGRAM FOR M92 is shown in figure 46. Red are HB stars, green are AGB stars, and blue are RGB stars. For stars colored green, we can not say for sure, if they are AGB stars or stars at the tip of the red giant branch. It can be seen that observed post main-sequence stars are well separated in HB, AGB and RGB groups.

The Python script to plot the H-R diagram for M92 with flagged stars can be found in Appendix A.6.

To make H-R diagrams with stellar parameters, we do a similar analysis as we did for spatial distribution diagrams. On the x and y axes we put magnitudes for r and g-r bands, and on z axis we put color-coded stellar parameters like we did for spatial distribution diagrams.

H-R diagrams for all six stellar parameters that we analyzed:

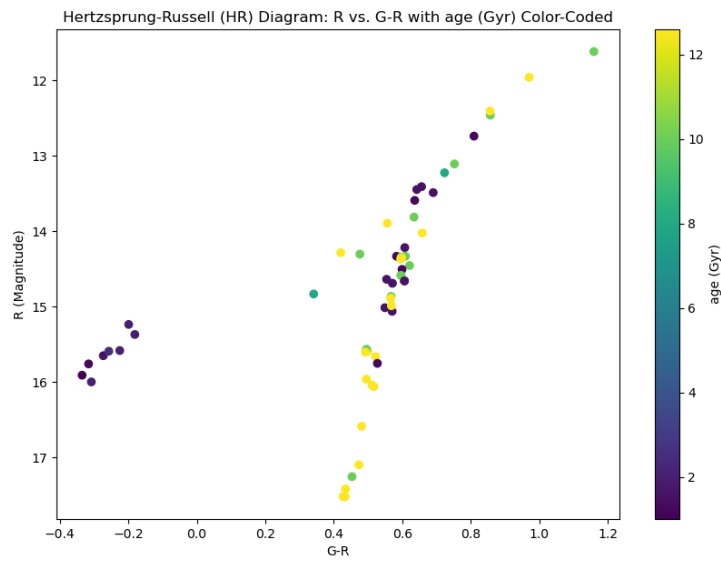


Figure 47: H-R diagram of M92 giants for age.

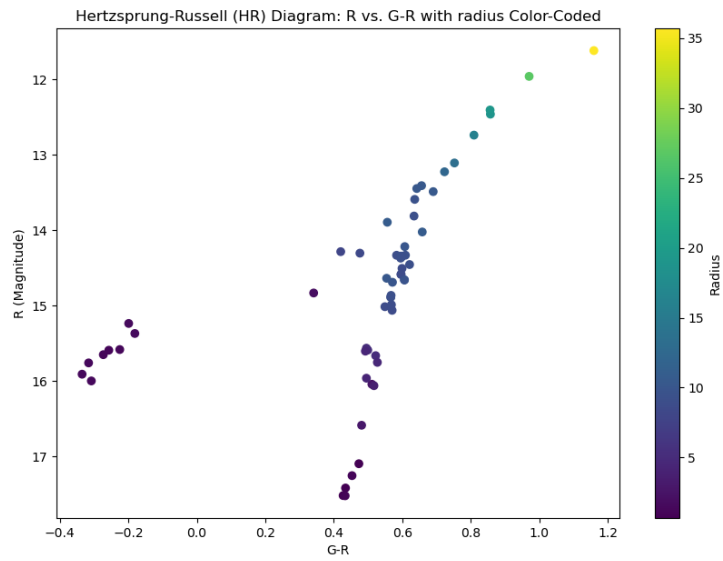


Figure 48: H-R diagram of M92 giants for radius.

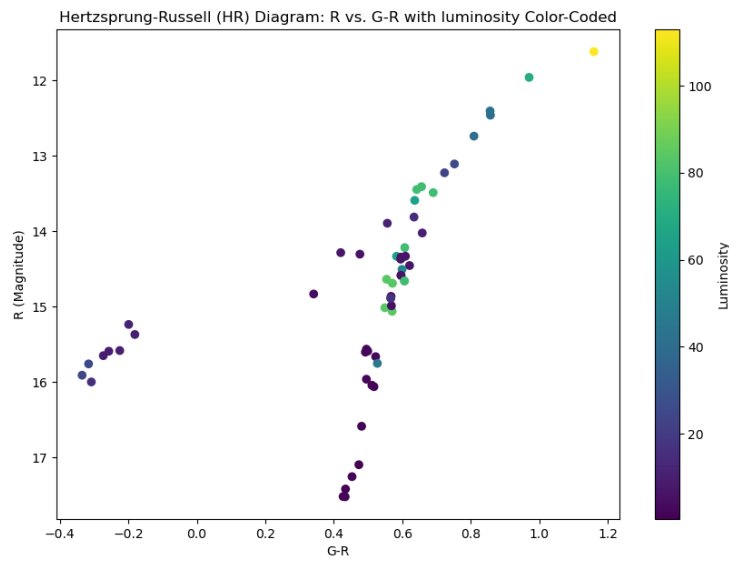


Figure 49: H-R diagram of M92 giants for luminosity.

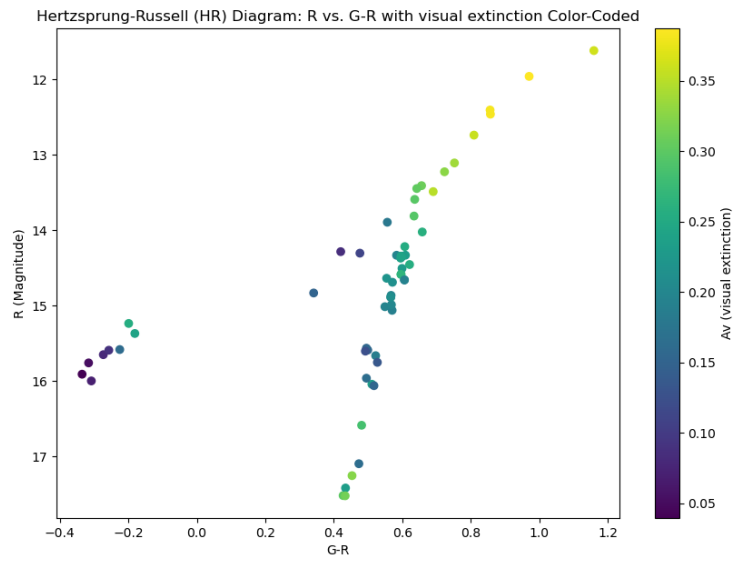


Figure 50: H-R diagram of M92 giants for visual extinction.

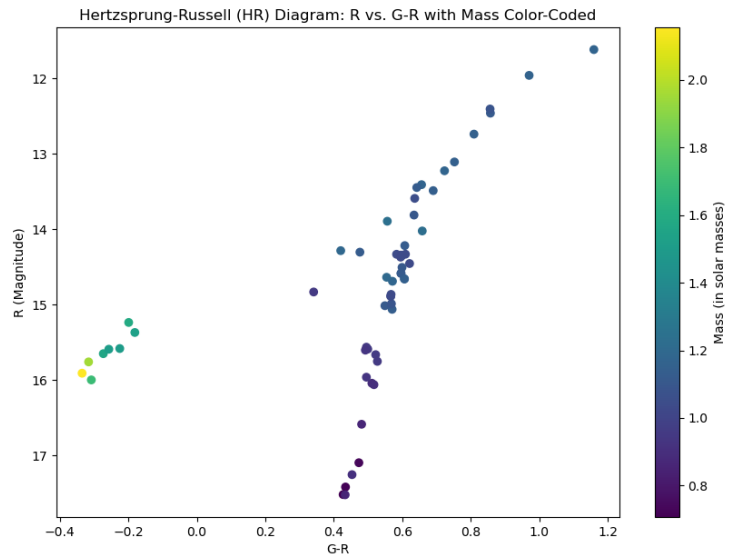


Figure 51: H-R diagram of M92 giants for mass.

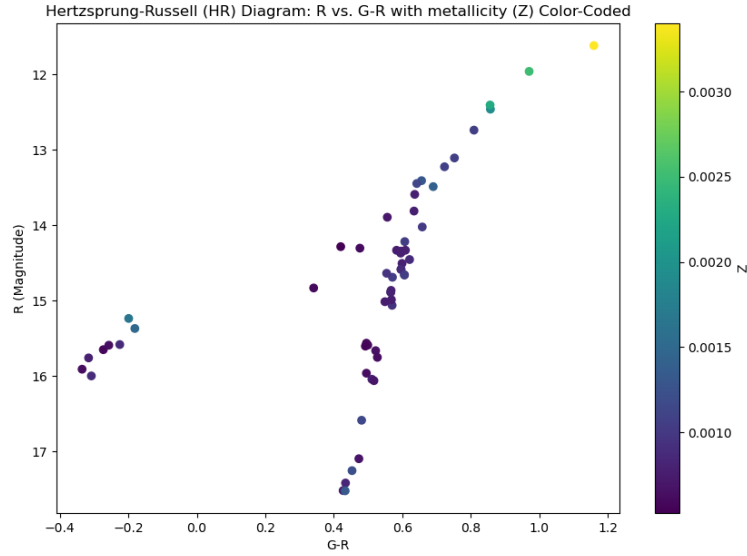


Figure 52: H-R diagram of M92 giants for metallicity.

We can see H-R diagram for age in figure 47. Yellow and orange color stars are the oldest and more dark color stars like blue and purple are the youngest stars. In theory RGB stars are first to form, after RGB phase, stars enter HB phase and finally, they enter AGB phase of their life cycle. In figure 47 we see that BEAST did not calculate that very well and therefore cannot determine stellar age without more strict prior. Most of the stars should be of similar age. While BEAST gives a large spread in age (between 2 and 13 Gyr), as can be seen, BEAST determined age the best for RGB stars.

For visual extinction, we can see in figure 50 that AGB stars has highest extinction, which is to be expected because they have the highest mass loss. Also, stellar wind creates the envelope of the gass and dust, creating higher extinction. RGB star have lower extinction because their mass loss is lower then in AGB stars.

For radius of a star, we know that AGB stars have larger radius than RGB stars and that HB is somewhere in the middle. BEAST performed well in the determination of stellar radius, which we can see in figure 48.

In figure 49 we can see that AGB stars have the highest luminosities and RGB star have the lowest. That is also in agreement with the expectations.

In figure 51, we can see that AGB stars have somewhat higher masses than RGB stars, and that is expected, but HB stars seems to have much higher masses than AGB and RGB stars. That is not as expected. HB stars should have masses in the between of AGB and RGB stars. That shows that BEAST do not perform

well in determination of the masses of HB stars.

The procedure to create the H-R diagram with stellar parameters on the z axis is described in the appendix A.7.

11.3.2 M13: H-R diagram

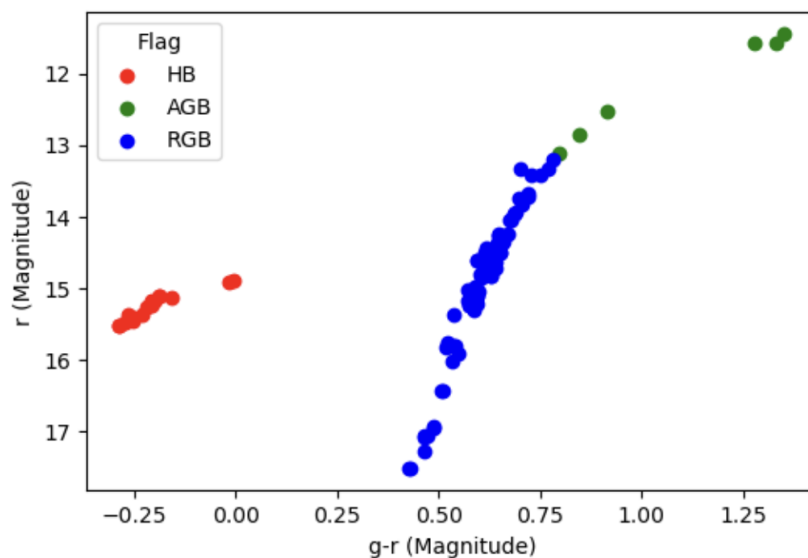


Figure 53: H-R diagram for M13.

H-R diagram for M13 is shown in figure 53. Red are HB stars, green are AGB stars, and blue are RGB stars. It is hard to distinguish between AGB and RGB stars. It is also possible that stars with $g-r > 0.6$ that we marked as AGB stars are also RGB stars that are on tip of their RGB part of evolution. It is also possible that all of these stars with $g-r > 0.6$ are AGB stars. In M13, HB stars are easy to distinguish, as well as lower luminosity RGB stars. It is hard to distinguish between higher luminosity RGB stars and AGB stars.

H-R diagrams for all six stellar parameters that we analyzed:

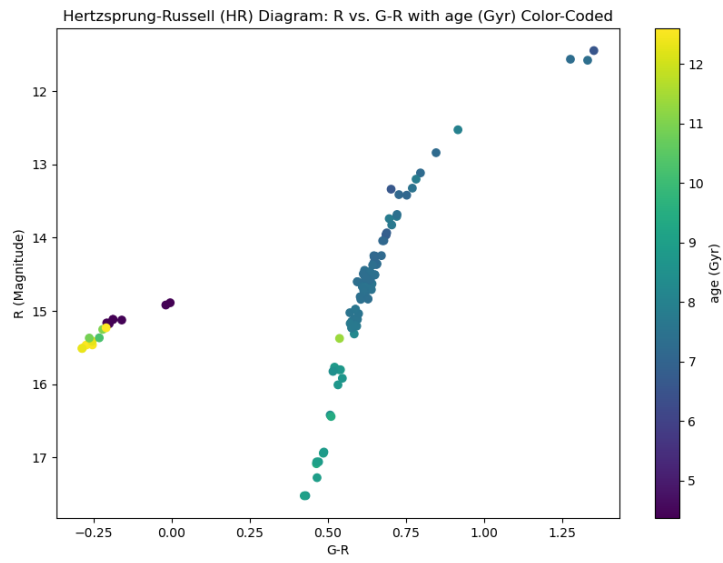


Figure 54: H-R diagram of M13 giants for age.

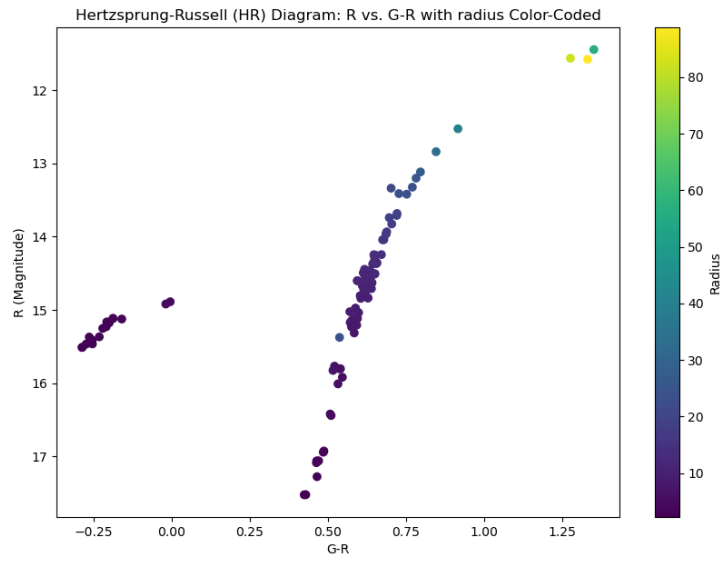


Figure 55: H-R diagram of M13 giants for radius.

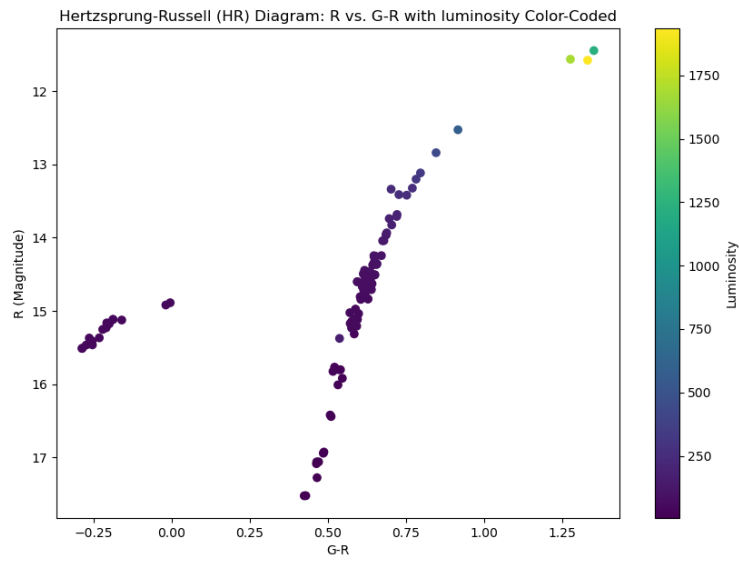


Figure 56: H-R diagram of M13 giants for luminosity.

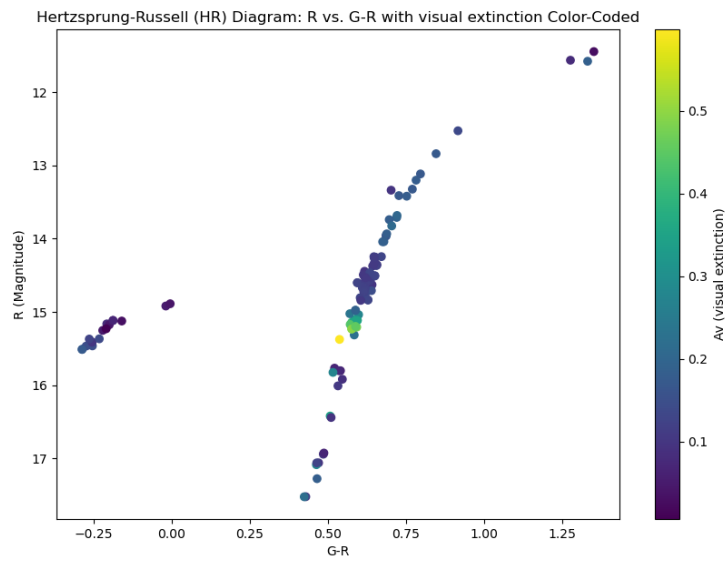


Figure 57: H-R diagram of M13 giants for visual extinction.

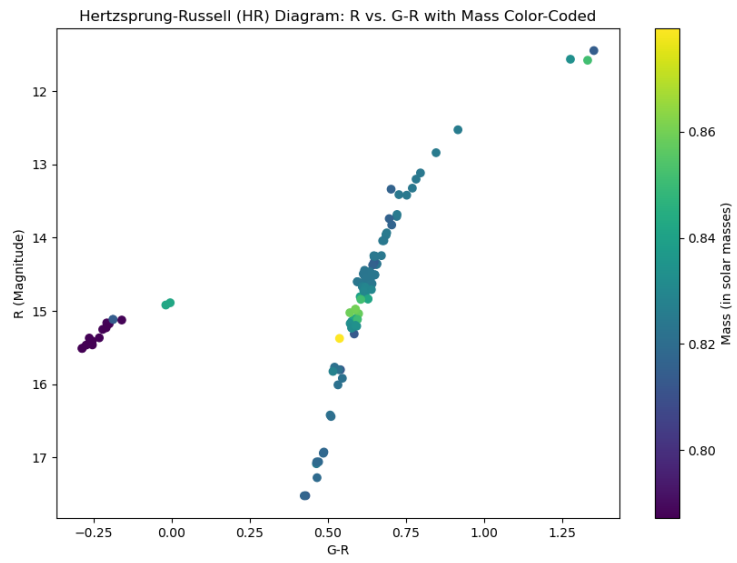


Figure 58: H-R diagram of M13 giants for mass.

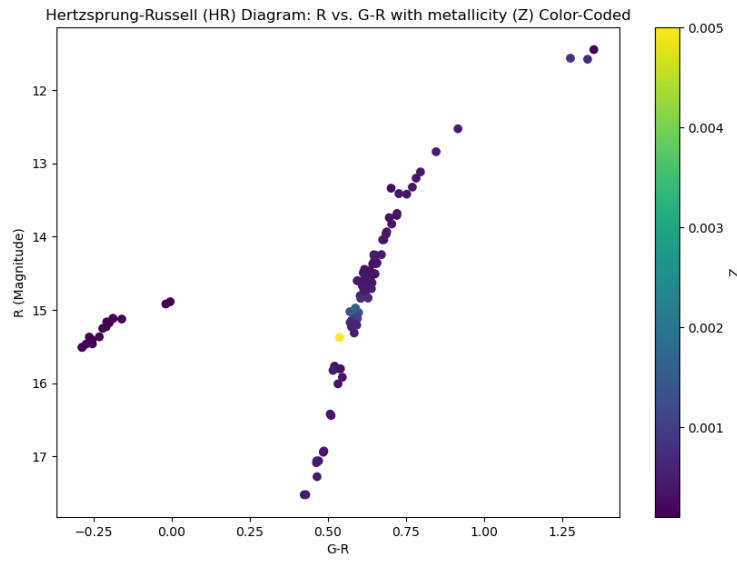
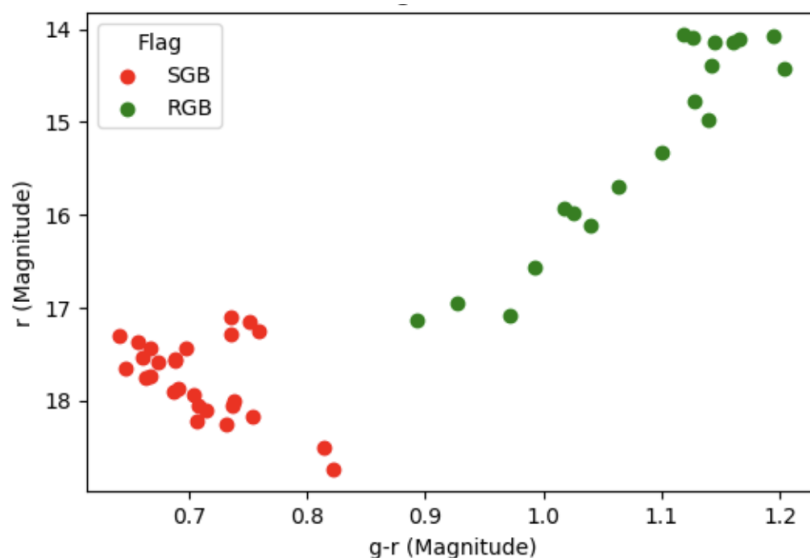


Figure 59: H-R diagram of M13 giants for metallicity.

In M13 we face the same problem as for M92. The age of half of the HB stars seems too large, compared to age of AGB and RGB stars. Age of RGB and AGB stars are similar, as expected. All other parameters seems to behave as expected. The radius is larger for AGB then for RGB stars, especially for high luminosity AGB stars. Luminosity behaves similar to stellar radius. Extinction is low in general and it seems somewhat higher for AGB stars, as expected there is a group of RGB stars that seems to have higher masses and extinction, but that could be a bogus. Besides that, HB stars seems to have the lowest masses and AGB and RGB stars seems to have similar masses, although AGB stars seems to be of higher masses, as expected. Metallicity is low and similar for all types of giants. Even the mass for HB stars was calculated much better. Now it is even a little bit smaller than AGB and RGB stars, but is still good.

11.3.3 NGC 6791: H-R diagram



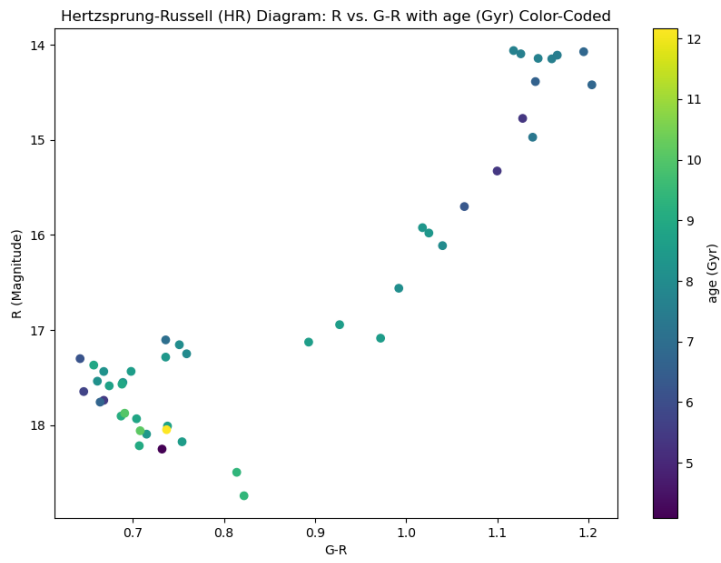


Figure 61: H-R diagram of NGC 6971 giants for age.

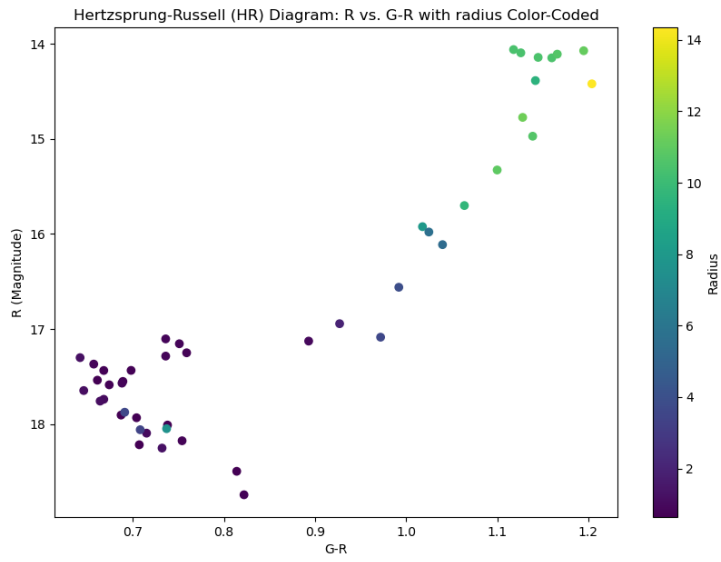


Figure 62: H-R diagram for radius.

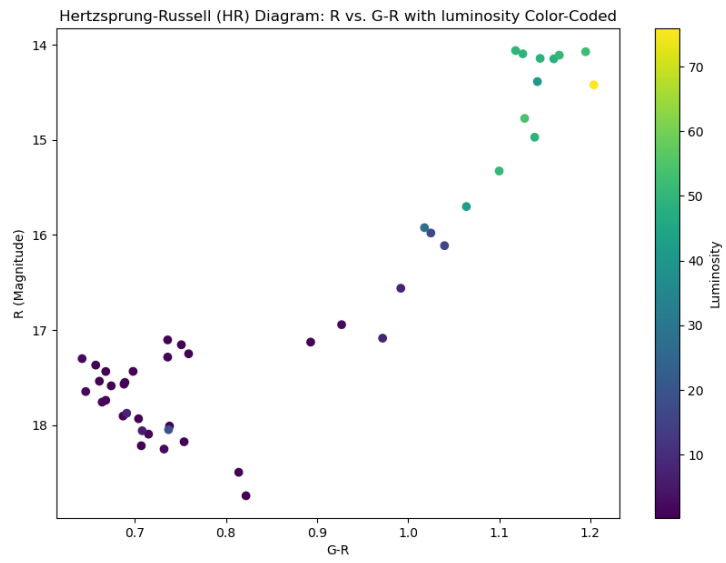


Figure 63: H-R diagram of NGC 6971 giants for luminosity.

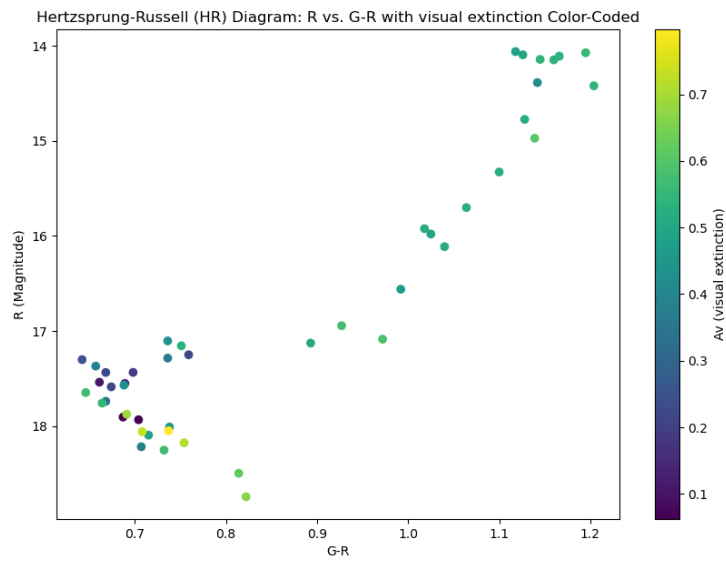


Figure 64: H-R diagram of NGC 6971 giants for visual extinction.

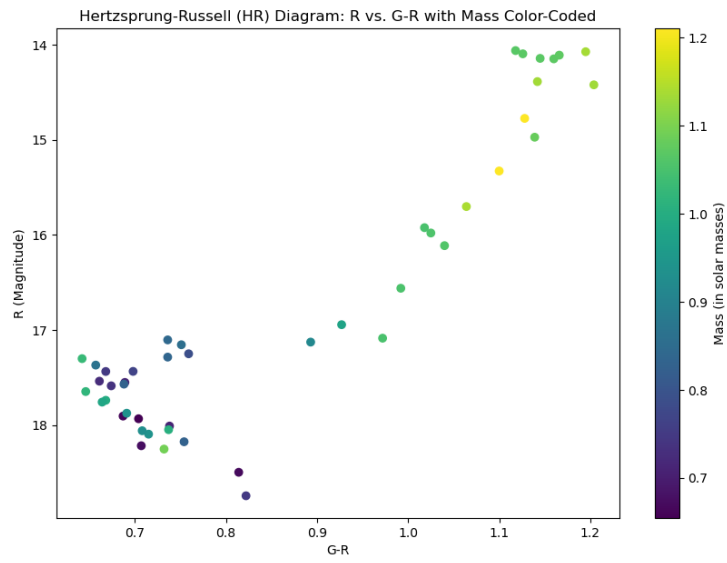


Figure 65: H-R diagram of NGC 6971 giants for mass.

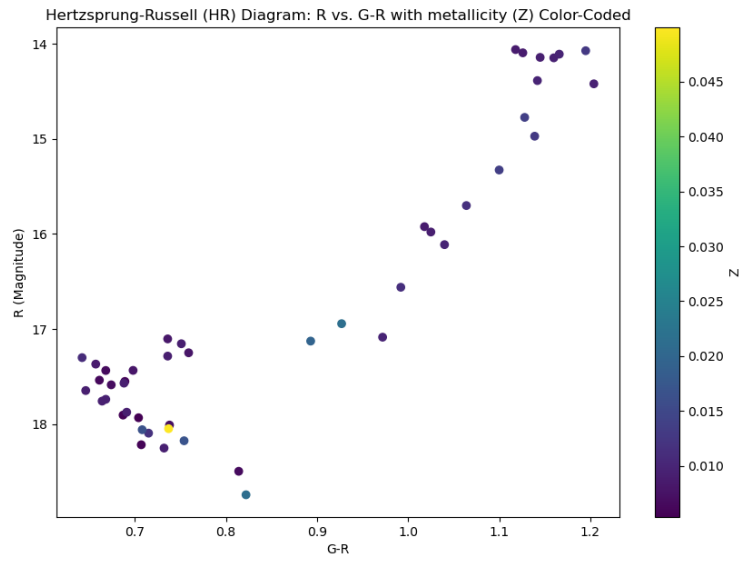


Figure 66: H-R diagram of NGC 6971 giants for metallicity.

It seems that all of the stars in NGC 6791 are of the same age, as expected, which is shown in figure 61. Age is much better determined than for stars in M92 and M13 cluster.

As expected, stellar radii are larger for RGB than for SGB stars, increasing toward the tip of the red giant branch, as it is shown in figure 62.

Luminosity is shown in figure 63. Luminosity is behaving as expected, similar to radii - the reddest RGB stars, nearer to the tip, have the highest luminosities.

Extinction seems to be higher for RGB stars than for SGB stars, as they have higher mass loss and stronger stellar wind. This is shown in figure 64.

RGB stars, especially the redder ones, seem to have higher masses, as expected. This is shown in figure 65. Higher mass stars evolve more rapidly, so it is expected for SGB stars to be less evolved and of lower mass than RGB stars. Notice that the stellar masses for SGB and RGB stars in younger open cluster NGC 6791 are considerably higher than RGB and HB stars in older globular clusters M13 and M92.

Again, metallicity seems to be the same for both RGB and SGB stars, as expected.

Beast determined the stellar properties very well for NGC 6791. It calculated stellar parameters as they are expected to be. In figure 61, we see that SGB stars are a bit younger than RGB stars. In figure 62, we see that SGB stars have lower radius than RGB stars, as expected. Same thing is with luminosity and mass.

Conclusion

To conclude, we determined all stellar parameters of giants in 3 clusters very well, with the exception of stellar age, which requires more strict prior.

11.4 Relationships between stellar parameters

We can also analyse the relationship between some stellar parameters.

11.4.1 M92: Relationships between stellar parameters

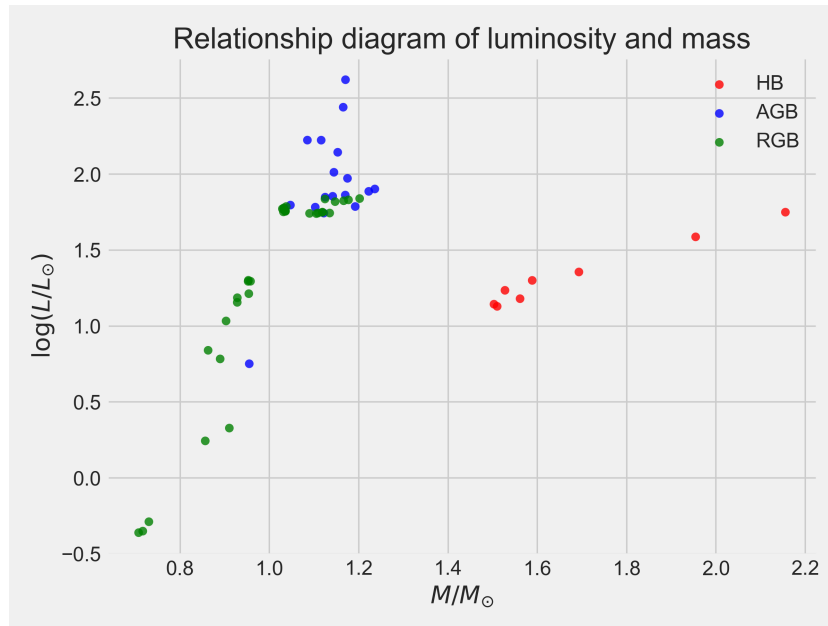


Figure 67: Relationship between stellar luminosity and its mass for M92 giants.

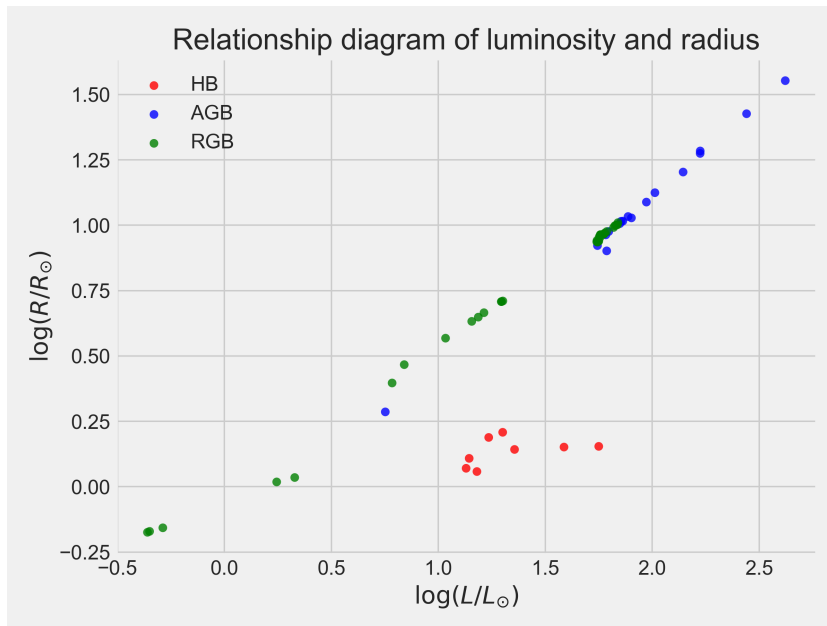


Figure 68: Relationship between stellar luminosity and its radius for M92 giants.

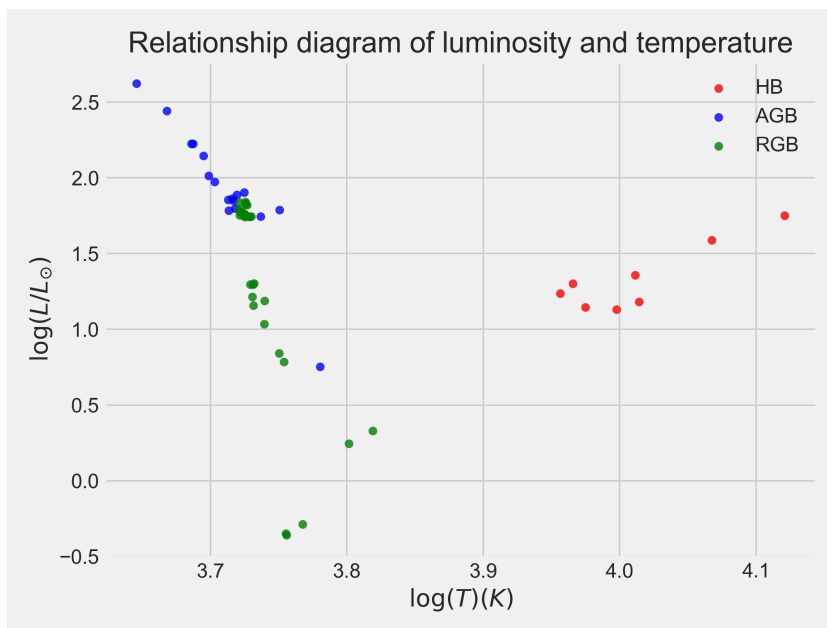


Figure 69: Relationship between stellar luminosity and temperature for M92 giants.

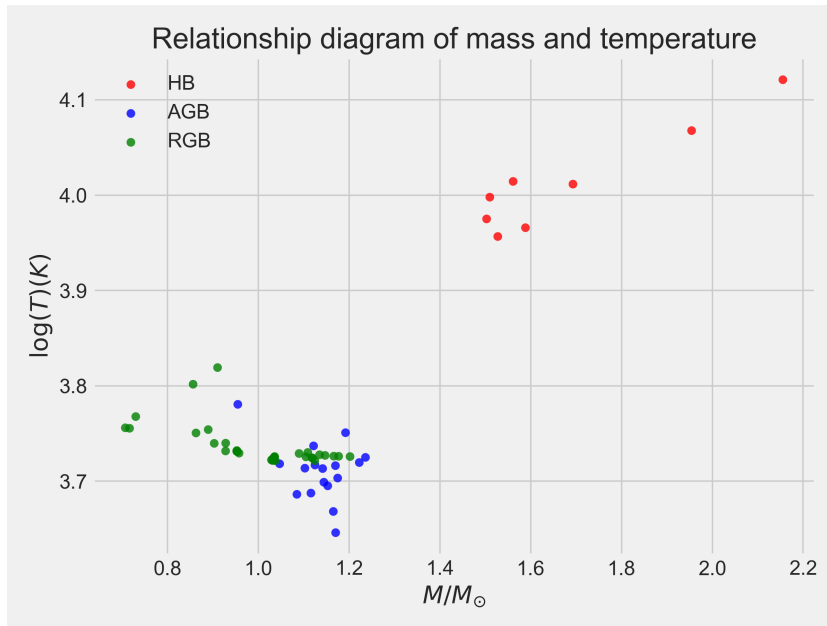


Figure 70: Relationship between stellar mass and its temperature for M92 giants.

The relationship between stellar luminosity and its radius, shown in figure 68 is in logarithmic scale, and we got linear logarithmic correlation between these parameters, as expected. We see that AGB stars have larger radius than RGB stars, as expected. A higher radius is responsible for higher luminosity, which can we also see in the graph. AGB stars shows around 10 times larger radii than RGB stars, as expected. HB stars are somewhere in the middle of an AGB and RGB star with luminosity and radius. This graph is in great correlation with theory.

The relationship between stellar luminosity and temperature is shown in figure 69. HB stars have the highest temperatures (around 10000 K). This makes sense because HB stars generally have higher temperatures compared to RGB and AGB stars due to helium fusion in their cores. Again, luminosity is the highest and the temperature the lowest for AGB stars, as they are the largest in the sample.

The relationship between stellar mass and its temperature is shown in figure 70. AGB stars have larger mass and lower temperature than RGB stars, which is in agreement with theory. AGB stars have lower temperature because they have a larger radius than RGB stars. They are also more evolved because they have a larger mass. HB stars should have a mass somewhere in between of the RGB and AGB stars, but on the graph we see that they have much higher mass. We can conclude that BEAST is not capable of performing precise calculations for the mass of HB stars. That is not a big problem because we do not have that many HB stars.

AGB stars larger masses than RGB stars, which is expected according to the stellar evolution. More massive stars evolve more rapidly towards AGB phase. HB stars have masses in between, as expected from the evolutionary standpoint. Luminosity increases linearly with mass in logarithmic scale, which is in accordance with theory.

Although, it seems that luminosity of HB stars is well determined (between RGB and AGB stars), it seems that their masses are overestimated and cannot be precisely determined.

The script for plotting various astrophysical relationships can be found in Appendix A.8.

11.4.2 M13: Relationships between stellar parameters

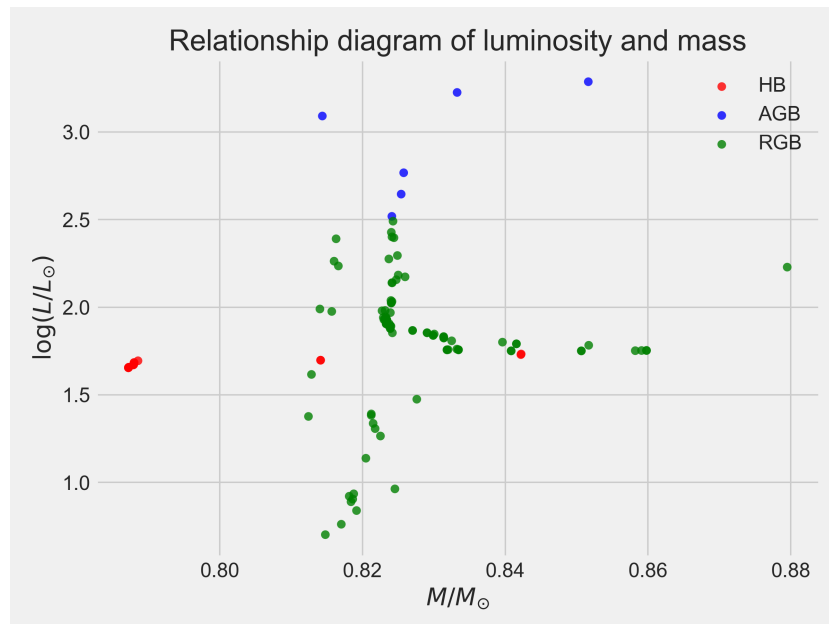


Figure 71: Relationship between stellar luminosity and its mass for M13 giants.

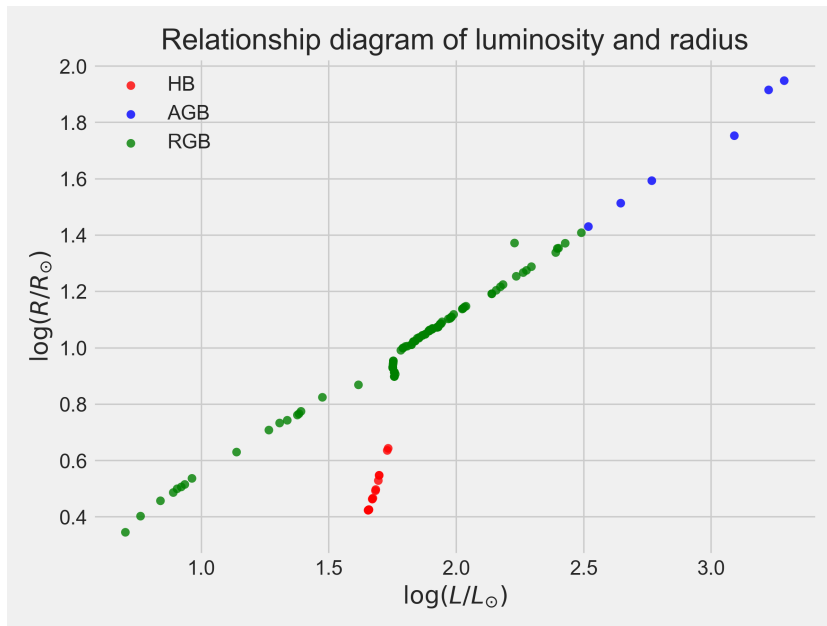


Figure 72: Relationship between stellar luminosity and its radius for M13 giants.

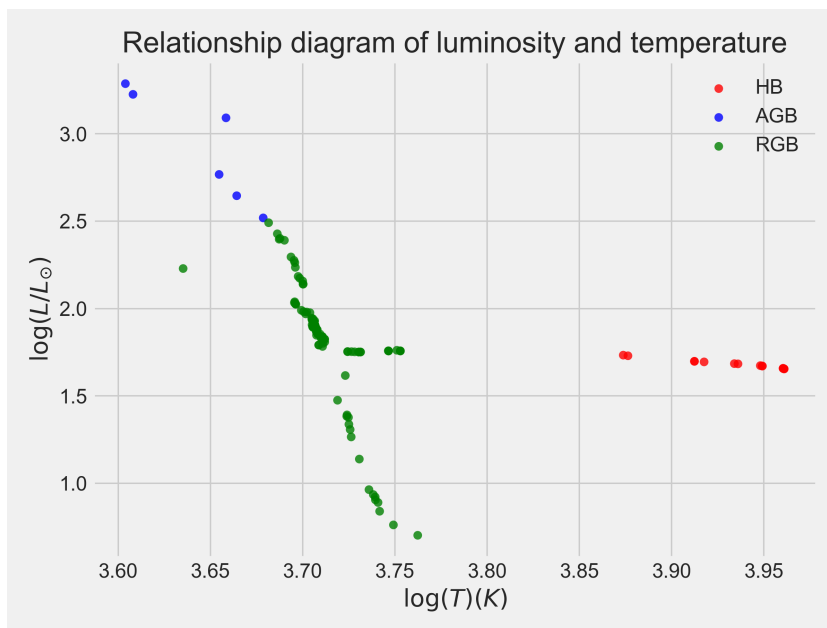


Figure 73: Relationship between stellar luminosity and temperature for M13 giants.

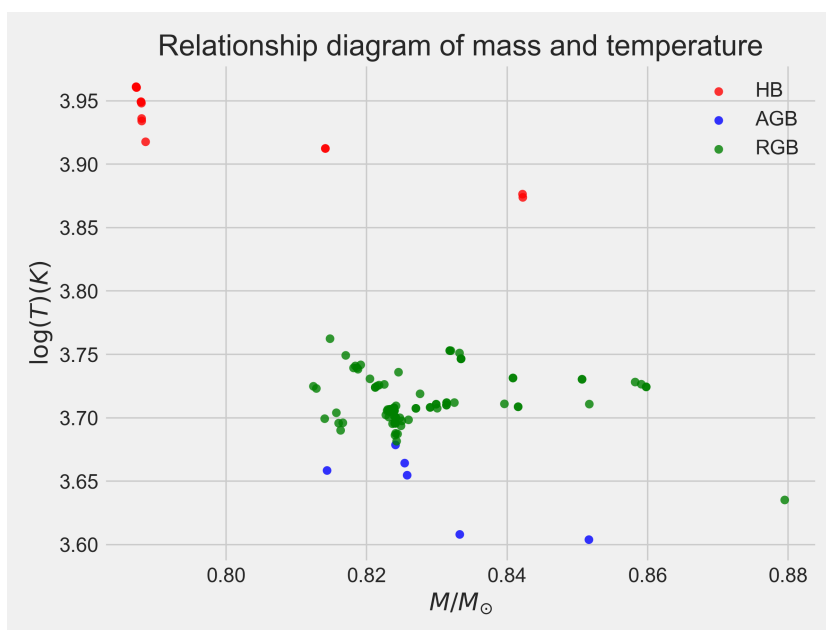


Figure 74: Relationship between stellar mass and its temperature for M13 giants.

For M13 we have the same story as we had for M92. AGB stars have higher luminosities and radii than RGB stars, as expected, with luminosities of HB stars in between. For M13, HB stars have lower radii than RGB stars. We can see that in figure 72. This is expected as HB stars increase their temperature and contract after their RGB phase, decreasing the radii.

HB stars also have higher temperatures than AGB and RGB stars, figure 73.

The behaviour of luminosity with stellar masses in M13 is much less clear than in M92, although the correlation is visible. Notice that the range of masses is much lower in M13 than in M92, so the correlation is less visible. That is shown in figure 71.

The only difference in M13 compared to the results for M92 is that now BEAST obtained much better masses for HB stars. Now, masses of HB stars are similar to masses of the AGB and RGB stars, even being slightly lower. That indicates that BEAST can precisely calculate masses for HB stars, but not very consistently. We can see that on figures 74 and 71.

11.4.3 NGC 6791: Relationships between stellar parameters

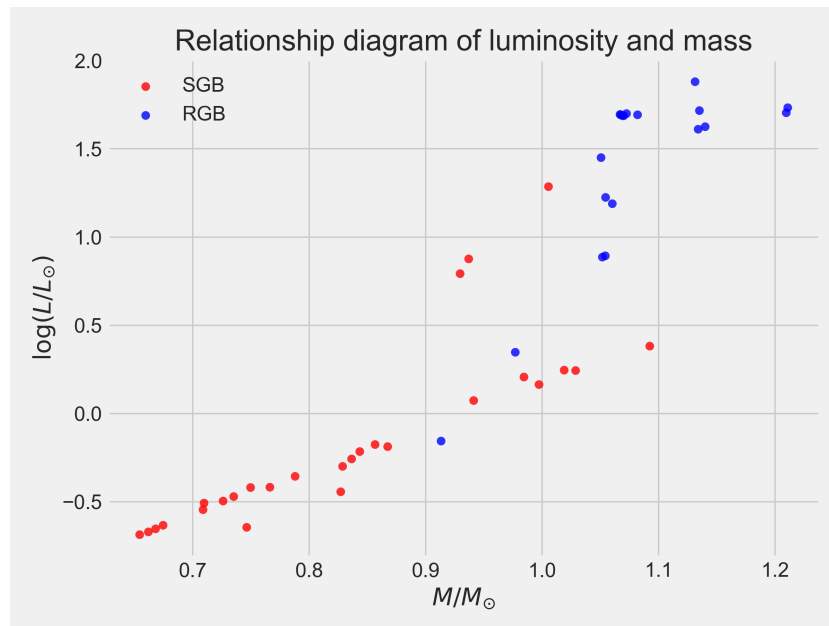


Figure 75: Relationship between stellar luminosity and its mass for NGC 6791 giants.

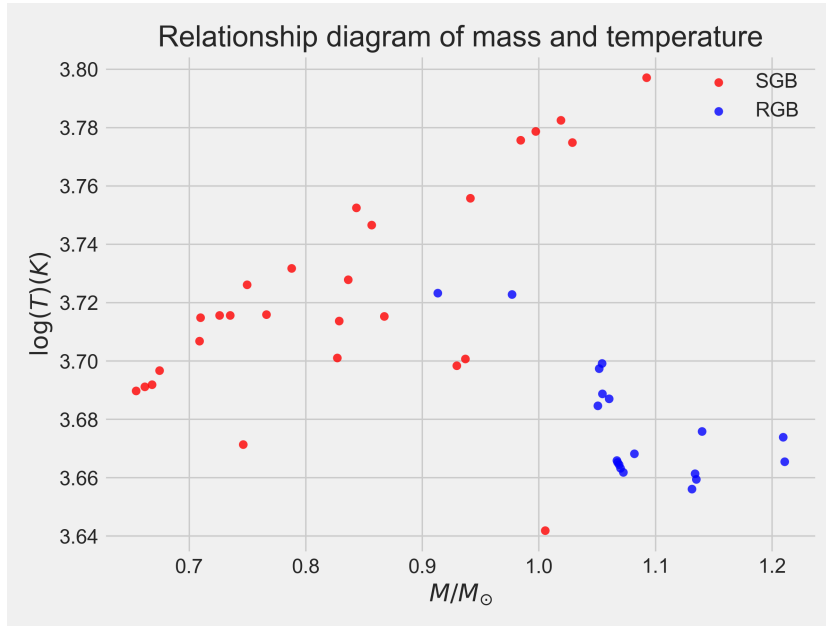


Figure 78: Relationship between stellar mass and its temperature for NGC 6791 giants.

For open cluster NGC 6791 we only have SGB and RGB stars, while we had RGB, HB, and AGB stars in two clusters before. But, we can still see some similarities. Similarly to clusters before, we can still see that for the relationship between stellar luminosity and its radius we can see a linear correlation, which indicates a logarithmic correlation between the two of these parameters. SGB stars are in a transitional phase where they have exhausted the hydrogen in their cores but are still burning hydrogen in a shell around the core. They tend to be hotter and slightly more luminous than main-sequence stars, but are not as cool or luminous as RGB stars. RGB stars are in a later evolutionary stage, where they have expanded significantly and cooled. They are cooler on the surface, giving them their characteristic red color, but they are much more luminous as a result of their larger size. We can see this in figures 76 and 77. It can clearly be seen that RGB stars have larger radii and luminosity than SGB stars 76. At the same time SGB stars are showing a decrease in luminosity as they get redder (cooler). RGB stars are cooler and significantly more luminous than SGB stars. As their luminosity increases they become cooler 77.

Luminosity - mass relation 75 for both SGB and AGB stars follows linear correlation, as expected, with more luminous RGB stars being more massive and thus more evolved than SGB stars.

Their masses are similar in theory, in figures 78 and 75 we see that BEAST

calculated that RGB stars have slightly higher masses, but this is still really good.

Open cluster differs significantly from two closed clusters M13 and M92, as it is much younger. So we expect to observe more massive stars as giants and subgiants in post main-sequence phase.

11.5 M92: Comparison between stellar parameters calculated with distance set as constant and distance being variable

Ideally, stellar parameters should be determined accurately regardless the distance to the star. In reality, the accuracy of determined stellar parameters can heavily depend on accuracy of distance determination. Therefore, BEAST also determines distance, and we wanted to analyse how much distance determination influences each of the stellar parameter. The value of the distance determined by the other authors from stellar parallax is 8.2 kpc [29], and BEAST measured distance is 5.46 kpc, which is not excellent.

In BEAST calculations, all parameters are based on distance and if we get distance wrong, then other parameters will be wrong as well. So, we wanted to determine how much the distance is influencing determination of other stellar parameters. In the following graphs, we will see that some parameters nicely follow the $y = x$ line, some are linearly correlated, and other not so much. Line $y=x$ is dotted red line on the graphs. No influence of the distance would be shown if all data followed that line.

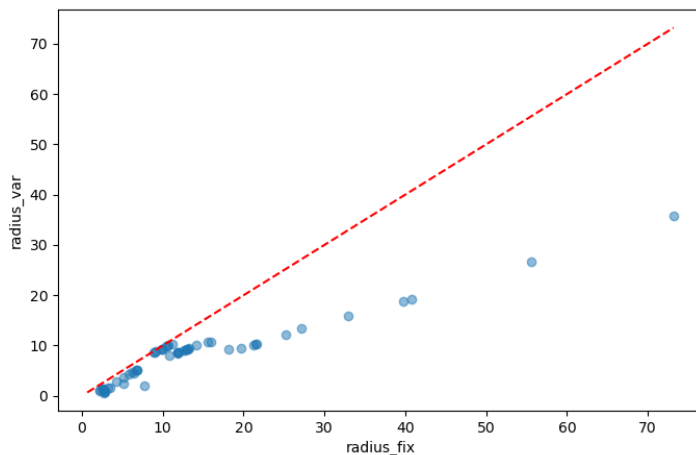


Figure 79: Comparison between radius of stars with fixed distance and with distance being a free parameter.

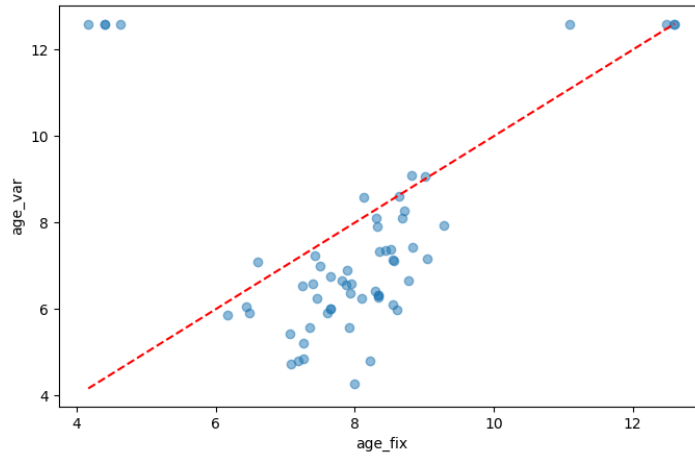


Figure 80: Comparison between age of stars with fixed distance and with distance being a free parameter.

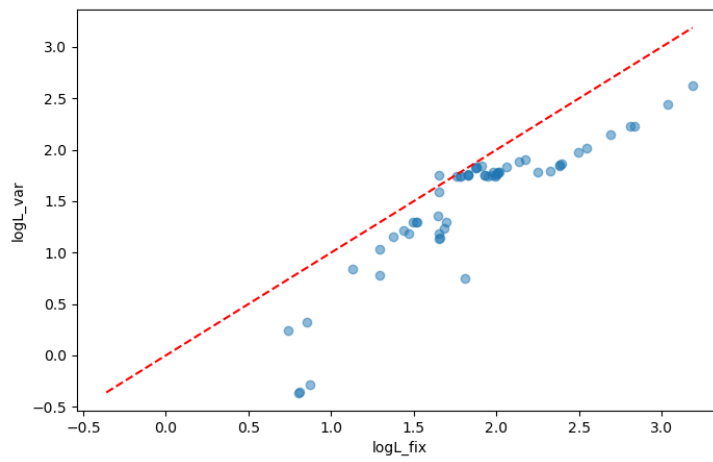


Figure 81: Comparison between luminosity of stars with fixed distance and with distance being a free parameter.

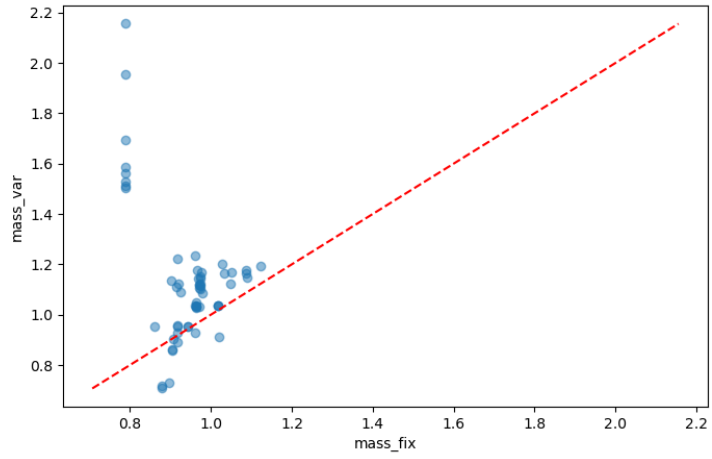


Figure 82: Comparison between mass of stars with fixed distance and with distance being a free parameter.

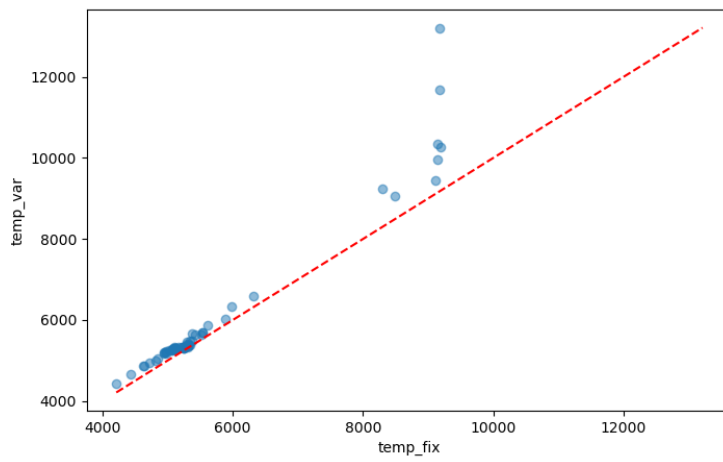


Figure 83: Comparison between temperature of stars with fixed distance and with distance being a free parameter.

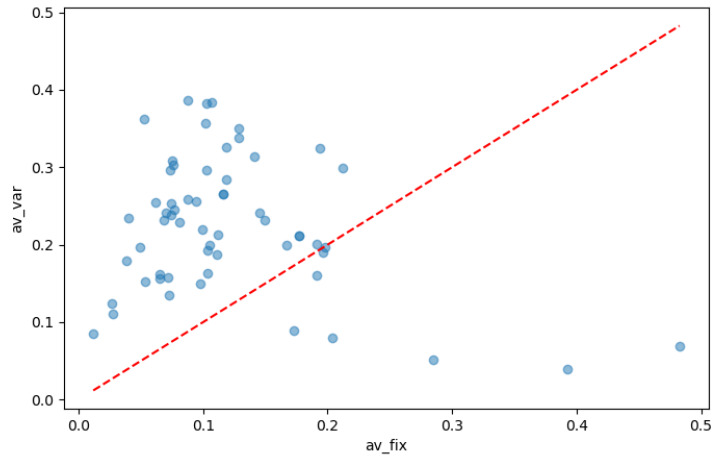


Figure 84: Comparison between visual extinction of stars with fixed distance and with distance being a free parameter.

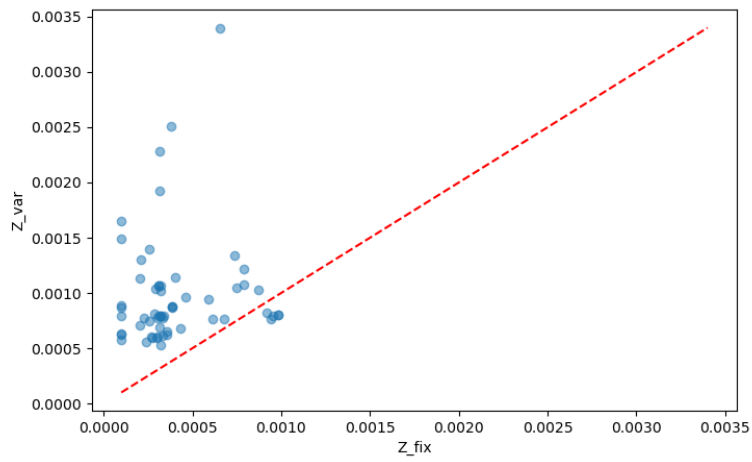


Figure 85: Comparison between metallicity of stars with fixed distance and with distance being a free parameter.

We can see in figure 79, that the radius for fixed and for variable distance calculations is following a linear relationship almost perfectly for small radii stars (up to $10 R_{\odot}$). But for stars with higher radii BEAST starts to underestimate it when we do not provide the correct distance (we put it as variable) in BEAST analysis.

That is caused by BEAST calculating that M92 is closer to us than it actually is. If the BEAST determines that stars are closer to us than they actually are, their luminosities will be smaller than they actually are. That is seen in figure 81 by the data on the graph being below $x=y$ line, although they follow red line parallelly very well.

Stellar ages are also underestimated by ~ 2 Gyrs when distance is free parameter. The stellar mass seems not influenced significantly by the distance, except for the few stars that were miscalculated, with very high masses, when the distance is free parameter, becoming stars with the lowest masses if distance is provided.

Determination of the distance does not influence temperature determination, except for the few hottest stars above 8000K.

Extinction is overestimated by ~ 0.2 magnitudes when distance is free parameter.

Metallicity is rather low regardless the distance determination, although it seems overestimated when the distance is free parameter.

We can see that in all of the graphs, most of the dots are around $x=y$ line with few stars being exceptions and probably being poorly calculated. Graphs are generally good.

The python script for plotting comparison between stellar parameters calculated with distance set as constant and distance being variable can be found in Appendix A.9.

11.6 M13: Comparison between stellar parameters calculated with distance and age set as constant and distance and age being variable

As we said, age cannot be set as constant in the BEAST, but we can set it in a very narrow range. Other authors have determined that the age of M13 to be around 11.65 Gyr [37], so we set age range to be between 10 and 13.5 Gyr. Other studies have obtained the value of distance for M13 of 7.87 kpc [34] and BEAST calculated it to be 5.01 kpc which can be considered acceptable.

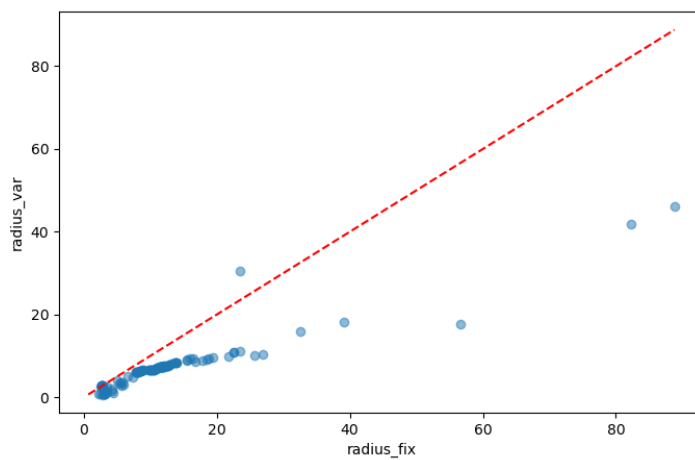


Figure 86: Comparison between radius of stars with fixed distance and age and with distance and age being a free parameter.

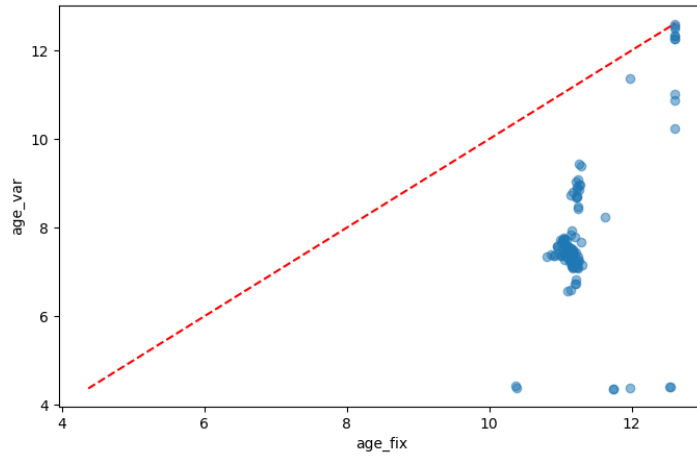


Figure 87: Comparison between age of stars with fixed distance and age and with distance and age being a free parameter.

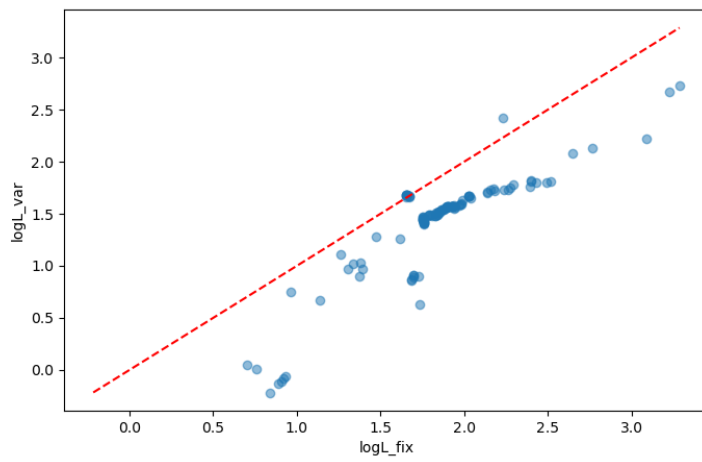


Figure 88: Comparison between luminosity of stars with fixed distance and age and with distance and age being a free parameter.

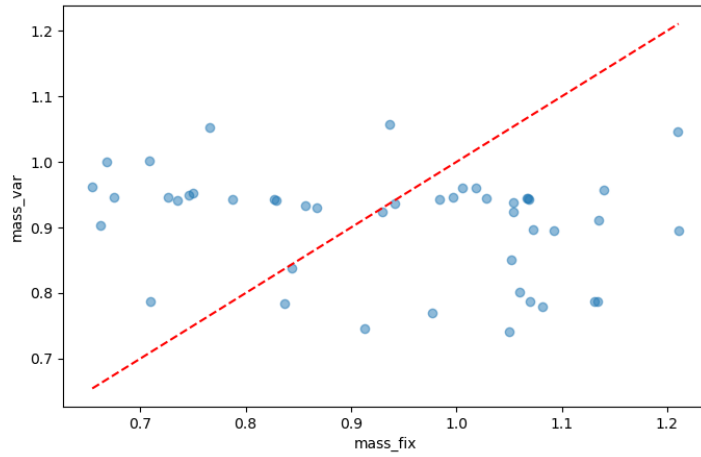


Figure 89: Comparison between mass of stars with fixed distance and age and with distance and age being a free parameter.

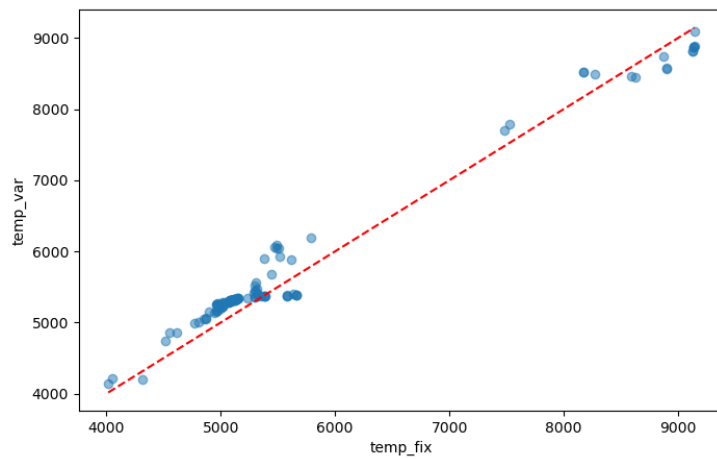


Figure 90: Comparison between temperature of stars with fixed distance and age and with distance and age being a free parameter.

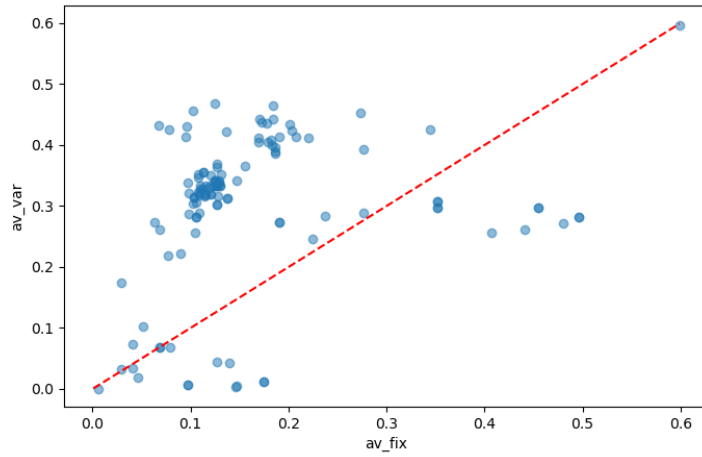


Figure 91: Comparison between visual extinction of stars with fixed distance and age and with distance and age being a free parameter.

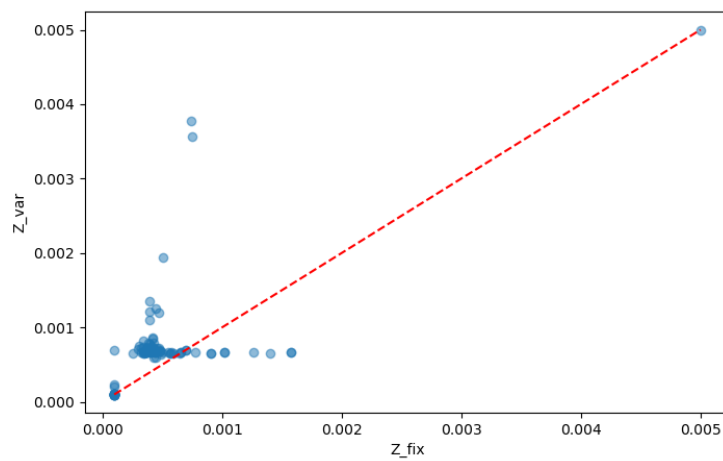


Figure 92: Comparison between metallicity of stars with fixed distance and age and with distance and age being a free parameter.

For M13 we see similar behaviour as for M92. Exception is that for M13 we did not only put distance as a constant in second BEAST analysis, but we also narrowed the age interval. We can see that in figure 87, that when we let BEAST determines age as almost free parameter (from 4 to 13.5 Gyr), age of the stars is underestimated and that is why the data are below the $x=y$ line. Other parameters are determined much better when compared to the values obtained with fixed distance and stellar age, being located around $x=y$ line, with some being better like for temperature and some being less good like for visual extinction.

As can be seen on 80 for M92 cluster, distance does not influence too significantly determination of the stellar age. Still, BEAST underestimate stellar age significantly when compared to expected value, by $\sim 30\%$. Fixing age and distance does not influence determination of the stellar radii up to $10 R_{\odot}$, similar to M92. Larger radii are underestimated when distance and stellar age are free parameters.

Luminosities are well determined, although slightly underestimated due to underestimated distance determined by BEAST like for M92.

Comparison of obtained stellar masses cannot be performed as the mass interval is very narrow. Distance and stellar age determination of the stellar effective temperatures.

Similarly, obtained metallicity remains low regardless of fixing distance and stellar age.

Finally, dust extinction is overestimated by ~ 0.15 magnitudes, mainly due to underestimate distance and not stellar age, like for M92, see figure 84.

12 Comparison with values from other studies

12.1 M92 - Comparison

Distance to the M92 from our solar system is 8.2 kpc (26700 ly) [29].

Some scientific papers estimate that the age of the cluster is around 11 Gyr [31] and some others to be 13.18 Gyr [56].

Some scientific papers estimate its metallicity to be 0.0051 [30], while others estimate it to be 0.007 [56]. We took the value of $Z = 0.00007310$ [57] which we can round to 0.0001 because it is that small that BEAST cannot compute such a small value for metallicity.

Also, M92 visual extinction in magnitude $A_v = 0.0568$ [58]. That is, the average of visual extinction in magnitudes for all bands. Its ratio of total to selective extinction $R_v = 3.1$ [58].

The BEAST calculated mean distance to be equal to 5.46 kpc. To calculate the accuracy of a obtained value by BEAST compared to a value from literature, we can use the following equation:

$$\text{Accuracy (\%)} = \left(1 - \frac{|\text{BEAST Value} - \text{Value from literature}|}{\max(\text{Value from literature}, \text{BEAST Value})} \right) \times 100 \quad (40)$$

The distance value from our BEAST analysis has the accuracy of measurement at 66.6%. That accuracy can be considered acceptable, although not excelent.

For metallicity, we get 0.0004. That shows that we have low metallicity, as expected for an old cluster. The theoretical value is 0.0001 but BEAST does not allow such small values, so the obtained value is as good as it gets.

The age of 7.45 Gyr was determined by BEAST. That is actually quite acceptable, because we know that this cluster is really old, but we do not know exactly how old it is. If we take the age to be 11 Gyr from the literature [31], that gives us the accuracy of 67.73%. Since 11 Gyr from literature has an error of 1.5 Gyr, our value of 7.45 Gyr does fall into two sigma interval of 11 ± 1.5 Gyr.

For visual extinction in magnitude we got $A_v = 0.12$ which has an accuracy of 47.33% and for the ratio of total to selective extinction, $R_v = 2.76$ we got an accuracy of 89.03%.

It can be seen that our analysis underestimates the distance and stellar age of M92 cluster, while dust extinction is overestimated. We have also performed analysis with fixed distance and stellar age, but no significant changes or improvements were achieved.

We can see all of the average stellar values and one sigma uncertainty intervals for M92 and its accuracies in the table below:

Table 3: Values of stellar parameters for M92, when distance is variable

	This work	Other works	accuracy
distance (kpc)	5464^{+2679}_{-2590}	8200 ref:[29]	66.63%
Age (Gyr)	$7.84^{+3.89}_{-2.93}$	11.0 ± 1.5 ref:[31]	71.27%
Mass initial (M_{\odot})	$0.92^{+0.12}_{-0.1}$		
log Luminosity ($\log L_{\odot}$)	$1.35^{+0.39}_{-0.46}$		
Luminosity (L_{\odot})	$22.4^{+32.6}_{-14.7}$		
Temperature (K)	5691^{+270}_{-199}		
Metallicity	$0.0008^{+0.0023}_{-0.0006}$	0.0001 ref:[57]	12.5%
Radius (R_{\odot})	$6.53^{+3.32}_{-3.08}$		
log g ($\log m/s^2$)	$3.02^{+0.5}_{-0.4}$		
Av	$0.2^{+0.2}_{-0.16}$	0.0568 ref:[58]	28.4%
Rv	$2.76^{+0.24}_{-0.21}$	3.1 ref:[58]	89%

Table 4: Values of stellar parameters for M92, when distance is constant

	This works	Other works	accuracy
Age (Gyr)	$7.45^{+3.27}_{-2.17}$	11.0 ± 1.5 ref:[31]	67.73%
Mass initial (M_{\odot})	$0.94^{+0.12}_{-0.1}$		
log Luminosity ($\log L_{\odot}$)	$1.86^{+0.0}_{-0.0}$		
Luminosity (L_{\odot})	$71.9^{+6.4}_{-4.9}$		
Temperature (K)	5571^{+129}_{-116}		
Metallicity	$0.0004^{+0.001}_{-0.0003}$	0.0001 ref:[57]	25%
Radius (R_{\odot})	$13.11^{+0.46}_{-0.46}$		
log g ($\log m/s^2$)	$2.48^{+0.05}_{-0.06}$		
Av	$0.12^{+0.13}_{-0.09}$	0.0568 ref:[58]	47.33%
Rv	$2.76^{+0.23}_{-0.22}$	3.1 ref:[58]	89.03%

Even tho, the distance is underestimated, expected value of 8.2 is within + 2 sigma error.

Expected value of age of the cluster, its metallicity and dust extinction does get in + one sigma error.

AGB, RGB and HB stars we analysed in M92 are very old and of mass $\sim 0.92 M_{\odot}$, luminosities of $\sim 22 L_{\odot}$, radius $\sim 6.5 R_{\odot}$, temperature ~ 5700 K and low metallicity.

We tried to determine influence of the distance on the determination of the other parameters in a way that we fixed distance. Fixing the distance on a value obtained by other methods did not significantly affect other parameters. Fixing the age did somewhat lower the age of the cluster and lowered and improved de-

termination of the metallicity and dust extinction. Fixing the distance did not significantly affect determination of the stellar masses and it lowered temperature by ~ 100 K. On the other hand, fixing the distance did significantly increase luminosities (from 22 to $72 L_{\odot}$) and radii (from 6.5 to $13.1 R_{\odot}$) of stars, as expected.

12.2 M13 - Comparison

Distance to the M92 from our solar system is estimated to be 7.87 kpc (26700 ly) [34].

The newest scientific papers estimate that the age of the cluster is 11.65 Gyr [37] and its metallicity to be 0.0005 [36].

Also, M13 visual extinction in magnitude $A_v = 0.012$ [38]. Its ratio of total to selective extinction $R_v = 3.1$ [38].

With that we can calculate the accuracies. BEAST gave us the value of distance to be 5.01 kpc, which corresponds to an accuracy of 63.67%. The value of 7.87 kpc from other studies is a little bit outside of one sigma uncertainty interval, but well inside two sigma.

For metallicity, we get 0.00048. That shows that we have very low metallicity, as expected for a globular cluster. The accuracy of 96% is excellent.

BEAST calculated age of M13 cluster to be 7.67 Gyr with the accuracy of 65.84%. Cluster age of 11.65 Gyr from other studies is on the edge of one sigma uncertainty interval.

For visual extinction in magnitude we obtained $A_v = 0.16$ which has very good accuracy of 87.5%, with the literature value well inside one sigma uncertainty interval. And for ratio of total to selective extinction, $R_v = 3.49$ which has accuracy of 88.83%, also very good.

We can see all of the average stellar values and their one sigma uncertainties for M13 and its accuracies in the table below:

Analysed AGB, RGB and HB stars in M13 cluster are very old, similar to M92. Mass is $\sim 0.92 M_{\odot}$, luminosity $\sim 27 L_{\odot}$ and radius $\sim 7.1 R_{\odot}$, temperature around 5700 K and low metallicity.

Stars analysed in M13 globular cluster are very similar to the star analysed in the M92 cluster, which is expected based on the age of these globular clusters. Big difference is only in metallicity, where M13 has much bigger metallicity than M92, even tho both of these clusters are very low in metals. And also dust extinction is somewhat higher in M13 than in M92.

We tried to determine the impact of the distance on determination of the other parameters by fixing the distance. Fixing the distance to the values obtained by the other methods had a great impact on the determination of other stellar parameters. It increased age significantly from 7.7 to 11.3 Gyr, which increased accuracy to 97%, which is excellent. It also lowered dust extinction and metallicity

Table 5: Values of stellar parameters for M13, when distance and age are variables

	This works	Other works	accuracy
distance (kpc)	5011^{+2413}_{-2104}	7870 ref:[34]	63.67%
Age (Gyr)	$7.67^{+3.95}_{-2.86}$	11.65 ref:[37]	65.84%
Mass initial (M_{\odot})	$0.92^{+0.14}_{-0.1}$		
log Luminosity ($\log L_{\odot}$)	$1.43^{+0.36}_{-0.46}$		
Luminosity (L_{\odot})	$27.1^{+34.5}_{-17.9}$		
Temperature (K)	5682^{+215}_{-212}		
Metallicity	$0.0007^{+0.0005}_{-0.0005}$	0.0005 ref:[36]	71.43%
Radius (R_{\odot})	$7.14^{+3.19}_{-3.18}$		
log g ($\log m/s^2$)	$2.92^{+0.51}_{-0.35}$		
Av	$0.3^{+0.17}_{-0.18}$	0.012 ref:[38]	40%
Rv	$3.56^{+0.89}_{-0.84}$	3.1 ref:[38]	87.08%

Table 6: Values of stellar parameters for M13, when distance and age are constant

	This works	Other works	accuracy
Age (Gyr)	$11.29^{+1.27}_{-1.11}$	11.65 ref:[37]	96.91%
Mass initial (M_{\odot})	$0.82^{+0.03}_{-0.02}$		
log Luminosity ($\log L_{\odot}$)	$1.84^{+0.03}_{-0.04}$		
Luminosity (L_{\odot})	$69.2^{+5.7}_{-5.8}$		
Temperature (K)	5519^{+90}_{-128}		
Metallicity	$0.00048^{+0.00004}_{-0.0003}$	0.0005 ref:[36]	96%
Radius (R_{\odot})	$12.15^{+0.48}_{-0.41}$		
log g ($\log m/s^2$)	$2.42^{+0.03}_{-0.04}$		
Av	$0.16^{+0.13}_{-0.12}$	0.012 ref:[38]	87.5%
Rv	$3.49^{+0.88}_{-0.87}$	3.1 ref:[38]	88.83%

and significantly improved their determination. Fixing the distance did lower stellar masses from $0.92 M_{\odot}$ to $0.82 M_{\odot}$ and lowered temperature by ~ 150 K. But, fixing the distance significantly increased stellar luminosities (from 27 to 69 L_{\odot}) and radii (from 7.1 to 12.1 R_{\odot}), as expected.

Similar to M92, our analysis underestimated distance and stellar age, while metallicity and dust extinction are overrated. We have also performed analysis with fixed stellar age and distance, but no significant improvements or changes were achieved.

12.3 NGC 6791 - Comparison

Other authors have determined the distance to NGC 6791 to be 4.23 kpc away from Earth [40].

The newest scientific papers estimate that the age of the cluster is 8.3 Gyr [41] and its metallicity 0.0258 [42].

Also, NGC 6791 visual extinction has been determined as $A_v = 0.7$ [41]. Its ratio of total to selective extinction $R_v = 3.1$ [41].

BEAST determined the distance value to be 4.55 kpc, which gives us an accuracy of 93%. That can be considered an excellent accuracy. BEAST performed very well in calculating distance of NGC 6791. We have seen that BEAST had some problems with doing calculations for HB stars in previous cluster, so maybe now that we have stars that are closer in evolution to the main-sequence like SGB and RGB, BEAST can perform better in calculating stellar parameters.

For metallicity, we obtained 0.0111, which gives us an accuracy of 43%.

BEAST calculated age of NGC 6791 cluster to be 7.77 Gyr. Accuracy of that value is 93.6%, which is excellent.

For visual extinction in magnitude, BEAST determined $A_v = 0.46$ which has accuracy of 65.71% And for ratio of total to selective extinction, we obtained $R_v = 3.01$ which has accuracy of 97.1%.

All of the average stellar values with one sigma uncertainty for NGC 6791 and their accuracies are shown in the table below. As the distance and the cluster age were determined very well, BEAST analysis with distance and age being constant did not improve or change stellar parameters significantly.

Table 7: Values of stellar parameters for NGC 6791.

	This works	Other works	accuracy
distance	4551_{-1736}^{+2690}	4230 ref:[40]	92.98%
Age (Gyr)	$7.77_{-3.64}^{+3.95}$	11.65 ref:[41]	93.61%
Mass initial (M_\odot)	$0.94_{-0.09}^{+0.18}$		
log Luminosity	$0.49_{0.22}^{+0.48}$		
Luminosity	$3.1_{-1.3}^{+6.3}$		
Temperature (K)	5066_{-213}^{+225}		
Metallicity	$0.0111_{-0.0053}^{+0.004}$	0.0026 ref:[42]	43%
Radius (R_\odot)	$4.22_{-1.08}^{+2.85}$		
log g ($\log m/s^2$)	$3.69_{-0.44}^{+0.21}$		
A_v	$0.46_{-0.24}^{+0.21}$	0.7 ref:[41]	65.71%
R_v	$3.01_{-0.25}^{+0.28}$	3.1 ref:[41]	97.01%

Analysed SGB and RGB stars in NGC 6791 have stellar age of around 8 Gyr,

which is significantly younger than stars in globular clusters M13 and M92. NGC 6791 is an open cluster and M13 and M92 are globular clusters, that is expected.

Stellar masses in NGC 6791 ($0.94 M_{\odot}$) are a little bit larger than in M13 and M92 ($0.92 M_{\odot}$), which is expected considering the age and evolution of the clusters.

Temperature of the stars in open cluster NGC 6791 is significantly lower than in globular clusters M13 and M92, by about 600 K. That is expected considering the phase in evolution and cluster age.

It can be concluded that our BEAST analysis can determine very well distances and stellar age of younger open cluster with SGB and RGB stars.

Luminosity ($\sim 3 L_{\odot}$) and radius ($\sim 4.2 R_{\odot}$) of stars in NGC 6791 are significantly lower than in M13 and M92, which is expected.

Metallicity is significantly higher in NGC 6791 (0.011) than in older clusters M13 and M92 (around 0.0005), which is as expected considering cluster age.

Dust extinction to the NGC 6791 cluster is much higher than for M13 and M92.

13 Conclusion

The BEAST and Bayesian inference are an excellent tools for doing analysis of stars and its parameters. It is also very useful for obtaining properties of dust through photometric SED fitting. With Bayesian statistics, BEAST provides estimates of key astrophysical parameters such as distance, masses, stellar age, while accounting for uncertainties.

In our study it provided a lot of useful information about the stellar and dust parameters. Even though it was not very precise in all circumstances such as in determination of distances, for other parameters it came close to the values obtained by the other methods. In some cases, differences between the calculated value from BEAST and the value from other studies for certain parameters might be due to different methodologies, assumptions, or the specific data sets used in each analysis. It is also important to consider that we provided BEAST with only around hundred stars for each cluster. With more data to analyze, BEAST would probably generate even more precise results. Additionally, we used more general priors, adequate for open and globular clusters, would probably lead to more accurate results.

BEAST has application in various research areas, including star clusters, galactic surveys, and exoplanet studies. This makes it an invaluable asset in modern astrophysics.

We have also shown that multiband photometric observations can be used for accurate determination of stellar distances and parameters when Bayesian inference with priors is used. This approach provided good results even in case of the most problematic objects such as the giant stars, which are well known to cause degenerative results.

Finally, we have shown that that this approach determined distances and stellar ages, as well as other stellar and dust parameters, very well in younger open cluster and in SGB and RGB stars.

Determination of stellar distances and ages were less accurate for older globular clusters, and for AGB, RGB and HB stars.

It must also be noticed that we used photometry in g , r , i and z band only, and that addition of u band photometry should improve results, especially in determination of metallicity, dust extinction and stellar ages.

References

- [1] Bradley W. Carroll and Dale A. Ostlie. *An Introduction to Modern Astrophysics*. Pearson, 2 edition, 2014.
- [2] Ben Lambert. *A Student's Guide to Bayesian Statistics*. SAGE Publications Ltd, 2018. ISBN 9781526418289.
- [3] Željko Ivezić, Andrew J Connolly, Jacob T VanderPlas, and Alexander Gray. *Statistics, Data Mining, and Machine Learning in Astronomy: A Practical Python Guide for the Analysis of Survey Data*. Princeton University Press, 2014.
- [4] William M. Bolstad. *Introduction to Bayesian Statistics*. John Wiley & Sons, 2nd edition, 2007. ISBN 9780470141151.
- [5] Karl D. Gordon et al. The panchromatic hubble andromeda treasury xv: Bayesian distance and extinction fitting of the phat stellar library. *arXiv preprint arXiv:1606.06182*, 2016. URL <https://arxiv.org/pdf/1606.06182>.
- [6] BEAST Documentation Contributors. Beast documentation. <https://beast.readthedocs.io/en/latest/>, 2024. Accessed: 2024-11-07.
- [7] Michael Berry, Željko Ivezić, Branimir Sesar, Mario Jurić, Edward F. Schlafly, Eric F. Bell, Jo Bovy, Krzysztof Findeisen, Alyson M. Brooks, Timothy C. Beers, et al. The milky way tomography with sloan digital sky survey. iv. dissecting dust. *The Astrophysical Journal*, 757(166):1–35, 2012. doi: 10.1088/0004-637X/757/2/166.
- [8] C. A. L. Baier-Jones, J. Rybizki, M. Fouesneau, D. Miettinen, and R. Andrae. Estimating distances from parallaxes. v. geometric and photogeometric distances to 1.47 billion stars in gaia early data release 3. *The Astronomical Journal*, 161(5):247, 2021. doi: 10.3847/1538-3881/abd806. URL <https://iopscience.iop.org/article/10.3847/1538-3881/abd806/pdf>. Received 2020 December 9; revised 2020 December 30; accepted 2020 December 31; published 2021 February 25.
- [9] Gregory Maurice Green, Edward F. Schlafly, Douglas P. Finkbeiner, Mario Jurić, Hans-Walter Rix, Will Burgett, Kenneth C. Chambers, Peter W. Draper,

- Heather Flewelling, Rolf-Peter Kudritzki, et al. Measuring distances and red- denings for a billion stars: Toward a 3d dust map from pan-starrs 1. *The Astrophysical Journal*, 783(2):114, 2014. doi: 10.1088/0004-637X/783/2/114. Received 2013 September 12; revised 2014 January 10; accepted 2014 January 24; published 2014 March 10.
- [10] Gregory M. Green, Edward F. Schlafly, Catherine Zucker, Joshua S. Speagle, and Douglas Finkbeiner. A 3d dust map based on gaia, pan-starrs 1, and 2mass. *The Astrophysical Journal*, 887(2):93, 2019. doi: 10.3847/1538-4357/ab5362. Received 2019 May 7; revised 2019 October 30; accepted 2019 October 30; published 2019 December 13.
- [11] R. Lallement, J.-L. Vergely, B. Valette, L. Puspitarini, L. Eyer, and L. Casagrande. 3d maps of the local ism from inversion of individual color excess measurements. *Astronomy & Astrophysics*, 561:A91, 2014. doi: 10.1051/0004-6361/201322032. Received 6 June 2013; Accepted 24 September 2013; Published 2014.
- [12] Eleanor Imster. Prehistoric cave art suggests ancient use of complex astronomy, 2018. URL <https://earthsky.org/human-world/prehistoric-cave-art-suggests-ancient-use-complex-astronomy/>.
- [13] Wikipedia contributors. History of astronomy — wikipedia, the free encyclopedia, 2024. URL https://en.wikipedia.org/wiki/History_of_astronomy. Accessed: 2024-11-06.
- [14] Donald D. Clayton. *Principles of Stellar Evolution and Nucleosynthesis*. University of Chicago Press, 1983.
- [15] Wikipedia contributors. Stellar classification — wikipedia, the free encyclopedia, 2024. URL https://en.wikipedia.org/wiki/Stellar_classification. Accessed: 2024-11-06.
- [16] Elizabeth Howell. Annie jump cannon: Biography, facts & contributions, 2017. URL <https://www.space.com/34707-annie-jump-cannon-biography.html>. Accessed: 2024-11-06.
- [17] Special topic: The hertzsprung-russell diagram, n.d. URL https://www.aal.lu/SPECIAL_TOPIC/6/. Accessed: 2024-11-06.
- [18] Nola Taylor Redd. Parallax: How astronomers measure stellar distances, 2015. URL <https://www.space.com/30417-parallax.html>. Accessed: 2024-11-06.

- [19] YouTube. Understanding bayesian inference and its applications in astrophysics. <https://www.youtube.com/watch?v=CWMh61yutjU&t=550s>, 2024. Accessed: 2024-11-06.
- [20] YouTube. A detailed explanation of the noise model and its applications in astrophysics. <https://www.youtube.com/watch?v=JWpJjsou99c&t=786s>, 2024. Accessed: 2024-11-06.
- [21] Wikiwand Contributors. Period-luminosity relation, accessed 2024. URL https://www.wikiwand.com/en/articles/Period-luminosity_relation. Accessed: 2024-11-10.
- [22] Wikipedia contributors. Luminosity — Wikipedia, The Free Encyclopedia. <https://en.wikipedia.org/wiki/Luminosity>, 2024. Accessed: 2024-11-06.
- [23] Pennsylvania State University. Astro 801: Lesson 7, part 3 - luminosity and flux. https://www.e-education.psu.edu/astro801/content/17_p3.html, 2024. Accessed: 2024-11-06.
- [24] Wikipedia contributors. Surface gravity — Wikipedia, The Free Encyclopedia. https://en.wikipedia.org/wiki/Surface_gravity, 2024. Accessed: 2024-11-06.
- [25] G. Schaller, D. Schaerer, G. Meynet, and A. Maeder. New Grids of Stellar Models from 0.8-SOLAR-MASS to 120-SOLAR-MASSSES at $Z=0.020$ and $Z=0.001$. , 96:269, December 1992.
- [26] Jr. Iben, Icko. Stellar Evolution. III. The Evolution of a $5 M_{\text{sun}}$ Star from the Main Sequence Through Core Helium Burning. , 143:483, February 1966. doi: 10.1086/148528.
- [27] Duncan A. Forbes, Nate Bastian, Mark Gieles, Robert A. Crain, J. M. Diederik Kruijssen, Søren S. Larsen, Sylvia Ploekinger, Oscar Agertz, Michele Trenti, Annette M. N. Ferguson, Joel Pfeffer, and Oleg Y. Gnedin. Globular cluster formation and evolution in the context of cosmological galaxy assembly: open questions. *Proceedings of the Royal Society A*, 474(2210), February 2018. doi: 10.1098/rspa.2017.0616. URL <https://doi.org/10.1098/rspa.2017.0616>.
- [28] NASA. Messier 92, 2023. URL <https://science.nasa.gov/mission/hubble/science/explore-the-night-sky/hubble-messier-catalog/messier-92/>.

- [29] C. W. Chen and W. P. Chen. Morphological distortion of galactic globular clusters. *The Astrophysical Journal*, 721(2):1790, 2010. doi: 10.1088/0004-637X/721/2/1790. URL <https://iopscience.iop.org/article/10.1088/0004-637X/721/2/1790>.
- [30] G. A. Drukier, H. N. Cohn, P. M. Lugger, S. D. Slavin, R. C. Berrington, and B. W. Murphy. The global kinematics of the globular cluster m92. *arXiv preprint arXiv:0611246*, 2006. doi: 10.1086/510721. URL <https://doi.org/10.1086/510721>.
- [31] A. Di Cecco, R. Beccuci, G. Bono, B. P. Monelli, P. B. Stetson, S. Degl’Innocenti, P. G. Prada Moroni, M. Nonino, A. Weiss, R. Buonanno, E. C. Calamida, F. Caputo, I. Corsi, G. Ferraro, G. Iannicola, L. Pulone, M. Romanelli, and A. R. Walker. On the absolute age of the globular cluster m92. *arXiv preprint arXiv:1006.5217*, 2010. doi: 10.48550/arXiv.1006.5217. URL <https://doi.org/10.48550/arXiv.1006.5217>.
- [32] Robert Thompson and Barbara Thompson. *Illustrated Guide to Astronomical Wonders: From Novice to Master Observer*. O’Reilly Media, Inc., 2007. ISBN 9780596526856.
- [33] SIMBAD Astronomical Database. M 13 (messier 13). https://simbad.u-strasbg.fr/simbad/sim-id?mescat.velocities=on&mescat.distance=on&mescat.fe_h=on&Ident=%402894585&Name=M++13&submit=display+selected+measurements#lab_meas. Accessed: 15-Oct-2024.
- [34] Eugene Vasiliev and Holger Baumgardt. Gaia EDR3 view on galactic globular clusters. *Monthly Notices of the Royal Astronomical Society*, 505:5978, 2021. doi: 10.1093/mnras/stab1475. URL <https://ui.adsabs.harvard.edu/abs/2021MNRAS.505.5978V/abstract>.
- [35] H. Baumgardt and M. Hilker. A catalogue of masses, structural parameters and velocity dispersion profiles of 112 milky way globular clusters. *arXiv preprint arXiv:1804.08359*, 2018.
- [36] Ricardo P. Schiavon, Siân G. Phillips, Natalie Myers, Danny Horta, Dante Minniti, Carlos Allende Prieto, Borja Anguiano, Rachael L. Beaton, Timothy C. Beers, and Joel R. Brownstein. The APOGEE value-added catalogue of Galactic globular cluster stars. *Monthly Notices of the Royal Astronomical Society*, 528:1393–1407, February 2024. doi: 10.1093/mnras/stad3020. URL <https://doi.org/10.1093/mnras/stad3020>.

- [37] Duncan A Forbes and Terry Bridges. Accreted versus in situ milky way globular clusters. *Monthly Notices of the Royal Astronomical Society*, 404(3): 1203–1214, 2010. doi: 10.1111/j.1365-2966.2010.16373.x.
- [38] George A. Gontcharov, Charles J. Bonatto, Olga S. Ryutina, Sergey S. Savchenko, Aleksandr V. Mosenkov, Vladimir B. Il'in, Maxim Yu. Khovritchev, Alexander A. Marchuk, Denis M. Poliakov, and Anton A. Smirnov. Isochrone fitting of Galactic globular clusters – V. NGC 6397 and NGC 6809 (M55). *Monthly Notices of the Royal Astronomical Society*, 526:5628–5647, December 2023. doi: 10.1093/mnras/stad3134. URL <https://doi.org/10.1093/mnras/stad3134>.
- [39] SIMBAD, Centre de Données astronomiques de Strasbourg. Ngc 6791 - simbad astronomical database. <https://simbad.u-strasbg.fr/simbad/sim-basic?Ident=NGC+6791>, 2024. Accessed: 15-October-2024.
- [40] E. Poggio, R. Drimmel, T. Cantat-Gaudin, P. Ramos, V. Ripepi, E. Zari, R. Andrae, R. Blomme, L. Chemin, G. Clementini, F. Figueras, M. Fouesneau, Y. Frémat, A. Lobel, D. J. Marshall, T. Muraveva, and M. Romero-Gómez. Galactic spiral structure revealed by gaiaedr3. *Astronomy & Astrophysics*, 651:A104, July 2021. doi: 10.1051/0004-6361/202140687. URL <https://doi.org/10.1051/0004-6361/202140687>.
- [41] K. Brogaard, F. Grundahl, E. L. Sandquist, D. Slumstrup, M. L. Jensen, J. B. Thomsen, J. H. Jørgensen, J. R. Larsen, S. T. Bjørn, C. T. G. Sørensen, H. Bruntt, T. Arentoft, S. Frandsen, J. Jessen-Hansen, A. Asplund, S. Mathis, A. Collet, B. N. Røed, S. Stello, L. M. Mejborn, and P. L. Plastino. Age and helium content of the open cluster ngc 6791 from multiple eclipsing binary members. *Astronomy & Astrophysics*, 649:A178, June 2021. doi: 10.1051/0004-6361/202140911. URL <https://doi.org/10.1051/0004-6361/202140911>.
- [42] L. Magrini, C. Viscasillas Vázquez, L. Spina, S. Randich, D. Romano, E. Franciosini, A. Recio-Blanco, T. Nordlander, V. D’Orazi, M. Baratella, R. Smiljanic, M. L. L. Dantas, L. Pasquini, E. Spitoni, G. Casali, M. Van der Swaelmen, T. Bensby, E. Stonkute, S. Feltzing, G. G. Sacco, A. Bragaglia, E. Pancino, U. Heiter, K. Biazzo, G. Gilmore, and M. Tosi. The gaiaeso survey: Mapping the shape and evolution of the radial abundance gradients with open clusters. *Astronomy & Astrophysics*, 669:A119, January 2023. doi: 10.1051/0004-6361/202244957. URL <https://doi.org/10.1051/0004-6361/202244957>.

- [43] D.S. Sivia and J. Skilling. *Data Analysis: A Bayesian Tutorial*. Oxford University Press, 2 edition, 2006.
- [44] Wikipedia contributors. File: Boxplot vs pdf — Wikipedia, The Free Encyclopedia. https://en.wikipedia.org/wiki/Probability_density_function#/media/File:Boxplot_vs_PDF.svg, 2024. Accessed: 2024-11-07.
- [45] M. S. Bessell. Standard photometric systems. *Annual Review of Astronomy and Astrophysics*, 43(1):293–336, 2005. doi: 10.1146/annurev.astro.41.082801.100251.
- [46] William H Press, Saul A Teukolsky, William T Vetterling, and Brian P Flannery. *Numerical Recipes: The Art of Scientific Computing*. Cambridge University Press, 3 edition, 2007.
- [47] Heather L. Morrison, Zhibo Ma, James L. Clem, An Deokkeun, Charlie Conroy, Ricardo P. Schiavon, Paul Harding, Luca Casagrande, Constance Rockosi, Jennifer A. Johnson, et al. Globular and open clusters observed by sdss/segue: The giant stars. *The Astronomical Journal*, 151(7):1, 2016. doi: 10.1088/0004-6256/151/1/7. Received 2014 November 14; revised 2014 December 27; accepted 2014 December 27; published 2016 January.
- [48] Wikipedia contributors. Sloan Digital Sky Survey — Wikipedia, The Free Encyclopedia, 2024. URL https://en.wikipedia.org/wiki/Sloan_Digital_Sky_Survey. [Online; accessed 8-November-2024].
- [49] Sloan Digital Sky Survey. SEGUE-2: Sloan Extension for Galactic Understanding and Exploration 2, 2024. URL <https://www.sdss3.org/surveys/segue2.php>. [Online; accessed 8-November-2024].
- [50] Wikipedia contributors. 2MASS — Wikipedia, The Free Encyclopedia, 2024. URL <https://en.wikipedia.org/wiki/2MASS>. [Online; accessed 8-November-2024].
- [51] Wikipedia contributors. Photometric system, 2024. URL https://en.wikipedia.org/wiki/Photometric_system. Accessed: 2024-11-08.
- [52] NASA/IPAC Extragalactic Database (NED). SDSS Photometry Help (Data Release 6), 2024. URL <https://ned.ipac.caltech.edu/help/sdss/dr6/photometry.html>. [Online; accessed 8-November-2024].
- [53] Wikipedia contributors. FITS — Wikipedia, The Free Encyclopedia, 2024. URL <https://en.wikipedia.org/wiki/FITS>. [Online; accessed 8-November-2024].

- [54] SIMBAD Astronomical Database. M 92 entry, 2024. URL <https://simbad.u-strasbg.fr/simbad/sim-id?Ident=M+92&NbIdent=1&Radius=2&Radius.unit=arcmin&submit=submit+id>. [Online; accessed 8-November-2024].
- [55] Edwin E. Salpeter. The luminosity function and stellar evolution. *The Astrophysical Journal*, 121:161, 1955. doi: 10.1086/145971.
- [56] Duncan A. Forbes and Terry Bridges. Accreted versus in situ milky way globular clusters. *arXiv preprint arXiv:1001.4289*, 2010. doi: 10.1111/j.1365-2966.2010.16637.x. URL <https://doi.org/10.1111/j.1365-2966.2010.16637.x>.
- [57] Duncan A. Forbes and Terry Bridges. Accreted versus in situ Milky Way globular clusters. *Monthly Notices of the Royal Astronomical Society*, 404(3): 1203–1214, 05 2010. ISSN 0035-8711. doi: 10.1111/j.1365-2966.2010.16373.x. URL <https://doi.org/10.1111/j.1365-2966.2010.16373.x>.
- [58] NASA/IPAC Extragalactic Database. M 92, 2023. URL https://ned.ipac.caltech.edu/cgi-bin/nph-objsearch?objname=M+92&extend=no&list_limit=5&img_stamp=YES. Accessed: 2023-10-01.

A Python Scripts for Data Handling

A.1 Script for Converting Excel to FITS

This script loads an .xlsx file into a Pandas DataFrame, converts it to an Astropy Table, and then writes it to a FITS file.

```
import pandas as pd
from astropy.table import Table
from astropy.io import fits

# Step 1: Load the .xlsx file into a Pandas DataFrame
xlsx_file = 'novo.xlsx'
df = pd.read_excel(xlsx_file)

# Step 2: Convert the DataFrame to an Astropy Table
table = Table.from_pandas(df)

# Step 3: Write the Astropy Table to a FITS file
fits_file = 'output_file.fits'
```

```
table.write(fits_file, format='fits', overwrite=True)

print(f"Converted {xlsx_file} to {fits_file}")
```

A.2 Script for Exploring HDF5 Files

This script demonstrates how to read and inspect the contents of an HDF5 file.

```
import h5py

file_path = 'filters.hd5'

with h5py.File(file_path, 'r') as f:
    print("Keys: %s" % f.keys())

    def print_structure(name, obj):
        print(f"{name}: {type(obj)}")

    f.visititems(print_structure)

    dataset_name = 'your_dataset_name'
    if dataset_name in f:
        dataset = f[dataset_name]
        print(f"\nDataset '{dataset_name}' contents:\n{dataset[:]}")
```

A.3 Script for Converting FITS to Excel

This script converts data from a FITS file into an Excel format.

```
from astropy.io import fits
import pandas as pd
import numpy as np

fits_file = 'Proba_stats.fits'

with fits.open(fits_file) as hdul:
    data = hdul[1].data

    columns = [name for name in data.columns.names]
    data_dict = {col: data[col] for col in columns}

    df = pd.DataFrame(data_dict)

    # Handle any potential issues with data types
```

```

df = df.applymap(lambda x: np.nan if isinstance(x, bytes) else x)

# Save DataFrame to an Excel file
excel_file = 'zavrsna.xlsx'
df.to_excel(excel_file, index=False, engine='openpyxl')

print(f"FITS data successfully converted to {excel_file}")

```

A.4 Script for Plotting Spatial distribution diagrams

This script plots a Spatial distribution diagrams using data from an Excel file.

```

import pandas as pd
import matplotlib.pyplot as plt

# Replace with your actual Excel file path
excel_file = 'distance_variable_M92_flag2.xlsx'

# Read the Excel file into a DataFrame
df = pd.read_excel(excel_file, engine='openpyxl')

# Extract columns for plotting
ra = df['R.A. ']
decl = df['Decl. ']
logT_best = df['radius_p50']

# Create the plot
plt.figure(figsize=(10, 7))
scatter = plt.scatter(ra, decl, c=logT_best, cmap='viridis')

# Add color bar
cbar = plt.colorbar(scatter)
cbar.set_label('radius')

# Labels and title
plt.xlabel('R.A. ')
plt.ylabel('Decl. ')
plt.title('Spatial distribution: R.A. and Decl. on x and y axis and
↪ radius on z axis')

# Save the static plot
plt.savefig('ccd_plot_mass4.png')
print('CCD plot saved as ccd_plot.png')

```

```
# Show the plot
plt.show()
```

A.5 Script for Flag Assignment Based on Conditions

This script loads an Excel file, applies a function to determine flags based on specific conditions for each row, and saves the modified DataFrame with the new flag values.

```
import pandas as pd

# Load the data from your Excel file
data = pd.read_excel('distance_variable_M92.xlsx')

# Define a function to determine the flag value based on conditions
def determine_flag(row):
    if row['g-r'] < 0:
        return 1
    elif row['r'] < 14.1:
        return 2
    elif row['r'] < 15 and row['g-r']:
        return 2
    else:
        return 3

# Apply the function to create a new column 'flag'
data['flag'] = data.apply(determine_flag, axis=1)

# Save the modified DataFrame to a new Excel file
data.to_excel('distance_variable_M92_flag.xlsx', index=False)
```

A.6 Script for Generating HR Diagrams with Flagged Data

This script generates HR diagrams based on different flags in the dataset, illustrating the differences in stellar characteristics according to the flag categories. Flags were given to stars based on their place in HR diagram.

```
import pandas as pd
import matplotlib.pyplot as plt

# Load the data from an Excel file
excel_file = 'distance_variable_M92_flag2.xlsx'
```

```

df = pd.read_excel(excel_file, engine='openpyxl')

# Filter the data by flag values
df_flag1 = df[df['flag'] == 1]
df_flag2 = df[df['flag'] == 2]
df_flag3 = df[df['flag'] == 3]

# Set up the figure and axes
fig, axs = plt.subplots(2, 2, figsize=(14, 10))
fig.subplots_adjust(hspace=0.5, wspace=0.3)

# Plot configurations for each subplot
plots = [
    {'ax': axs[0, 0], 'x': 'g-r', 'y': 'r', 'xlabel': 'G-R', 'ylabel': 'R
    ↪ (Magnitude)', 'title': 'HR Diagram: R vs. G-R'},
]

# Function to plot each diagram
def plot_hr_diagram(ax, x, y, xlabel, ylabel, title):
    ax.scatter(df_flag1[x], df_flag1[y], color='red', label='HB')
    ax.scatter(df_flag2[x], df_flag2[y], color='green', label='AGB')
    ax.scatter(df_flag3[x], df_flag3[y], color='blue', label='RGB')
    ax.invert_yaxis()
    ax.set_xlabel(xlabel)
    ax.set_ylabel(ylabel)
    ax.set_title(title)
    ax.legend(title='Flag')

# Generate each plot
for plot in plots:
    plot_hr_diagram(**plot)

# Save the full figure
plt.savefig('hr_diagrams.png')
print('HR diagrams saved as hr_diagrams.png')

# Display the plots
plt.show()

```

A.7 Script for Plotting HR Diagram with stellar parameters

This script generates an HR diagram using data from an Excel file.

```

import pandas as pd
import matplotlib.pyplot as plt

excel_file = 'distance_variable_M92_flag2.xlsx'

# Read the Excel file into a DataFrame
df = pd.read_excel(excel_file, engine='openpyxl')

b_v = df['g-r']
v_mag = df['r']
logT_best = df['Luminosity']

# Create the HR diagram
plt.figure(figsize=(10, 7))
scatter = plt.scatter(b_v, v_mag, c=logT_best, cmap='viridis')

# Invert the y-axis (HR diagram convention: brighter stars at the top)
plt.gca().invert_yaxis()

# Add color bar
cbar = plt.colorbar(scatter)
cbar.set_label('Luminosity')

# Labels and title
plt.xlabel('G-R')
plt.ylabel('R (Magnitude)')
plt.title('Hertzsprung-Russell (HR) Diagram: R vs. G-R with luminosity
↪ Color-Coded')

# Save the static plot
plt.savefig('hr_diagram_logL4.png')
print('HR diagram saved as hr_diagram.png')

# Show the plot
plt.show()

```

A.8 Script for Multiple Relationship Diagrams

This script plots multiple relationships between different stellar parameters.

```

import pandas as pd
import matplotlib.pyplot as plt

```

```

# Replace with your actual Excel file path
excel_file = 'M13_flag.xlsx'

# Read the Excel file into a DataFrame
df = pd.read_excel(excel_file, engine='openpyxl')

# Filter data based on the flag
df_flag1 = df[df['flag'] == 1]
df_flag2 = df[df['flag'] == 2]
df_flag3 = df[df['flag'] == 3]

# Define a function to plot based on flag, for individual plots, and save
↳ them in high resolution
def plot_individual(x_col, y_col, x_label, y_label, title, file_name):
    plt.figure(figsize=(8, 6), dpi=300) # Specify figure size and
    ↳ resolution
    plt.scatter(df_flag1[x_col], df_flag1[y_col], c='red', alpha=0.8,
    ↳ label='HB', edgecolor='none')
    plt.scatter(df_flag2[x_col], df_flag2[y_col], c='blue', alpha=0.8,
    ↳ label='AGB', edgecolor='none')
    plt.scatter(df_flag3[x_col], df_flag3[y_col], c='green', alpha=0.8,
    ↳ label='RGB', edgecolor='none')
    plt.xlabel(x_label)
    plt.ylabel(y_label)
    plt.title(title)
    plt.legend()
    plt.tight_layout() # Adjust layout to make sure nothing is cut off
    plt.savefig(file_name, format='png', dpi=300) # Save the plot as a
    ↳ PNG file
    plt.close() # Close the plot to free memory

# Plot and save logL_Best vs logR (with LaTeX-style labels)
plot_individual('logL_p50', 'logR', r'$\log(L/L_{\odot})$',
↳ r'$\log(R/R_{\odot})$', 'Relationship diagram of luminosity and
↳ radius', 'relationship-luminosity_radius.png')

# Plot and save logL_Best vs M_ini_Best (with LaTeX-style labels)
plot_individual('M_ini_p50', 'logL_p50', r'$\log(M/M_{\odot})$',
↳ r'$\log(L/L_{\odot})$', 'Relationship diagram of luminosity and
↳ mass', 'relationship-luminosity_mass.png')

# Plot and save M_ini_Best vs logT_Best (with LaTeX-style labels)

```

```

plot_individual('M_ini_p50', 'logT_p50', r'\log(M/M_{\odot})$',
↳ r'\log(T) (K)$', 'Relationship diagram of mass and temperature',
↳ 'relationship-mass_temperature.png')

# Plot and save logT_Best vs logL_Best (with LaTeX-style labels)
plot_individual('logT_p50', 'logL_p50', r'\log(T) (K)$',
↳ r'\log(L/L_{\odot})$', 'Relationship diagram of luminosity and
↳ temperature', 'relationship-luminosity_temperature.png')

```

A.9 Script for Pairwise Comparison of Fixed and Variable Estimates

This script loads data from an Excel file and iterates through pairs of columns to create scatter plots for pairwise comparisons, so that we can see how well did BEAST work with different fixed parameters.

```

import pandas as pd
import matplotlib.pyplot as plt

# Load the data from your Excel file
data = pd.read_excel('M92_fix_vs_var (3).xlsx')

# Define column pairs
column_pairs = [
    ("logL_fix", "logL_var"),
    ("radius_fix", "radius_var"),
    ("age_fix", "age_var"),
    ("temp_fix", "temp_var"),
    ("mass_fix", "mass_var"),
    ("Z_fix", "Z_var"),
    ("av_fix", "av_var")
]

# Iterate through each pair of columns and create separate plots
for col1, col2 in column_pairs:
    plt.figure(figsize=(8, 5)) # Define a new figure for each plot
    plt.scatter(data[col1], data[col2], alpha=0.5) # Create scatter plot
    # Adding the y=x line
    min_val = min(data[col1].min(), data[col2].min())
    max_val = max(data[col1].max(), data[col2].max())

```

```
plt.plot([min_val, max_val], [min_val, max_val], 'r--') # Red dashed
↳ line for y=x
plt.xlabel(col1)
plt.ylabel(col2)
plt.title(f'Relationship between {col1} and {col2}')
plt.savefig(f"{col1}_vs_{col2}.png") # Save the figure
plt.close() # Close the figure to free up memory

print("All plots have been saved successfully.")
```

A.10 Tables that show rates (fluxes) for different bands for given stellar positions (R.A. and Decl.)

Table 8: M92 part 1: Rates (Flux) for Different Bands for given R.A. and Decl.

R.A.	Decl.	G RATE	R RATE	I RATE	Z RATE	J RATE	H RATE	K RATE
259.199700	43.104400	9.32e-07	1.65e-06	2.12e-06	2.43e-06	5.85e-06	9.71e-06	1.02e-05
259.183100	43.125500	1.17e-06	2.05e-06	2.65e-06	3.08e-06	7.51e-06	1.15e-05	1.30e-05
259.142900	43.126800	2.36e-06	4.33e-06	5.74e-06	7.19e-06	1.66e-05	2.74e-05	2.91e-05
259.157200	43.144800	2.31e-06	4.18e-06	5.54e-06	6.53e-06	1.62e-05	2.65e-05	2.76e-05
259.251400	43.196600	2.04e-06	3.66e-06	4.85e-06	5.69e-06	1.42e-05	2.27e-05	2.39e-05
259.245200	43.253200	2.63e-06	5.12e-06	7.02e-06	8.20e-06	2.10e-05	3.60e-05	3.90e-05
259.228000	43.174000	1.08e-06	1.85e-06	2.35e-06	2.65e-06	6.29e-06	9.78e-06	1.05e-05
259.207800	43.178100	4.70e-06	1.04e-05	1.49e-05	1.79e-05	4.87e-05	8.20e-05	9.11e-05
259.240600	43.236500	2.85e-06	5.71e-06	7.91e-06	9.25e-06	2.43e-05	4.10e-05	4.51e-05
259.231300	43.084300	1.66e-06	2.98e-06	4.06e-06	4.76e-06	1.16e-05	1.91e-05	2.11e-05
259.149100	42.944300	8.46e-07	1.46e-06	1.88e-06	2.18e-06	5.39e-06	8.51e-06	9.02e-06
259.248700	43.018300	1.06e-06	1.83e-06	2.37e-06	2.72e-06	6.63e-06	1.06e-05	1.14e-05
259.220200	43.058200	1.31e-06	1.93e-06	2.31e-06	2.46e-06	5.46e-06	8.02e-06	8.20e-06
259.340500	43.214900	7.74e-06	2.25e-05	3.57e-05	4.58e-05	1.34e-04	2.43e-04	2.73e-04
259.318900	43.179200	3.81e-06	8.02e-06	1.12e-05	1.33e-05	3.46e-05	6.01e-05	6.44e-05
259.340300	43.184200	1.34e-06	2.46e-06	3.17e-06	3.67e-06	8.93e-06	1.37e-05	1.58e-05
259.293500	43.185500	6.72e-06	1.64e-05	2.54e-05	3.22e-05	8.65e-05	1.51e-04	1.73e-04
259.332000	43.245100	1.66e-06	2.77e-06	3.54e-06	4.09e-06	9.62e-06	1.49e-05	1.61e-05
259.337600	43.103500	1.22e-06	1.90e-06	2.31e-06	2.60e-06	5.86e-06	8.82e-06	9.59e-06
259.314600	43.083100	1.06e-06	1.85e-06	2.39e-06	2.73e-06	6.46e-06	1.02e-05	1.14e-05
259.304800	43.000100	8.52e-07	1.17e-06	1.33e-06	1.46e-06	3.11e-06	4.37e-06	4.51e-06
259.266400	43.034100	1.03e-06	1.78e-06	2.31e-06	2.67e-06	6.39e-06	1.03e-05	1.09e-05
259.382100	43.094900	4.95e-06	1.09e-05	1.54e-05	1.90e-05	5.12e-05	8.90e-05	9.63e-05
259.369900	43.167500	9.07e-07	1.57e-06	2.04e-06	2.35e-06	5.47e-06	8.76e-06	9.19e-06
259.370900	43.115300	7.86e-07	1.33e-06	1.69e-06	1.94e-06	4.72e-06	7.13e-06	7.73e-06
259.373000	43.204100	1.05e-06	1.81e-06	2.36e-06	2.68e-06	6.58e-06	1.01e-05	1.10e-05
259.342500	43.080500	2.13e-06	4.02e-06	5.37e-06	6.43e-06	1.60e-05	2.66e-05	2.86e-05
259.519700	43.171200	7.83e-07	1.37e-06	1.75e-06	1.96e-06	4.59e-06	6.59e-06	8.07e-06
259.459800	43.229500	6.58e-07	1.11e-06	1.42e-06	1.62e-06	3.83e-06	6.30e-06	6.36e-06
259.052700	43.173900	7.19e-07	5.85e-07	5.00e-07	4.69e-07	7.21e-07	7.48e-07	9.12e-07
259.124500	43.100900	3.35e-07	5.43e-07	6.69e-07	7.71e-07	1.83e-06	2.83e-06	3.15e-06
259.151600	43.115600	6.72e-07	1.13e-06	1.42e-06	1.65e-06	3.78e-06	6.08e-06	6.72e-06
259.192500	43.082900	5.58e-07	9.44e-07	1.18e-06	1.35e-06	3.14e-06	4.93e-06	5.34e-06
259.212000	43.189700	6.64e-07	4.97e-07	4.07e-07	3.68e-07	4.94e-07	4.77e-07	5.25e-07
259.178300	43.246500	3.67e-07	5.81e-07	7.25e-07	8.18e-07	1.87e-06	2.78e-06	3.36e-06
259.201200	43.171300	5.95e-07	9.86e-07	1.24e-06	1.42e-06	3.43e-06	4.93e-06	5.61e-06
259.268100	43.069600	3.08e-07	5.00e-07	6.10e-07	6.97e-07	1.53e-06	2.72e-06	2.43e-06
259.189800	43.229600	3.77e-07	5.94e-07	7.49e-07	8.61e-07	1.93e-06	2.93e-06	3.31e-06
259.149000	42.944300	8.46e-07	1.46e-06	1.88e-06	2.18e-06	5.39e-06	8.51e-06	9.02e-06
259.347100	42.948800	8.38e-07	1.40e-06	1.81e-06	2.11e-06	4.97e-06	7.68e-06	8.48e-06
259.252800	43.217500	7.06e-07	5.49e-07	4.65e-07	4.27e-07	7.49e-07	5.42e-07	6.29e-07
259.290100	43.079600	7.35e-07	5.80e-07	4.87e-07	4.52e-07	6.30e-07	5.99e-07	8.23e-07
259.313000	43.264500	2.39e-07	3.83e-07	4.66e-07	5.13e-07	1.17e-06	1.73e-06	1.73e-06
259.401700	43.019900	9.66e-07	8.04e-07	7.04e-07	6.80e-07	1.16e-06	1.20e-06	1.36e-06
259.329600	43.215200	5.99e-07	1.01e-06	1.27e-06	1.44e-06	3.49e-06	5.29e-06	5.57e-06
259.344600	43.158700	5.89e-07	4.33e-07	3.45e-07	3.09e-07	4.06e-07	4.77e-07	1.49e-07
259.449900	43.307000	8.26e-08	1.25e-07	1.43e-07	1.47e-07	3.54e-07	4.25e-07	1.27e-07
259.366000	43.147500	8.40e-07	7.11e-07	6.29e-07	6.05e-07	1.02e-06	1.13e-06	1.19e-06
259.321400	43.074200	3.64e-07	5.73e-07	6.87e-07	7.59e-07	1.71e-06	2.57e-06	2.76e-06
259.381200	43.246900	6.63e-08	9.83e-08	1.14e-07	1.21e-07	3.18e-07	4.02e-07	6.47e-07

Table 9: M92 part 2: Rates (Flux) for Different Bands for given R.A. and Decl.

R.A.	Decl.	G_RATE	R_RATE	I_RATE	Z_RATE	J_RATE	H_RATE	K_RATE
259.393800	43.071100	2.61e-07	4.12e-07	5.03e-07	5.64e-07	1.37e-06	2.14e-06	2.27e-06
259.484400	43.059500	7.22e-08	1.08e-07	1.27e-07	1.38e-07	3.14e-07	5.87e-07	5.18e-07
259.432200	43.063400	1.49e-07	2.32e-07	2.77e-07	3.12e-07	7.30e-07	9.89e-07	1.34e-06
259.577200	43.199000	2.34e-07	3.76e-07	4.57e-07	4.96e-07	1.10e-06	1.60e-06	1.95e-06
259.459800	43.229500	6.58e-07	1.11e-06	1.42e-06	1.62e-06	3.83e-06	6.30e-06	6.36e-06
259.519700	43.171200	7.83e-07	1.37e-06	1.75e-06	1.96e-06	4.59e-06	6.59e-06	7.78e-06
259.404200	43.131000	5.29e-07	3.98e-07	3.26e-07	2.95e-07	3.98e-07	3.66e-07	5.62e-07
259.390500	43.189600	6.58e-08	9.80e-08	1.14e-07	1.22e-07	2.36e-07	2.68e-07	4.27e-07
259.437400	43.135600	9.38e-08	1.45e-07	1.73e-07	1.86e-07	3.45e-07	6.15e-07	6.04e-07

Table 10: M13 part 1: Rates (Flux) for Different Bands for given R.A. and Decl.

R.A.	Decl.	G_RATE	R_RATE	I_RATE	Z_RATE	J_RATE	H_RATE	K_RATE
250.474200	36.309800	9.72e-08	1.50e-07	1.82e-07	1.94e-07	4.76e-07	6.79e-07	6.78e-07
250.512500	36.321100	1.69e-07	2.70e-07	3.31e-07	3.58e-07	1.09e-06	1.61e-06	1.91e-06
250.466400	36.409300	1.03e-06	8.92e-07	7.81e-07	7.50e-07	1.18e-06	1.21e-06	1.13e-06
250.297500	36.656600	6.59e-08	9.80e-08	1.16e-07	1.23e-07	2.71e-07	4.63e-07	1.40e-07
250.363700	36.539500	8.69e-07	1.54e-06	2.01e-06	2.24e-06	5.51e-06	8.76e-06	9.44e-06
250.315400	36.581800	6.62e-08	9.79e-08	1.15e-07	1.22e-07	3.07e-07	3.07e-07	6.01e-07
250.348800	36.637100	8.00e-08	1.23e-07	1.47e-07	1.54e-07	3.51e-07	5.19e-07	7.17e-07
250.355900	36.608400	1.07e-07	1.67e-07	1.99e-07	2.15e-07	4.91e-07	7.56e-07	8.34e-07
250.416200	36.592700	1.08e-07	1.70e-07	2.04e-07	2.22e-07	5.11e-07	7.39e-07	7.62e-07
250.377600	36.560600	1.66e-07	2.65e-07	3.26e-07	3.54e-07	8.42e-07	1.19e-06	1.37e-06
250.452500	36.731100	4.37e-07	7.49e-07	9.35e-07	1.05e-06	2.39e-06	3.66e-06	4.07e-06
250.533400	36.323900	3.05e-07	4.93e-07	6.11e-07	6.78e-07	1.69e-06	2.40e-06	2.45e-06
250.489400	36.332100	8.35e-07	1.44e-06	1.87e-06	2.18e-06	5.38e-06	8.89e-06	9.04e-06
250.490600	36.363500	8.13e-07	6.25e-07	5.28e-07	4.73e-07	7.44e-07	7.32e-07	8.61e-07
250.450500	36.393300	9.86e-07	1.81e-06	2.32e-06	2.63e-06	6.64e-06	1.06e-05	1.09e-05
250.466200	36.326300	9.03e-07	1.62e-06	2.04e-06	2.39e-06	5.80e-06	9.66e-06	1.03e-05
250.352200	36.409500	5.16e-07	8.77e-07	1.11e-06	1.23e-06	2.96e-06	4.70e-06	4.82e-06
250.452000	36.301800	8.65e-07	6.84e-07	5.77e-07	5.22e-07	8.75e-07	8.54e-07	7.45e-07
250.408500	36.303900	5.26e-07	9.02e-07	1.12e-06	1.27e-06	3.20e-06	4.89e-06	5.23e-06
250.275600	36.422900	1.09e-06	1.99e-06	2.57e-06	2.96e-06	7.35e-06	1.19e-05	1.29e-05
250.260800	36.437700	7.33e-07	1.29e-06	1.64e-06	1.88e-06	4.56e-06	6.92e-06	7.36e-06
250.312900	36.398300	9.79e-07	1.79e-06	2.32e-06	2.65e-06	6.74e-06	1.05e-05	1.11e-05
250.307800	36.417400	7.10e-07	1.26e-06	1.60e-06	1.83e-06	4.53e-06	7.31e-06	7.41e-06
250.326100	36.347100	4.75e-07	8.08e-07	1.01e-06	1.11e-06	2.80e-06	4.23e-06	4.66e-06
250.238900	36.587100	9.56e-08	1.47e-07	1.75e-07	1.91e-07	4.90e-07	7.59e-07	9.66e-07
250.267300	36.586400	9.77e-08	1.50e-07	1.81e-07	2.00e-07	5.05e-07	7.12e-07	7.04e-07
250.242900	36.708600	2.59e-07	4.29e-07	5.29e-07	6.06e-07	1.32e-06	2.17e-06	2.20e-06
250.333900	36.614500	1.07e-06	8.99e-07	7.89e-07	7.24e-07	1.26e-06	1.37e-06	1.36e-06
250.331100	36.507700	6.85e-07	1.20e-06	1.52e-06	1.78e-06	4.16e-06	6.57e-06	7.54e-06
250.361800	36.424600	8.08e-07	1.42e-06	1.81e-06	1.98e-06	4.96e-06	8.17e-06	8.68e-06
250.315400	36.463900	8.77e-07	1.57e-06	2.01e-06	2.33e-06	5.81e-06	8.99e-06	9.71e-06
250.316000	36.554900	7.76e-07	1.36e-06	1.75e-06	2.04e-06	4.92e-06	8.02e-06	8.39e-06
250.323900	36.491600	1.10e-06	2.00e-06	2.60e-06	3.05e-06	7.69e-06	1.22e-05	1.34e-05
250.375500	36.591200	8.45e-07	1.50e-06	1.96e-06	2.23e-06	5.53e-06	8.86e-06	9.42e-06
250.450700	36.594800	5.20e-07	8.99e-07	1.16e-06	1.30e-06	3.24e-06	4.90e-06	5.28e-06
250.397800	36.604600	1.04e-06	8.61e-07	7.68e-07	7.13e-07	1.20e-06	1.35e-06	1.31e-06
250.460900	36.555100	1.10e-06	1.08e-06	1.04e-06	1.01e-06	1.86e-06	1.99e-06	2.12e-06
250.331800	36.689700	8.06e-07	1.42e-06	1.83e-06	2.16e-06	5.01e-06	8.16e-06	8.57e-06
250.388600	36.541200	1.09e-06	1.98e-06	2.59e-06	3.00e-06	7.39e-06	1.21e-05	1.29e-05
250.405100	36.680700	2.90e-07	4.78e-07	5.94e-07	6.71e-07	1.58e-06	2.14e-06	2.38e-06
250.439300	36.430600	1.11e-06	1.11e-06	1.07e-06	9.97e-07	1.71e-06	1.99e-06	1.87e-06
250.418800	36.526800	1.02e-06	1.85e-06	2.39e-06	2.76e-06	6.75e-06	1.09e-05	1.18e-05
250.453800	36.534700	4.79e-07	8.26e-07	1.04e-06	1.17e-06	2.78e-06	4.16e-06	4.75e-06
250.433000	36.411600	7.79e-07	1.41e-06	1.79e-06	2.06e-06	4.73e-06	7.65e-06	8.22e-06
250.469200	36.514700	8.37e-07	6.51e-07	5.40e-07	4.94e-07	7.68e-07	7.31e-07	6.72e-07
250.542400	36.630800	8.65e-07	1.57e-06	2.00e-06	2.33e-06	5.79e-06	8.81e-06	9.86e-06
250.520700	36.526800	4.85e-07	8.34e-07	1.05e-06	1.17e-06	2.91e-06	4.44e-06	4.97e-06
250.556900	36.554100	5.57e-07	9.66e-07	1.22e-06	1.40e-06	3.34e-06	5.04e-06	5.64e-06
250.504500	36.562600	8.24e-07	6.53e-07	5.50e-07	4.95e-07	8.08e-07	8.22e-07	6.44e-07
250.468700	36.450400	8.69e-07	1.56e-06	2.00e-06	2.23e-06	6.70e-06	9.90e-06	1.04e-05
250.539200	36.566400	6.52e-07	1.16e-06	1.48e-06	1.69e-06	4.31e-06	6.62e-06	6.84e-06
250.545500	36.409200	8.43e-07	1.50e-06	1.93e-06	2.20e-06	5.56e-06	8.65e-06	8.98e-06
250.507400	36.389600	8.80e-07	1.55e-06	1.98e-06	2.29e-06	5.75e-06	8.91e-06	9.67e-06
250.444100	36.501300	7.07e-07	1.25e-06	1.59e-06	1.84e-06	4.43e-06	6.84e-06	7.11e-06
250.571500	36.525900	5.94e-07	1.02e-06	1.29e-06	1.46e-06	3.55e-06	5.76e-06	5.65e-06
250.582600	36.496100	8.99e-07	1.59e-06	2.06e-06	2.34e-06	5.94e-06	9.44e-06	1.01e-05
250.612300	36.650700	2.42e-07	3.95e-07	4.81e-07	5.41e-07	1.34e-06	2.00e-06	1.99e-06
250.579500	36.617600	7.35e-07	1.30e-06	1.65e-06	1.90e-06	4.67e-06	7.24e-06	7.54e-06

Table 11: M13 part 2: Rates (Flux) for Different Bands for given R.A. and Decl.

R.A.	Decl.	G_RATE	R_RATE	I_RATE	Z_RATE	J_RATE	H_RATE	K_RATE
250.608400	36.451300	7.63e-07	1.35e-06	1.73e-06	1.95e-06	4.84e-06	7.94e-06	7.99e-06
250.584700	36.450900	9.71e-07	7.93e-07	6.96e-07	6.33e-07	1.10e-06	1.05e-06	9.77e-07
250.486700	36.697500	7.25e-07	1.31e-06	1.65e-06	1.95e-06	4.64e-06	7.33e-06	8.33e-06
250.554500	36.267800	2.92e-07	4.78e-07	5.90e-07	6.56e-07	1.56e-06	2.48e-06	2.29e-06
250.546400	36.306200	9.44e-07	1.67e-06	2.15e-06	2.45e-06	6.20e-06	9.64e-06	1.01e-05
250.408500	36.303900	5.26e-07	9.02e-07	1.12e-06	1.27e-06	3.20e-06	4.89e-06	5.23e-06
250.452000	36.301800	8.65e-07	6.84e-07	5.77e-07	5.22e-07	8.75e-07	8.54e-07	7.45e-07
250.411100	36.377700	3.35e-06	7.31e-06	1.01e-05	1.23e-05	3.41e-05	6.04e-05	6.71e-05
250.404100	36.351500	5.04e-07	8.54e-07	1.07e-06	1.19e-06	2.91e-06	4.38e-06	4.84e-06
250.490600	36.363500	8.13e-07	6.25e-07	5.28e-07	4.73e-07	7.44e-07	7.32e-07	8.61e-07
250.428900	36.330100	8.78e-07	1.57e-06	2.00e-06	2.32e-06	5.75e-06	9.20e-06	9.33e-06
250.489400	36.332100	8.35e-07	1.44e-06	1.87e-06	2.18e-06	5.38e-06	8.89e-06	9.04e-06
250.234900	36.371800	1.30e-06	2.42e-06	3.15e-06	3.66e-06	9.29e-06	1.54e-05	1.64e-05
250.361500	36.390400	9.06e-07	1.60e-06	2.04e-06	2.22e-06	5.72e-06	9.31e-06	9.54e-06
250.313600	36.387800	1.02e-06	8.51e-07	7.47e-07	6.84e-07	1.14e-06	1.20e-06	1.16e-06
250.326100	36.347100	4.75e-07	8.08e-07	1.01e-06	1.11e-06	2.80e-06	4.23e-06	4.66e-06
250.401700	36.285500	1.69e-06	3.28e-06	4.32e-06	5.13e-06	1.32e-05	2.18e-05	2.36e-05
250.314600	36.517400	5.78e-07	9.78e-07	1.24e-06	1.44e-06	3.43e-06	5.40e-06	5.68e-06
250.230900	36.595300	1.08e-06	2.00e-06	2.61e-06	3.04e-06	7.52e-06	1.22e-05	1.31e-05
250.332600	36.410600	2.21e-06	4.32e-06	5.89e-06	7.01e-06	1.83e-05	3.07e-05	3.34e-05
250.291100	36.569400	9.06e-07	7.11e-07	5.99e-07	5.43e-07	9.66e-07	9.50e-07	9.59e-07
250.307800	36.417400	7.10e-07	1.26e-06	1.60e-06	1.83e-06	4.53e-06	7.31e-06	7.41e-06
250.260800	36.437700	7.33e-07	1.29e-06	1.64e-06	1.88e-06	4.56e-06	6.92e-06	7.36e-06
250.378400	36.503500	2.42e-06	4.62e-06	6.10e-06	7.16e-06	1.83e-05	2.95e-05	3.13e-05
250.442200	36.429200	9.81e-07	8.09e-07	7.00e-07	6.28e-07	7.16e-07	6.97e-07	5.61e-07
250.391000	36.452900	4.31e-07	7.08e-07	9.09e-07	9.80e-07	1.61e-05	2.55e-05	2.70e-05
250.396400	36.400800	8.34e-07	1.48e-06	1.89e-06	2.17e-06	5.48e-06	8.64e-06	8.86e-06
250.368100	36.451000	2.72e-06	5.67e-06	7.72e-06	9.02e-06	2.49e-05	4.28e-05	4.63e-05
250.313400	36.489900	2.14e-06	4.29e-06	5.83e-06	6.96e-06	1.81e-05	3.05e-05	3.29e-05
250.378700	36.425400	1.68e-06	3.19e-06	4.21e-06	4.86e-06	1.28e-05	2.11e-05	2.28e-05
250.333900	36.614500	1.07e-06	8.99e-07	7.89e-07	7.24e-07	1.26e-06	1.37e-06	1.36e-06
250.316000	36.554900	7.76e-07	1.36e-06	1.75e-06	2.04e-06	4.92e-06	8.02e-06	8.39e-06
250.438100	36.470200	4.19e-06	9.75e-06	1.37e-05	1.69e-05	4.75e-05	8.52e-05	9.48e-05
250.362600	36.566100	2.91e-07	4.68e-07	5.82e-07	6.59e-07	1.57e-06	3.03e-06	3.40e-06
250.459500	36.404200	7.30e-06	2.37e-05	3.80e-05	5.11e-05	1.63e-04	3.22e-04	3.74e-04
250.442000	36.454600	1.73e-06	3.36e-06	4.49e-06	5.24e-06	1.43e-05	2.35e-05	2.48e-05
250.388600	36.541200	1.09e-06	1.98e-06	2.59e-06	3.00e-06	7.39e-06	1.21e-05	1.29e-05
250.424700	36.447600	7.60e-06	2.64e-05	4.53e-05	6.21e-05	7.71e-06	1.24e-05	1.48e-05
250.436500	36.390900	2.30e-06	4.68e-06	6.28e-06	7.55e-06	1.97e-05	3.26e-05	3.62e-05
250.438600	36.518500	2.55e-06	5.24e-06	7.20e-06	8.55e-06	2.27e-05	3.88e-05	4.29e-05
250.485700	36.500700	1.38e-06	2.60e-06	3.44e-06	3.96e-06	1.03e-05	1.72e-05	1.83e-05
250.420000	36.569800	1.54e-06	2.95e-06	3.94e-06	4.51e-06	1.19e-05	1.94e-05	2.17e-05
250.443000	36.553800	8.82e-07	7.13e-07	6.17e-07	5.63e-07	9.68e-07	1.03e-06	8.77e-07
250.450800	36.594800	5.20e-07	8.99e-07	1.16e-06	1.30e-06	3.24e-06	4.90e-06	5.28e-06
250.462000	36.481700	6.85e-06	2.34e-05	3.92e-05	5.23e-05	1.81e-04	3.66e-04	4.16e-04
250.465400	36.459000	1.39e-06	2.62e-06	3.50e-06	3.92e-06	1.00e-05	1.64e-05	1.71e-05
250.501500	36.423500	1.29e-06	2.42e-06	3.16e-06	3.66e-06	9.45e-06	1.53e-05	1.62e-05
250.471700	36.423100	9.84e-07	1.78e-06	2.32e-06	2.57e-06	6.44e-06	1.04e-05	1.09e-05
250.571500	36.525900	5.94e-07	1.02e-06	1.29e-06	1.46e-06	3.55e-06	5.76e-06	5.65e-06
250.541100	36.495500	8.33e-07	1.50e-06	1.93e-06	2.23e-06	5.41e-06	8.49e-06	9.09e-06
250.578600	36.504300	8.23e-07	1.47e-06	1.90e-06	2.15e-06	5.31e-06	8.54e-06	9.07e-06
250.539200	36.566400	6.52e-07	1.16e-06	1.48e-06	1.69e-06	4.31e-06	6.62e-06	6.84e-06
250.510500	36.542400	8.63e-07	1.55e-06	1.99e-06	2.27e-06	5.50e-06	8.85e-06	9.48e-06
250.520700	36.526800	4.85e-07	8.34e-07	1.05e-06	1.17e-06	2.91e-06	4.44e-06	4.97e-06
250.608400	36.451300	7.63e-07	1.35e-06	1.73e-06	1.95e-06	4.84e-06	7.94e-06	7.99e-06
250.568800	36.416200	1.42e-06	2.67e-06	3.52e-06	4.08e-06	1.07e-05	1.73e-05	1.90e-05
250.556500	36.476800	6.62e-07	1.16e-06	1.47e-06	1.68e-06	4.09e-06	6.49e-06	6.77e-06
250.568700	36.437100	9.14e-07	1.64e-06	2.10e-06	2.41e-06	6.19e-06	9.66e-06	1.04e-05

Table 12: NGC 6791:Rates (Flux) for Different Bands for given R.A. and Decl.

R.A.	Decl.	G RATE	R RATE	I RATE	Z RATE	J RATE	H RATE	K RATE
290.310500	37.775800	7.11e-08	1.67e-07	2.22e-07	2.68e-07	6.92e-07	1.03e-06	1.19e-06
290.277900	37.802300	3.66e-08	6.89e-08	8.50e-08	9.81e-08	1.92e-07	3.47e-07	4.77e-07
290.256000	37.801400	2.69e-07	7.40e-07	1.06e-06	1.34e-06	3.87e-06	6.53e-06	7.76e-06
290.289400	37.784000	1.38e-07	3.59e-07	4.98e-07	6.23e-07	1.68e-06	2.91e-06	3.13e-06
290.276200	37.749900	8.48e-07	2.37e-06	3.46e-06	4.30e-06	1.25e-05	2.20e-05	2.51e-05
290.308400	37.752600	1.67e-07	4.27e-07	5.90e-07	7.15e-07	1.99e-06	3.45e-06	4.06e-06
290.268900	37.721200	6.20e-08	1.41e-07	1.86e-07	2.17e-07	5.46e-07	8.16e-07	9.70e-07
290.244800	37.720300	7.53e-07	2.19e-06	3.24e-06	4.03e-06	1.21e-05	2.09e-05	2.46e-05
290.208500	37.797700	6.19e-08	1.22e-07	1.49e-07	1.68e-07	4.11e-07	6.84e-07	7.83e-07
290.230800	37.797100	5.99e-08	1.47e-07	2.01e-07	2.38e-07	6.50e-07	1.13e-06	1.39e-06
290.253600	37.759400	7.81e-07	2.35e-06	3.49e-06	4.48e-06	1.37e-05	2.39e-05	2.80e-05
290.253600	37.777700	7.76e-07	2.27e-06	3.30e-06	4.21e-06	1.27e-05	2.19e-05	2.59e-05
290.220300	37.759200	8.16e-07	2.30e-06	3.31e-06	4.15e-06	1.22e-05	2.15e-05	2.48e-05
290.188200	37.742800	5.62e-07	1.70e-06	2.58e-06	3.31e-06	1.01e-05	1.83e-05	2.08e-05
290.130300	37.775200	5.74e-08	1.06e-07	1.31e-07	1.40e-07	3.14e-07	4.27e-07	6.96e-07
290.188900	37.788300	7.67e-07	2.20e-06	3.17e-06	4.07e-06	1.24e-05	2.13e-05	2.44e-05
290.127700	37.754800	6.17e-08	1.13e-07	1.38e-07	1.52e-07	3.33e-07	5.34e-07	1.02e-06
290.163500	37.743700	6.14e-07	1.76e-06	2.51e-06	3.15e-06	9.12e-06	1.60e-05	1.86e-05
290.143300	37.801100	6.89e-08	1.38e-07	1.73e-07	1.98e-07	5.22e-07	6.27e-07	9.09e-07
290.196100	37.761200	3.51e-08	6.72e-08	8.29e-08	9.25e-08	1.68e-07	1.56e-07	5.42e-07
290.168800	37.785200	9.53e-08	2.38e-07	3.23e-07	3.86e-07	1.01e-06	1.61e-06	1.79e-06
290.176700	37.764200	1.97e-07	5.24e-07	7.41e-07	9.18e-07	2.73e-06	4.49e-06	5.59e-06
290.174200	37.706000	6.66e-08	1.20e-07	1.46e-07	1.62e-07	3.13e-07	5.25e-07	1.87e-07
290.180800	37.721400	1.58e-07	4.06e-07	5.61e-07	6.93e-07	1.80e-06	3.10e-06	3.48e-06
290.124700	37.811500	7.32e-08	1.44e-07	1.83e-07	2.03e-07	5.07e-07	5.07e-07	7.91e-07
290.240500	37.817000	3.59e-07	1.03e-06	1.53e-06	1.96e-06	5.90e-06	1.03e-05	1.16e-05
290.192700	37.819600	4.36e-07	1.23e-06	1.80e-06	2.34e-06	6.79e-06	1.20e-05	1.39e-05
290.163300	37.834600	3.75e-08	7.09e-08	8.97e-08	9.99e-08	2.28e-07	9.55e-07	7.21e-07
290.157900	37.819000	6.26e-08	1.26e-07	1.63e-07	1.86e-07	3.78e-07	6.65e-07	5.60e-07
290.286000	37.717500	2.70e-08	5.17e-08	6.39e-08	7.19e-08	1.94e-07	2.67e-07	5.75e-07
290.292600	37.752100	4.97e-08	9.24e-08	1.11e-07	1.21e-07	2.28e-07	4.75e-07	6.74e-07
290.267500	37.732500	5.26e-08	9.66e-08	1.17e-07	1.29e-07	2.79e-07	4.90e-07	4.80e-07
290.169600	37.707400	1.49e-08	3.19e-08	4.19e-08	4.65e-08	2.34e-07	3.92e-07	5.60e-07
290.233100	37.779500	2.68e-08	5.38e-08	6.69e-08	7.53e-08	4.02e-07	4.44e-07	6.27e-07
290.234000	37.725500	2.99e-08	5.79e-08	7.13e-08	7.83e-08	1.92e-07	3.30e-07	2.53e-07
290.233200	37.695000	5.59e-08	1.06e-07	1.31e-07	1.45e-07	2.92e-07	6.77e-07	5.71e-07
290.191700	37.750200	3.17e-08	6.26e-08	7.71e-08	8.29e-08	2.06e-07	3.05e-07	6.62e-07
290.161800	37.722400	4.34e-08	8.03e-08	9.67e-08	1.07e-07	2.50e-07	3.20e-07	2.22e-07
290.185100	37.733300	4.82e-08	8.74e-08	1.07e-07	1.18e-07	3.27e-07	3.61e-07	3.78e-07
290.162000	37.777000	2.55e-08	5.01e-08	6.29e-08	7.03e-08	1.85e-07	1.35e-07	1.60e-07
290.148600	37.759500	1.89e-08	4.00e-08	5.06e-08	5.54e-08	1.80e-07	3.01e-07	5.47e-07
290.183800	37.777400	3.06e-08	6.04e-08	7.50e-08	8.34e-08	2.13e-07	1.82e-06	2.46e-06
290.213500	37.741200	3.12e-08	5.98e-08	7.40e-08	8.59e-08	3.38e-07	6.45e-07	9.05e-07
290.144300	37.786400	4.28e-08	7.89e-08	9.70e-08	1.06e-07	2.74e-07	3.29e-07	3.98e-07
290.125700	37.764300	5.06e-08	9.55e-08	1.16e-07	1.26e-07	2.64e-07	3.75e-07	6.14e-07
290.119300	37.798000	4.98e-08	9.39e-08	1.17e-07	1.28e-07	2.63e-07	2.63e-07	9.38e-07

A.11 Tables that show stellar parameters obtained with BEAST

Table 13: M92: Stellar parameters obtained with BEAST

R.A.°	Decl.°	Luminosity (L_{\odot})	Radius (R_{\odot})	Age (Gyr)	Temperature (K)	Mass (M_{\odot})	Metallicity	Av	Rv
259.199700	43.104400	95.940063	12.609997	6.422435	5081.496429	0.976927	0.000383	0.094329	2.753792
259.183100	43.125500	117.760597	14.182576	7.104617	5050.355654	0.661960	0.000295	0.074770	2.752295
259.142900	43.126800	253.512863	21.586128	5.854105	4949.243897	1.209518	0.000209	0.075463	2.751016
259.157200	43.144800	248.313311	21.205383	5.901772	4958.758121	1.060225	0.000204	0.075845	2.751494
259.251400	43.196600	215.278173	19.623780	6.889315	4968.217633	1.066867	0.000229	0.073636	2.751666
259.245200	43.253200	321.366054	25.218821	6.599834	4846.436917	1.050536	0.000308	0.118891	2.755688
259.228000	43.174000	96.161228	12.700859	6.258713	5104.255070	0.913243	0.000256	0.048957	2.748915
259.207800	43.178100	636.795521	39.691437	6.102978	4633.031764	1.069980	0.000317	0.106884	2.753931
259.240600	43.236500	343.557948	27.187262	6.542756	4807.423522	0.836424	0.000321	0.128280	2.756206
259.231300	43.084300	177.418948	18.086901	6.370877	4967.846831	1.051669	0.000331	0.102477	2.754498
259.149100	42.944300	86.297855	11.836464	6.316920	5120.009970	1.134995	0.000385	0.116449	2.755336
259.248700	43.018300	106.414302	13.307905	6.762561	5067.786888	1.072408	0.000321	0.076610	2.752145
259.220200	43.058200	95.279616	10.761022	4.272720	5510.684982	1.067492	0.000319	0.011867	2.744401
259.340500	43.214900	1510.080154	73.161808	5.212113	4209.548781	1.131266	0.000655	0.052562	2.748320
259.318900	43.179200	463.446920	32.936783	6.254562	4720.079384	0.749692	0.000309	0.101533	2.753759
259.340300	43.184200	140.928880	15.556607	7.246950	5018.994985	1.068777	0.000320	0.088127	2.753219
259.293500	43.185500	1020.939484	55.550007	5.421448	4436.275954	0.867375	0.000381	0.087380	2.753239
259.332000	43.245100	144.543977	15.886818	7.003693	5080.076651	1.133906	0.000205	0.038300	2.748189
259.337600	43.103500	96.382902	11.867864	4.813925	5298.928781	0.856539	0.000272	0.027810	2.746423
259.314600	43.083100	106.414302	13.157594	6.671805	5075.990740	0.654491	0.000309	0.068754	2.751306
259.304800	43.000100	59.292532	7.681245	8.601889	5884.882416	1.054182	0.000274	0.097832	2.756250
259.266400	43.034100	100.925289	13.000875	6.594610	5078.662693	1.139929	0.000319	0.074297	2.751703
259.382100	43.094900	672.976656	40.756554	5.991285	4620.408043	1.028701	0.000318	0.102771	2.754122
259.369900	43.167500	86.696188	11.945863	6.270144	5123.413079	1.054451	0.000341	0.081122	2.752160
259.370900	43.115300	74.473197	10.628423	4.858113	5220.218896	0.843424	0.000746	0.112056	2.754409
259.373000	43.204100	100.925289	13.025275	6.571296	5082.416247	1.081882	0.000303	0.070152	2.751005
259.342500	43.080500	251.767693	21.459547	6.050977	4936.221800	1.210814	0.000255	0.128551	2.755644
259.519700	43.171200	74.473197	10.552544	4.803087	5229.240348	0.936923	0.000792	0.105168	2.753940
259.459800	43.229500	62.950618	9.849491	5.999542	5247.913216	0.787907	0.000985	0.177344	2.762778
259.052700	43.173900	44.771330	2.680927	12.600000	9116.353002	0.674602	0.000100	0.191233	2.774348
259.124500	43.100900	33.036954	6.752709	7.353623	5289.031384	0.735196	0.000356	0.111390	2.755988
259.151600	43.115600	64.120958	9.864725	5.922282	5248.620046	0.726090	0.000955	0.167035	2.762923
259.192500	43.082900	52.239619	8.839982	8.579840	5315.481603	0.746357	0.000592	0.196608	2.766041
259.212000	43.189700	44.157045	2.629377	12.600000	9180.046592	0.827061	0.000100	0.284633	2.819655
259.178300	43.246500	33.419504	6.812121	7.140267	5295.704955	0.941210	0.000305	0.072262	2.752578
259.201200	43.171300	56.754461	8.984877	8.098644	5325.476351	0.766291	0.000614	0.197692	2.764839
259.268100	43.069600	27.415742	6.211535	7.341877	5312.186856	0.708878	0.000336	0.072870	2.751804
259.189800	43.229600	33.419504	6.862844	7.125726	5294.446585	0.997280	0.000297	0.065083	2.751421
259.149000	42.944300	86.297855	11.836464	6.316920	5120.009970	1.018873	0.000385	0.116449	2.755336
259.347100	42.948800	82.413812	11.176366	5.573103	5170.368195	1.092365	0.000460	0.099140	2.754160
259.252800	43.217500	44.771330	2.644757	12.600000	9147.309058	0.668155	0.000100	0.204208	2.781343
259.290100	43.079600	44.771330	2.650372	12.600000	9140.554546	1.005411	0.000100	0.173132	2.777651
259.313000	43.264500	19.633603	5.133998	7.154531	5377.637254	0.929548	0.000289	0.040343	2.747756
259.401700	43.019900	49.888449	3.454628	12.599855	8297.278632	0.984357	0.000100	0.062148	2.751398
259.329600	43.215200	56.754461	9.111243	7.915908	5303.016018	0.709744	0.000681	0.191019	2.763411
259.344600	43.158700	44.157045	2.629502	12.600000	9179.698353	0.828677	0.000100	0.392950	2.857184
259.449900	43.307000	6.934258	2.241825	5.569635	6320.569563	1.020576	0.000792	0.194204	2.748875
259.366000	43.147500	48.977882	3.209784	12.600000	8485.782453	0.788160	0.000100	0.145599	2.760333
259.321400	43.074200	28.840315	6.369604	6.650277	5334.434429	0.960004	0.000239	0.026804	2.746849
259.381200	43.246900	5.902011	2.749850	9.068350	5540.768857	0.879952	0.000943	0.212480	2.775175
259.393800	43.071100	24.210290	5.742799	7.394379	5334.631131	0.916992	0.000355	0.103686	2.755415
259.484400	43.059500	5.902011	2.769773	9.084981	5536.298427	0.879639	0.000921	0.149800	2.763502
259.432200	43.063400	13.061709	4.187599	7.929720	5422.183645	0.903491	0.000405	0.118930	2.758558
259.577200	43.199000	19.633603	5.143583	7.439361	5370.568173	0.907954	0.000313	0.053716	2.750178
259.459800	43.229500	62.950618	9.849491	5.999542	5247.913216	1.016276	0.000985	0.177344	2.762778
259.519700	43.171200	74.644876	10.438103	4.743762	5238.501291	1.088770	0.000871	0.103692	2.753191
259.404200	43.131000	44.157045	2.627883	12.600000	9183.998953	0.788160	0.000100	0.482664	2.885324
259.390500	43.189600	4.731513	2.159186	8.095002	5973.431466	0.904942	0.000737	0.141364	2.763691
259.437400	43.135600	7.194490	2.892489	8.283526	5615.281812	0.897858	0.000433	0.065057	2.752911

Table 14: M13 part 1: Stellar parameters obtained with BEAST

R.A.°	Decl.°	Luminosity (L_{\odot})	Radius (R_{\odot})	Age (Gyr)	Temperature (K)	Mass (M_{\odot})	Metallicity	Av	Rv
250.474200	36.309800	7.759603	3.065010	8.866598	5506.609183	0.818387	0.000396	0.096596	3.447018
250.512500	36.321100	18.404263	5.106610	8.425274	5325.105171	0.822513	0.000426	0.344745	3.660943
250.466400	36.409300	48.346563	3.141670	4.407438	8590.722466	0.787984	0.000100	0.029403	3.397721
250.297500	36.656600	5.035287	2.214921	8.739467	5786.028331	0.814788	0.000424	0.108779	3.440320
250.363700	36.539500	80.358435	11.640271	7.307417	5089.700903	0.823309	0.000368	0.103858	3.454938
250.315400	36.581800	5.773876	2.527156	9.025786	5613.248649	0.817024	0.000432	0.220660	3.593211
250.348800	36.637100	6.911540	2.865087	8.956611	5517.509085	0.819159	0.000469	0.183843	3.555912
250.355900	36.608400	8.611657	3.274559	9.088347	5473.889226	0.818767	0.000423	0.102112	3.465748
250.416200	36.592700	8.342495	3.208738	8.845850	5486.931354	0.818134	0.000389	0.066942	3.429993
250.377600	36.560600	13.746851	4.266339	9.384347	5379.433684	0.820470	0.000394	0.094899	3.454029
250.452500	36.731100	41.341287	7.391078	8.227920	5286.014847	0.812845	0.000493	0.224909	3.590507
250.533400	36.323900	24.604332	5.950850	8.806768	5297.247026	0.821227	0.000326	0.068333	3.427970
250.489400	36.332100	78.590054	11.564631	7.326989	5074.880610	0.823890	0.000406	0.124491	3.471828
250.490600	36.363500	45.307067	2.659643	12.322642	9133.944780	0.787207	0.000100	0.174436	3.613147
250.450500	36.393300	95.421040	12.823029	7.283506	5037.761147	0.822733	0.000371	0.109739	3.454281
250.466200	36.326300	86.518226	12.158588	7.432621	5070.090632	0.823301	0.000371	0.126755	3.475165
250.352200	36.409500	57.251700	8.201925	7.689012	5577.586683	0.833423	0.000644	0.407191	3.622321
250.452000	36.301800	45.436226	2.664532	12.261705	9129.559718	0.787244	0.000100	0.097103	3.477313
250.408500	36.303900	56.357834	8.487314	7.573448	5387.598660	0.840830	0.000909	0.352269	3.601870
250.275600	36.422900	105.599581	13.737819	7.093544	4969.625001	0.824018	0.000439	0.108020	3.464687
250.260800	36.437700	66.741196	10.258667	7.418920	5151.480021	0.831385	0.000448	0.105896	3.454102
250.312900	36.398300	95.859895	12.884859	7.239495	5018.435842	0.823165	0.000382	0.120340	3.459854
250.307800	36.417400	67.904813	10.519677	7.421843	5128.689685	0.831365	0.000479	0.137906	3.475464
250.326100	36.347100	57.144303	7.911085	7.747065	5662.176908	0.831834	0.000571	0.495797	3.669021
250.238900	36.587100	9.187827	3.440984	9.431810	5444.561386	0.824536	0.000473	0.273811	3.637420
250.267300	36.586400	8.034619	3.160107	8.971839	5488.404390	0.818628	0.000426	0.124369	3.462736
250.242900	36.708600	21.729013	5.532910	8.694922	5309.770952	0.821486	0.000375	0.089228	3.448146
250.333900	36.614500	49.846469	3.528685	4.368214	8173.017413	0.814124	0.000100	0.068644	3.447061
250.331100	36.507700	63.185499	10.113491	7.375419	5140.115475	0.839610	0.000549	0.128087	3.481651
250.361800	36.424600	75.507900	11.171492	7.438205	5103.210695	0.823892	0.000401	0.115658	3.468411
250.315400	36.463900	84.947711	11.883163	7.347855	5079.118325	0.823253	0.000364	0.123720	3.463241
250.316000	36.554900	73.655587	11.067727	7.478264	5098.553523	0.827012	0.000439	0.126566	3.471566
250.323900	36.491600	109.198974	14.052096	7.235753	4962.389413	0.823983	0.000429	0.126524	3.479652
250.375500	36.591200	80.648035	11.721261	7.338843	5071.113293	0.823725	0.000402	0.124850	3.468014
250.450700	36.594800	56.345459	8.550440	7.553158	5374.961270	0.850662	0.001022	0.351456	3.590724
250.397800	36.604600	49.474382	3.380240	4.389078	8272.433957	0.788536	0.000100	0.079386	3.460328
250.460900	36.555100	54.076875	4.399381	4.420642	7478.402076	0.842231	0.000100	0.052069	3.410457
250.331800	36.689700	75.663975	11.179640	7.426791	5103.972744	0.823883	0.000399	0.114587	3.461340
250.388600	36.541200	106.314548	13.804262	7.116858	4967.024621	0.824048	0.000441	0.112573	3.468126
250.405100	36.680700	23.808193	5.774766	8.925817	5306.955644	0.812421	0.000323	0.062928	3.421595
250.439300	36.430600	53.626451	4.323793	4.382803	7522.439373	0.842188	0.000100	0.040669	3.406103
250.418800	36.526800	97.685841	13.144545	7.162453	5003.791926	0.814028	0.000406	0.108294	3.460446
250.453800	36.534700	57.229176	7.921242	7.756025	5661.034219	0.831988	0.000574	0.480179	3.658478
250.433000	36.411600	71.406081	10.824597	7.557557	5121.946363	0.824183	0.000418	0.098075	3.450646
250.469200	36.514700	45.144322	2.653463	12.547302	9140.604499	0.787191	0.000100	0.146314	3.577396
250.542400	36.630800	84.783840	11.890365	7.358139	5075.165798	0.823401	0.000377	0.128777	3.465580
250.520700	36.526800	57.137306	8.182497	7.691594	5579.019803	0.833445	0.000651	0.454368	3.662148
250.556900	36.554100	56.485332	8.737240	7.521721	5347.926133	0.858220	0.001264	0.276424	3.552467
250.504500	36.562600	45.247696	2.657391	12.501688	9136.183656	0.787199	0.000100	0.147294	3.552825
250.468700	36.450400	93.112314	12.670899	7.435152	5031.264969	0.823903	0.000396	0.203621	3.508649
250.539200	36.566400	61.796938	9.982881	7.355678	5113.423542	0.841565	0.000697	0.130335	3.465086
250.545500	36.409200	78.715463	11.520982	7.302227	5092.887780	0.823639	0.000388	0.110161	3.453917
250.507400	36.389600	84.171455	11.823241	7.336785	5083.594612	0.823191	0.000357	0.119410	3.463741
250.444100	36.501300	64.297223	10.139866	7.375343	5152.073090	0.832491	0.000502	0.108608	3.454013
250.571500	36.525900	56.648564	8.989727	7.588310	5301.216739	0.859794	0.001575	0.190748	3.495501
250.582600	36.496100	86.386209	12.112215	7.414624	5073.137210	0.823233	0.000362	0.129381	3.473021
250.612300	36.650700	20.282875	5.410025	8.712243	5318.134788	0.821765	0.000385	0.104698	3.452168
250.579500	36.617600	69.031619	10.576224	7.464913	5137.087862	0.829897	0.000438	0.126560	3.465153
250.608400	36.451300	71.487598	10.878189	7.526509	5107.487707	0.829043	0.000443	0.121021	3.465790
250.584700	36.450900	47.097581	2.928045	11.009293	8873.734589	0.787944	0.000100	0.045801	3.407466
250.486700	36.697500	70.318034	10.814677	7.491662	5099.581378	0.830048	0.000477	0.146776	3.486691
250.554500	36.267800	24.155287	5.835491	8.687699	5295.639275	0.821222	0.000348	0.077415	3.434313
250.546400	36.306200	87.279972	12.192150	7.383346	5076.717859	0.822914	0.000339	0.098535	3.449859

Table 15: M13 part 2: Stellar parameters obtained with BEAST

R.A.°	Decl.°	Luminosity (L_{\odot})	Radius (R_{\odot})	Age (Gyr)	Temperature (K)	Mass (M_{\odot})	Metallicity	Av	Rv
250.408500	36.303900	56.357834	8.487314	7.573448	5387.598660	0.840830	0.000909	0.352269	3.601870
250.452000	36.301800	45.436226	2.664532	12.261705	9129.559718	0.787244	0.000100	0.097103	3.477313
250.411100	36.377700	441.900500	32.624069	7.226484	4615.936167	0.825414	0.000447	0.172224	3.507321
250.404100	36.351500	57.661213	8.065531	7.722213	5637.389980	0.833219	0.000598	0.441269	3.647158
250.490600	36.363500	45.307067	2.659643	12.322642	9133.944780	0.787207	0.000100	0.174436	3.613147
250.428900	36.330100	83.900549	11.817699	7.319136	5082.173656	0.823214	0.000362	0.114156	3.456597
250.489400	36.332100	78.590054	11.564631	7.326989	5074.880610	0.823890	0.000406	0.124491	3.471828
250.234900	36.371800	137.868021	15.560500	7.124275	5014.189919	0.824159	0.000373	0.186139	3.506068
250.361500	36.390400	84.924190	11.845936	7.314656	5087.822327	0.822999	0.000340	0.102064	3.456228
250.313600	36.387800	48.203646	3.111564	4.399136	8629.853602	0.787973	0.000100	0.041242	3.411061
250.326100	36.347100	57.144303	7.911085	7.747065	5662.176908	0.831834	0.000571	0.495797	3.669021
250.401700	36.285500	188.539943	18.832020	7.716067	4958.087337	0.823690	0.000304	0.190317	3.500330
250.314600	36.517400	56.604235	8.856085	7.539769	5326.981692	0.859099	0.001403	0.237208	3.531451
250.230900	36.595300	107.821698	13.970439	7.178413	4960.643919	0.824127	0.000454	0.126649	3.476347
250.332600	36.410600	251.972165	22.582550	7.124836	4872.492879	0.824129	0.000365	0.169593	3.496204
250.291100	36.569400	46.839014	2.905429	10.881399	8896.879844	0.787876	0.000100	0.126510	3.508593
250.307800	36.417400	67.904813	10.519677	7.421843	5128.689685	0.831365	0.000479	0.137906	3.475464
250.260800	36.437700	66.741196	10.258667	7.418920	5151.480021	0.831385	0.000448	0.105896	3.454102
250.378400	36.503500	245.686459	21.792610	6.586972	4899.157905	0.816296	0.000257	0.096955	3.445940
250.442200	36.429200	45.104998	2.651966	12.596279	9142.491260	0.787190	0.000100	0.006213	3.381356
250.391000	36.452900	169.319779	23.553740	11.365987	4317.260379	0.879513	0.005000	0.598917	3.167829
250.396400	36.400800	78.222957	11.471541	7.309241	5094.172268	0.823775	0.000395	0.115091	3.458282
250.368100	36.451000	329.983854	26.945078	7.204285	4771.183092	0.824108	0.000393	0.170322	3.497173
250.313400	36.489900	249.137475	22.530550	7.088740	4867.119182	0.824404	0.000387	0.178832	3.496686
250.378700	36.425400	183.118120	18.503285	7.784200	4963.215496	0.816012	0.000295	0.181834	3.504071
250.333900	36.614500	49.846469	3.528685	4.368214	8173.017413	0.814124	0.000100	0.068644	3.447061
250.316000	36.554900	73.655587	11.067727	7.478264	5098.553523	0.827012	0.000439	0.126566	3.471566
250.438100	36.470200	585.061623	39.209626	7.937648	4515.689832	0.825766	0.000508	0.136752	3.491492
250.362600	36.566100	29.850255	6.675086	8.460605	5234.942800	0.827604	0.000448	0.276393	3.643722
250.459500	36.404200	1680.932828	82.326050	7.270441	4055.487040	0.833255	0.000753	0.078569	3.432209
250.442000	36.454600	197.211895	19.413023	7.363679	4939.618668	0.824889	0.000342	0.201678	3.504536
250.388600	36.541200	106.314548	13.804262	7.116858	4967.024621	0.824048	0.000441	0.112573	3.468126
250.424700	36.447600	1233.353743	56.626032	6.572403	4454.636740	0.814366	0.000101	0.028993	3.368167
250.436500	36.390900	267.612191	23.512404	7.513804	4855.940236	0.824033	0.000370	0.169062	3.491099
250.438600	36.518500	309.655914	25.623428	7.839339	4803.421357	0.824269	0.000390	0.178077	3.500972
250.485700	36.500700	149.023738	16.472803	6.739517	4993.493208	0.825963	0.000422	0.186607	3.509532
250.420000	36.569800	171.961144	17.947795	7.661334	4966.396639	0.816614	0.000340	0.207775	3.522392
250.443000	36.553800	46.880841	2.908248	10.236642	8894.339173	0.787894	0.000100	0.139826	3.507401
250.450800	36.594800	56.345459	8.550440	7.553158	5374.961270	0.850662	0.001022	0.351456	3.590724
250.462000	36.481700	1935.136465	88.800737	7.339272	4017.136122	0.851639	0.000743	0.184588	3.489792
250.465400	36.459000	143.514081	16.008611	6.741854	5012.139199	0.824725	0.000393	0.155861	3.478638
250.501500	36.423500	137.874464	15.549796	7.111410	5015.330998	0.824115	0.000370	0.186168	3.501088
250.471700	36.423100	94.588069	12.718545	7.335415	5057.854113	0.815689	0.000357	0.107653	3.456599
250.571500	36.525900	56.648564	8.989727	7.588310	5301.216739	0.859794	0.001575	0.190748	3.495501
250.541100	36.495500	78.263720	11.484310	7.311718	5089.120249	0.823784	0.000399	0.111530	3.455852
250.578600	36.504300	77.907786	11.473646	7.323165	5077.805834	0.823985	0.000415	0.119207	3.463985
250.539200	36.566400	61.796938	9.982881	7.355678	5113.423542	0.841565	0.000697	0.130335	3.465086
250.510500	36.542400	80.846017	11.690906	7.316465	5081.392103	0.823397	0.000379	0.108934	3.457691
250.520700	36.526800	57.137306	8.182497	7.691594	5579.019803	0.833445	0.000651	0.454368	3.662148
250.608400	36.451300	71.487598	10.878189	7.526509	5107.487707	0.829043	0.000443	0.121021	3.465790
250.568800	36.416200	152.617878	16.772637	6.824462	4983.909224	0.825005	0.000413	0.183226	3.507260
250.556500	36.476800	60.637259	9.803812	7.389308	5138.038532	0.851695	0.000773	0.105245	3.458071
250.568700	36.437100	88.032042	12.370436	7.430831	5069.272915	0.823258	0.000369	0.131493	3.472937
250.579500	36.617600	69.031619	10.576224	7.464913	5137.087862	0.829897	0.000438	0.126560	3.465153
250.542400	36.630800	84.783840	11.890365	7.358139	5075.165798	0.823401	0.000377	0.128777	3.465580
250.363700	36.539500	80.358435	11.640271	7.307417	5089.700903	0.823309	0.000368	0.103858	3.454938

Table 16: NGC 6791: Stellar parameters obtained with BEAST

R.A.°	Decl.°	Luminosity (L_{\odot})	Radius (R_{\odot})	Age (Gyr)	Temperature (K)	Mass (M_{\odot})	Metallicity	Av	Rv
290.310500	37.775800	2.223936	1.957129	8.539993	5281.789607	0.976927	0.021538	0.574103	3.004025
290.277900	37.802300	0.213414	0.644561	9.133536	4910.667309	0.661960	0.005626	0.064791	2.981855
290.256000	37.801400	50.629363	10.940208	5.398252	4719.140479	1.209518	0.013580	0.522450	3.001727
290.289400	37.784000	15.450112	5.444043	7.967931	4864.398984	1.060225	0.009813	0.514738	3.002567
290.276200	37.749900	49.520062	10.440607	7.603309	4633.086508	1.066867	0.008741	0.479072	3.005691
290.308400	37.752600	28.194753	7.999622	8.346384	4837.632553	1.050536	0.008723	0.523139	3.012947
290.268900	37.721200	0.697991	0.921660	8.601412	5287.442492	0.913243	0.019478	0.509757	3.005024
290.244800	37.720300	48.688512	10.469243	7.537183	4605.098237	1.069980	0.009411	0.529593	3.003250
290.208500	37.797700	0.552820	0.812239	8.381271	5343.568366	0.836424	0.009114	0.370252	3.009047
290.230800	37.797100	7.698310	3.598095	8.535023	4981.570798	1.051669	0.009728	0.588101	3.023287
290.253600	37.759400	52.078317	11.104542	6.802367	4564.722368	1.134995	0.012784	0.551728	3.022215
290.253600	37.777700	50.077452	10.681312	7.476127	4590.022560	1.072408	0.009792	0.535642	3.007423
290.220300	37.759200	49.229446	10.432401	7.578789	4626.112996	1.067492	0.008820	0.494062	3.004445
290.188200	37.742800	75.904188	14.353374	6.769669	4529.911362	1.131266	0.009499	0.541230	3.001303
290.130300	37.775200	0.380682	0.722319	8.184716	5322.373698	0.749692	0.006569	0.224196	2.999936
290.188900	37.788300	48.804094	10.467710	7.612073	4618.114172	1.068777	0.009287	0.539763	3.004144
290.127700	37.754800	0.649463	0.851786	8.903746	5191.160243	0.867375	0.008605	0.394948	3.043791
290.163500	37.743700	40.837478	9.445728	6.602134	4585.154368	1.133906	0.009819	0.416819	2.995646
290.143300	37.801100	0.667293	0.850951	8.012433	5579.074368	0.856539	0.009036	0.536655	3.012005
290.196100	37.761200	0.205858	0.639074	8.834290	4894.820353	0.654491	0.005336	0.062191	2.981373
290.168800	37.785200	7.829787	3.888669	8.043948	5002.006364	1.054182	0.011379	0.462260	2.995413
290.176700	37.764200	42.204246	9.642328	6.276266	4740.651066	1.139929	0.011543	0.525936	3.005274
290.174200	37.706000	1.752637	1.203656	6.198864	5954.481144	1.028701	0.010890	0.255191	2.975171
290.180800	37.721400	16.774460	5.646169	8.351379	4883.438079	1.054451	0.009131	0.487618	3.002748
290.124700	37.811500	0.608884	0.811302	6.993813	5655.465738	0.843424	0.008186	0.432951	2.994840
290.240500	37.817000	49.287976	10.674412	7.288493	4657.885102	1.081882	0.012873	0.605895	3.009589
290.192700	37.819600	54.066472	11.317912	5.377780	4628.750933	1.210814	0.013843	0.517774	3.002182
290.163300	37.834600	7.521316	3.596625	10.001157	5019.777603	0.936923	0.008997	0.690494	3.079811
290.157900	37.819000	0.440533	0.755411	7.913382	5391.668668	0.787907	0.007950	0.224699	2.981381
290.286000	37.717500	0.232752	0.654092	9.002331	4973.898518	0.674602	0.005825	0.379896	3.036222
290.292600	37.752100	0.338338	0.707461	8.698901	5195.238270	0.735196	0.006808	0.217563	3.003081
290.267500	37.732500	0.319211	0.689214	8.155232	5195.183053	0.726090	0.006235	0.109235	2.984927
290.169600	37.707400	0.226515	0.708552	9.418303	4691.861509	0.746357	0.021335	0.663978	3.058485
290.233100	37.779500	0.360287	0.783730	8.519418	5023.751422	0.827061	0.016851	0.713686	3.016504
290.234000	37.725500	1.184793	1.031902	8.395860	5698.439868	0.941210	0.011743	0.486946	3.001172
290.233200	37.695000	0.382237	0.741042	8.542491	5198.574658	0.766291	0.007970	0.186145	2.990687
290.191700	37.750200	0.285216	0.687651	8.751867	5090.854236	0.708878	0.007173	0.445236	3.047963
290.161800	37.722400	1.459561	1.064382	5.460823	6007.048677	0.997280	0.009376	0.351473	2.972277
290.185100	37.733300	1.760872	1.173110	5.720344	6059.942368	1.018873	0.009152	0.569756	2.989108
290.162000	37.777000	2.409126	1.269405	4.088868	6267.225024	1.092365	0.009237	0.570779	2.947831
290.148600	37.759500	0.222060	0.653042	9.362447	4918.868779	0.668155	0.006634	0.617737	3.066786
290.183800	37.777400	19.303236	7.656188	12.168076	4383.829183	1.005411	0.049960	0.797752	3.070813
290.213500	37.741200	6.203460	3.379818	10.119482	4993.066033	0.929548	0.016550	0.738197	3.088922
290.144300	37.786400	1.610514	1.136060	6.701628	5965.376338	0.984357	0.009174	0.555311	3.004745
290.125700	37.764300	0.310827	0.685614	8.359695	5185.976460	0.709744	0.005922	0.136833	2.990510
290.119300	37.798000	0.501781	0.800465	8.905076	5172.294620	0.828677	0.009155	0.438443	3.051412